

**ALKYLATION OF ZINC THIOLATE PROTEINS:
REACTIONS WITH MODEL COMPOUNDS**

THESIS

Presented to the Graduate Council of
Southwest Texas State University
in Partial Fulfillment of the Requirements

For the Degree

Master of Science

By

Jennifer Nicole Smith, B.S.

San Marcos, Texas
August 2003

For my loving parents,
Dr. Thomas Michael and Karlene Smith

ACKNOWLEDGEMENTS

The author wishes to recognize those persons who provided assistance throughout the course of this experience, and to those colleagues who supported this research endeavor. Without their aid, this project would not have been possible.

DR. CARL J. CARRANO for affording guidance, ideas, patience, aid in preparation of this thesis, and the opportunity for this experience.

DR. DEBRA A. FEAKES, DR. MICHAEL T. BLANDA, and DR. WALTER E. RUDZINSKI for their direction in the completion of this project, and for their guidance.

DR. ZAHIDA SHIRIN AND DR. BALWONT CHOCHAN for their exemplary display of patience and assistance throughout the course of this project, and for their friendships.

KARLENE, HEATHER, and DR. THOMAS MICHAEL SMITH for their never ending love, counsel, encouragement and support (both financial and emotional). The author would be lost without them.

ELIZABETH POOLE for true friendship and love and support.

JASON WHITSON for encouraging and loving me.

TABLE OF CONTENTS

	Page
LIST OF ABBREVIATIONS.....	viii
LIST OF FIGURES AND SCHEMES.....	x
LIST OF TABLES.....	xii
ABSTRACT.....	xiii
I. INTRODUCTION.....	1
Background and History.....	1
The Problem.....	9
Research Goals.....	11
Applications.....	13
II. MATERIALS	
Model Compounds.....	14
NMR Spectrometer.....	15
X-ray Crystallography.....	16
IR Spectroscopy.....	16
Elemental Analysis.....	16
III. METHODS	
Synthesis of [(L3S)ZnI].....	17
Synthesis of [(L1O)Zn(SPh)].....	17

Synthesis of [(L1O)Zn(NAcSPh)].....	18
Synthesis of [(L4O)Zn(NAcSPh)].....	19
Synthesis of [(L1O)Zn(NCOCF ₃ SPh)].....	20
Synthesis of [(L3S)Zn(NAcSPh)].....	21
Synthesis of [(L3SCH ₃)Zn(NAcSPh)].....	21
X-ray Crystallography.....	21
Kinetic Experiments.....	22
Kinetic Data Analysis.....	24

IV. RESULTS

Synthesis and Crystallography.....	25
1. Synthesis of [(L3S)ZnI].....	25
2. Synthesis of [(L1O)Zn(SPh)].....	26
3. Synthesis of [(L1O)Zn(NAcSPh)].....	28
4. Synthesis of [(L1O)Zn(NCOCF ₃ SPh)]	30
5. Synthesis of [(L4O)Zn(NAcSPh)].....	31
6. Synthesis of [(L3S)Zn(NAcSPh)].....	33
7. Synthesis of [(L3SCH ₃)Zn(NAcSPh)].....	35
Reactivity.....	37
1. Methylation of [(L3S)ZnI].....	37
2. Methylation of [(L1O)Zn(SPh)].....	38
3. Methylation of [(L1O)Zn(NAcSPh)].....	39
4. Methylation of [(L1O)Zn(NCOCF ₃ SPh)].....	40
5. Methylation of [(L4O)Zn(SPh)].....	41
6. Methylation of [(L4O)Zn(NAcSPh)].....	43

V. DISCUSSION

Kinetics: Solvent Effects.....	45
Kinetics: Hydrogen Bonding in [(L1O)Zn(NAcSPh)] and [(L4O)Zn(NAcSPh)].....	48
Hydrogen Bonding: [(L3S)Zn(NAcSPh)].....	51
Kinetics: Hydrogen Bonding of [(L1O)Zn(NAcSPh)] and [(L1O)Zn(NCOCF ₃ SPh)].....	52
Conclusions.....	53
Future Research.....	54

REFERENCES.....	56
APPENDIX A: Kinetic Data.....	60
APPENDIX B: Graphs and ¹ H NMR Spectra.....	70
APPENDIX C: X-ray Crystallographic Data Tables.....	135

LIST OF ABBREVIATIONS

1. $\text{NCOCF}_3\text{CH}_3\text{SPh}$ = 2,2,2-Trifluoro-N-(mercaptophenyl)acetamide
2. NAcCH_3SPh = N-(2-methylmercaptophenyl)acetamide
3. CH_3SPh = Benzenemethylthiol
4. [L3S] ligand = (2-Methylethanethiol-bis-3,5-dimethylpyrazolyl)methane
5. [L1O] ligand = (3-*tert*-butyl-2-hydroxy-5-methylphenyl)bis(3,5-dimethylpyrazolyl)methane
6. [L4O] ligand = Bis(3,5-dimethylpyrazolyl)acetate
7. (L3S)ZnI = (2-Methylethanethiol-bis-3,5-dimethylpyrazolyl) zinc iodide
8. (L3SCH₃)ZnI = (2-Methyl-2-methylthiol-bis-3,5-dimethylpyrazolyl) zinc iodide
9. (L3S)Zn(NAcSPh) = (2-Methylethanethiol-bis-3,5-dimethylpyrazolyl) zinc N-(2-mercaptophenyl)acetamide
10. (L3SCH₃)Zn(NAcSPh) = (2-Methyl-2-methylthiol-bis-3,5-dimethylpyrazolyl) zinc N-(2-mercaptophenyl)acetamide
11. (L1O)Zn(SPh) = (3-*tert*-Butyl-2-hydroxy-5-methylphenyl)bis(3,5-dimethylpyrazolyl) zinc benzenethiol
12. (L1O)Zn(NAcSPh) = (3-*tert*-Butyl-2-hydroxy-5-methylphenyl)bis(3,5-dimethylpyrazolyl) zinc N-(2-mercaptophenyl)acetamide

13. (L1O)ZnI = (3-*tert*-Butyl-2-hydroxy-5-methylphenyl)bis(3,5-dimethylpyrazolyl)
zinc iodide
14. (L1O)Zn(NCOCF₃SPh) = (3-*tert*-Butyl-2-hydroxy-5-methylphenyl)bis(3,5-
dimethylpyrazolyl) zinc 2,2,2-trifluoro-N-(2-mercaptophenyl)acetamide
15. (L4O)Zn(SPh) = Bis(3,5-dimethylpyrazolyl)acetyl zinc benzenethiol
16. (L4O)ZnI = Bis(3,5-dimethylpyrazolyl)acetyl zinc iodide
17. (L4O)Zn(NAcSPh) = Bis(3,5-dimethylpyrazolyl)acetyl zinc N-(2-
mercaptophenyl)acetamide

LIST OF FIGURES AND SCHEMES

	Page
Figure 1. Pseudotetrahedral coordination of zinc in proteins.....	2
Figure 2. Zinc coordination of NCp7 protein.....	4
Figure 3. Space-filled model of Ada protein, with four cysteine donor residues.....	6
Figure 4. Pathway of Methionine synthesis.....	8
Figure 5. The pathways of zinc thiolate reactivity.....	10
Figure 6. Family of ligands used for model compounds.....	12
Figure 7. ORTEP diagram of [(L3S)ZnI].....	26
Figure 8. ORTEP diagram of [(L1O)Zn(NAcSPh)].....	29
Figure 9. ORTEP diagram of [(L1O)Zn(NCOCF ₃ SPh)].....	31
Figure 10. ORTEP diagram of [(L4O)Zn(NAcSPh)].....	33
Figure 11. ORTEP diagram of [(L3S)Zn(NAcSPh)].....	35
Figure 12. ORTEP diagram of [(L3SCH ₃)Zn(NAcSPh)].....	36
Figure 13. Ingold Analysis for nucleophile determination.....	47
Scheme 1. Synthesis of [(L3S)ZnI].....	25
Scheme 2. Synthesis of [(L1O)Zn(SPh)].....	27
Scheme 3. Synthesis of [(L1O)Zn(NAcSPh)].....	28

Scheme 4. Synthesis of [(L1O)Zn(NCOCF ₃ SPh)].....	30
Scheme 5. Synthesis of [(L4O)Zn(NAcSPh)].....	32
Scheme 6. Synthesis of [(L3S)Zn(NAcSPh)].....	34

LIST OF TABLES

	Page
Table 1. Concentrations for each reaction.....	23
Table 2. Relative Rate Comparisons for each ligand in methyl iodide.....	45
Table 3. Relative Rate Comparisons for each ligand in $(\text{CH}_3)_3\text{OBF}_4$	46
Table 4. Relative Rate Comparisons between the [L1O] analogs in CH_3I	49
Table 5. Relative Rate Comparisons between the [L1O] analogs in $(\text{CH}_3)_3\text{OBF}_4$	49
Table 6. Relative Rate Comparisons between the [L4O] analogs in CH_3I	50
Table 7. Relative Rate Comparisons between the [L4O] analogs in $(\text{CH}_3)_3\text{OBF}_4$	50

ABSTRACT

ALKYLATION OF ZINC THIOLATE PROTEINS: REACTIONS WITH MODEL COMPOUNDS

by

Jennifer Nicole Smith, B.S.
Southwest Texas State University
August 2003

Supervising Professor: Dr. Carl J. Carrano

Many metalloproteins are known to tetrahedrally coordinate a zinc atom into their folded conformation. The zinc is ligated to nitrogen, sulfur, and/or oxygen donor atoms, which come from amino acid residues, such as histidine, cysteine, tyrosine, aspartic acid, and glutamic acid. The operative roles of the proteins are classified as either for structural support, or for enzymatic activity. The reactive proteins can utilize the same tetrahedral coordination to the same donor atoms as the non-enzymatic proteins. To date, it is unclear how nature is controlling the reactivity of zinc thiolate proteins. Learning how to control the reactivity of zinc-thiolate bonds can have major implications in the development of new pharmaceuticals, in addition to fundamental protein chemistry.

The research presented here involves the synthesis and characterization of small molecule chemical models, which mimic the active sites of zinc-thiolate proteins. The zinc complexes studied are of the general type, LZn-SR, where L represents a tripodal heteroscorpionate ligand, and SR represents a thiophenol. ¹H NMR kinetic studies were performed to determine the influence of the ligand donor atoms and of the hydrogen bonding interactions during the alkylation of a variety of model compounds. The reactions were run in chloroform, acetonitrile, and methanol with either of two methylating agents, methyl iodide or trimethyloxonium tetrafluoroborate. The comparison of rate constants firstly shows that hydrogen bonding to the sulfur donor decreases the rate of alkylation, and secondly that the strength of the hydrogen bond only mildly influences the rate. In addition to controlling zinc thiolate reactivity, it is shown that hydrogen bonding also generates exquisite specificity when multiple thiolate targets are present. Finally, the data also support the proposal that a zinc-bound thiolate is the actual nucleophile in the alkylation mechanism.

CHAPTER I

INTRODUCTION

Background and History

Zinc is the most abundant metal in biological systems. There are over 300 enzymes that involve zinc¹, and hundreds of other proteins that coordinate a zinc ion into their structures. The donor atoms that coordinate the zinc, usually nitrogen and oxygen, originate either from the surrounding amino acid side chains, typically histidine, aspartate or glutamate, or from water. While histidine is the most common donor¹, it has been shown that the sulfur from cysteine residues can also function as a donor atom. Zinc thiolate proteins are of interest because relatively little is known about the zinc thiolate reactivity, or how nature controls the reactivity. As a result, there is a lack of knowledge of how to exploit the reactivity of zinc thiolate proteins.

Zinc thiolate proteins have both structural and enzymatic roles², although the geometry of the binding sites are extremely similar. All zinc thiolate proteins have the donor atoms pseudotetrahedrally coordinated around the zinc¹, as shown in Figure 1. Thus their differing reactivity cannot stem from the geometry of the active site. Rather, it must be a reflection of the electronic state generated by the differing donor atoms.

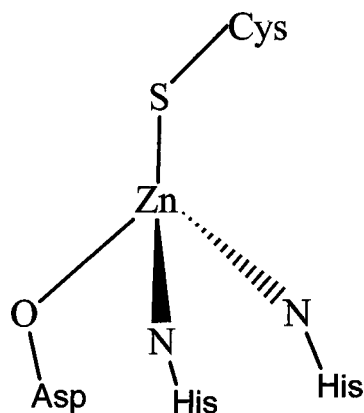


Figure 1. Pseudotetrahedral coordination of zinc in proteins

Zinc thiolate proteins are ubiquitous. In particular, the zinc finger proteins are so numerous that about 1% of the human genome encodes for them³. The zinc fingers are small, metal binding peptides that are involved in gene regulation and the recognition between nucleic acids and proteins.³ This role of the zinc is strictly structural. They contain a core of histidine and cysteine residues that assemble in three motifs of coordination, CCCC, CCHC, CCHH, where the C is cysteine and the H is histidine⁴. While the motifs are highly conserved, there is variability in the sequence of amino acids that are between these residues, to allow for the large diversity seen between organisms. One example of the CCCC coordination is the GATA family of zinc fingers. The GATA family consists of proteins that are transcription factors. The proteins recognize a six-nucleotide motif of T/AGATAG/A, within a gene sequence.⁵ GATA proteins regulate gene expression during embryonic development⁶. GATA proteins contain a zinc finger motif of the amino acid sequence CXNCX(17)CNXC⁷. This coordination gives four sulfur donor

atoms to the zinc in a pseudotetrahedral array. While these proteins vary slightly from species to species, there is a universal function and thus the motifs are conserved⁸.

Since the zinc fingers are a structural motif, the zinc atom must be bound to the proper donor atoms in order for the protein to fold into its spatial conformation. Any modification of the zinc finger is not tolerated in the organism, resulting in a non-functional protein. Since a thiolate is an excellent nucleophile, zinc thiolate proteins are susceptible to oxidizing agents and alkylating agents. While in nature, it is undesirable for zinc fingers to have reactivity, it is obvious that this susceptibility could be exploited for drug therapy targets. If the thiolate ligand of a zinc finger reacts, the zinc atom may be ejected causing the protein to lose its folded structure and thereby rendering it unable to function⁹.

This idea has been applied to the HIV nucleocapsid protein (NCp7). HIV is a retrovirus that encodes a Gag precursor polyprotein. The polyprotein is cleaved into several smaller proteins, including the nucleocapsid protein¹⁰. The role of NCp7 is to aid in the recognition and packaging of the newly replicated viral genome during the late stages of the lytic cycle^{10, 11}. In this protein, the zinc is pseudotetrahedrally coordinated to one histidine and three cysteine residues, shown in Figure 2.

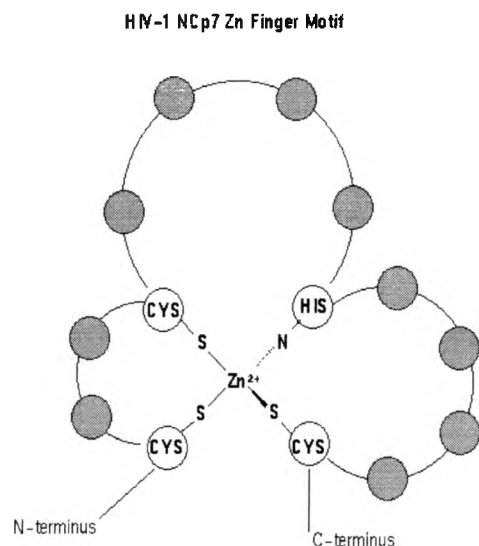


Figure 2. Zinc coordination of NCp7 protein¹²

Interestingly, these amino acid residues and the spacing between them are conserved amongst all retroviruses, although the amino acids between these residues can vary between organisms. The zinc fingers in the NCp7 protein are of interest because they are unusually susceptible to alkylation, causing the protein to lose its vital role during the packaging of the newly replicated viral genome, and thus be a potential treatment for HIV patients¹³. The ejection of the zinc from the protein appears to be the cause for the collapse of the folded structure. Since zinc finger proteins are so ubiquitous, understanding how nature controls zinc thiolate reactivity is key to the development of new HIV therapies and other drug targets.

Another class of zinc thiolate proteins with similar active site geometry is the metalloregulatory proteins. These proteins function to control the intracellular concentrations of metal ions, and to detoxify heavy metal pollutants. An example in this class of proteins is the *Zur* protein of *E. coli*. This protein represses the zinc

transporter genes on the *znuABC* operon¹⁴. Due to this repression, the uptake of zinc(II) is inhibited. *Zur* is “turned on” when it perceives a high level of zinc(II) inside the organism. *Zur* has two zinc fingers, one having a structural role, and the other involved in metal sensing. However, both sites have a tetrahedral coordination to the zinc, S_3N/O and $S(N/O)_3$ ¹⁴. These zinc thiolate proteins serve an important, albeit nonenzymatic purpose.

The final role of zinc thiolate proteins is that of enzymatic activity. There is still the same pseudotetrahedral coordination around the zinc, but the thiolate bound to the zinc becomes reactive towards electrophiles. An example of this type of reactivity comes from the Ada protein in *E. coli*. This protein has two functions. One, it can detect a DNA-methylphosphotriester and repair it.^{15,16} This DNA lesion occurs due to various environmental factors, and if not repaired, results in many cellular dysfunctions. Therefore the Ada protein is crucial for the survival of an organism.

Ada protein will undergo alkylation at a Zn-S site by removing the methyl group from the DNA backbone to its Cys38 residue^{15,16}, see Figure 3.

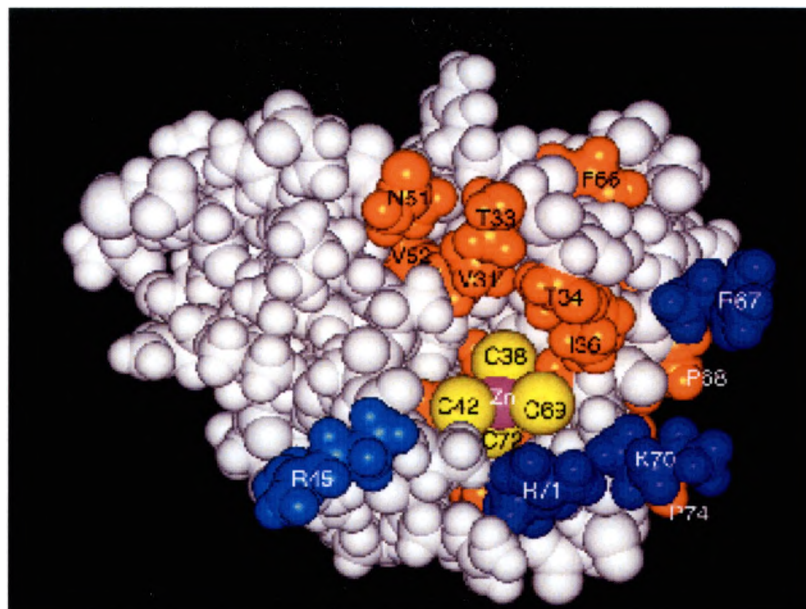


Figure 3. Space-filled model of Ada, with four donor Cysteine residues

Recent research has revealed that it is the Cys38 residue that is targeted for alkylation, not Cys69, as previously reported¹⁵. Then, Ada performs a second task of acting as a transcription factor, to activate the transcription of more Ada proteins and other DNA repair enzymes. In this aspect, it is regarded as a chemosensor for alkylation damage to a cell. These two functions occur at different active sites in the protein. Another interesting aspect of the Ada protein is that after the Cys38 residue is alkylated, the thioether remains bound to the zinc. It had previously been thought that thioethers are not good zinc ligands.

It is important to note that the Ada protein involves the CCCC coordination of zinc at the alkylation site¹⁷. The GATA family of zinc fingers and some nuclear hormone receptors, such as the human estrogen receptor, also utilize the same CCCC

coordination to zinc, but are completely unreactive. There must be a controlling factor in nature that is involved to regulate which zinc thiolate proteins will be involved in alkyl transfer reactions and which will simply hold the protein in the proper three-dimensional conformation. A second unanswered question is how only one of the many thiolates in a CCCC site can be targeted for reactivity leaving the others unaffected. It is currently unclear how nature can control this reactivity.

Other zinc thiolate proteins that are involved in alkyl transfer reactions are the enzymes MetE, MetH, and farnesyltransferase. MetE and MetH are methionine synthases, which are cobalamin-independent and dependent, respectively¹⁸. These enzymes are crucial for the transfer of a methyl group from methyl tetrahydrofolate ($\text{CH}_3\text{-H}_4\text{folate}$) to homocysteine in order to produce methionine de novo, see Figure 4.

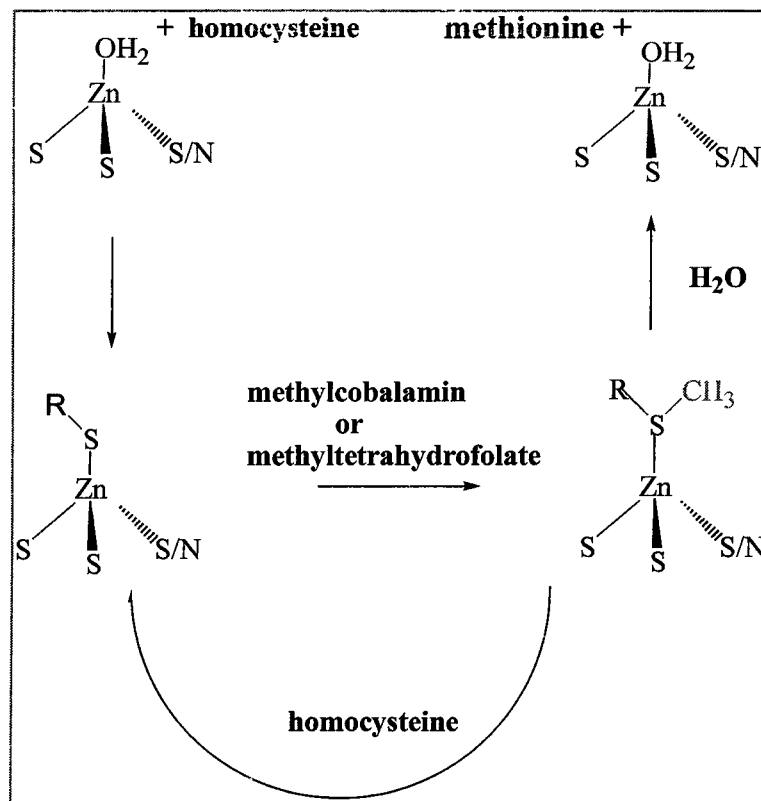


Figure 4. Pathway of methionine synthesis

In MetE, the zinc is ligated in a $[S_2(N/O)_2]$ environment, which when exposed to homocysteine converts to a $[S_3(N/O)]$ site as the homocysteine binds. However in MetH, the zinc is ligated in a $[S_3(N/O)]$ system, which is then changed to a $[S_4]$ environment upon reaction with homocysteine¹⁸. These proteins have the same function, yet have different coordination to the zinc. This is more evidence to support the idea that the protein functions do not stem from the coordination structure.

The protein farnesyltransferase (PFTase) selectively catalyzes the methylation of a cysteine in protein substrates. These protein substrates are characterized as having a motif of CaaX at the C-terminus, where “C” is cysteine, “a” is a small hydrophobic amino acid, and “X” is any of the amino acids A, S, M, or N¹⁹. Examples of the protein substrate for PFTase are Ras, nuclear lamins, Rho proteins,

and various kinases¹⁹. Farnesyl diphosphate (FPP) is the needed cofactor that provides the alkyl group. This alkylation allows the substrate proteins to be inserted into the cell membrane. The yeast PFTase coordinates a zinc ion to D307, C309, H363, and a water molecule¹⁹, and there appears to be similar coordination in other organisms. The alkyl group is transferred to the substrate's cysteine residue by a nucleophilic attack in the PFTase, protein substrate, FPP complex.

The Problem

Much less is known about the reactivity of zinc thiolates than more widely studied Zn-O/N interactions. The normal paradigm of “different structures lead to different functions” appears not to hold for this group since zinc thiolate proteins can have exactly the same donor atoms and tetrahedral structure, but have completely different functions. In addition, as seen in the PFTase, MetE, and MetH enzymes, there can be similar function but different coordination. These enigmas have yet to be resolved. The key point is to understand the chemical difference between the reactive and unreactive thiolates.

It is well established that the thiolate anion is an excellent nucleophile, while the protonated thiol is a poor one. However the reactivity of a zinc-bound thiolate needs to be characterized in this inherent reactivity scheme of nucleophiles. When a zinc thiolate reacts, it can proceed via one of two pathways, an associative or a dissociative one, see Figure 5.

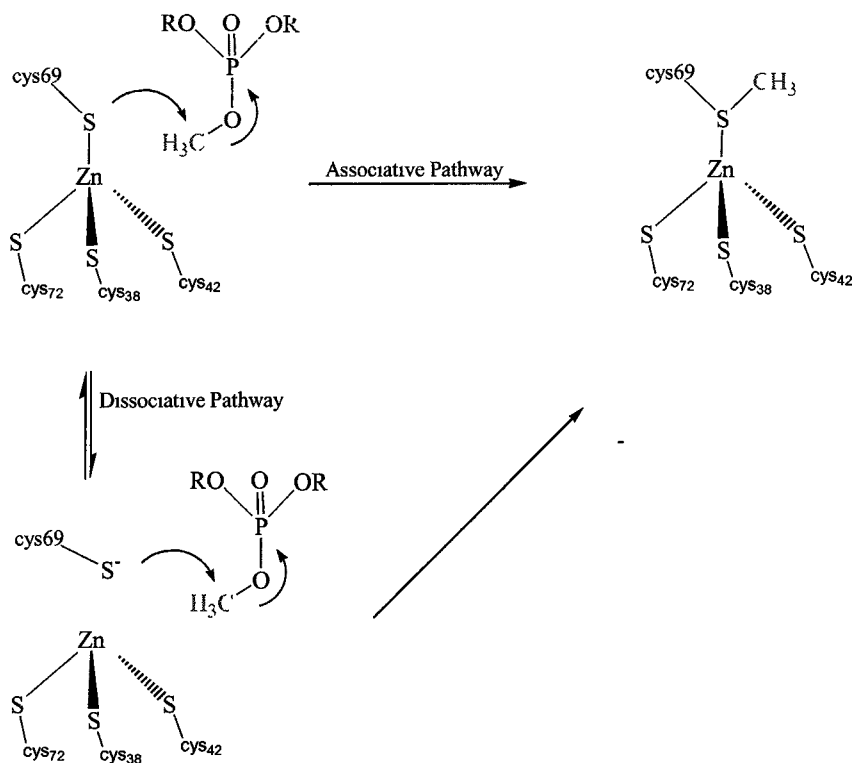


Figure 5. The pathways of zinc thiolate reactivity

In the associative pathway, the thiolate stays bound to the zinc and it is the zinc-bound thiol that is the nucleophile. In the dissociative pathway, the thiolate dissociates from the zinc as an anion, which subsequently reacts with the electrophile. In either case, a thioether is the final product. In previous work the conclusion had been reached based on the behavior of certain model systems that indicate that a dissociative pathway was operative¹⁷. This idea has been embraced as a mechanism for all zinc thiolate proteins, however this may not be an appropriate generalization.

It is also important to understand how nature controls the reactivity of zinc thiolate proteins. Why does the Ada protein react with electrophiles while the GATA proteins do not? They have exactly the same coordination to the zinc, but have different functions. Learning how to exploit this difference in reactivity will also

have major implications in many other areas of research. One way that nature exploits reactivity is to use hydrogen bonds. Recent literature cites that in the Ada protein, the three unreactive cysteine donor atoms, Cys42, -69, and 72, are involved in hydrogen bonding to protons of the protein's main chain¹⁵. Hydrogen bonding presents one option that could be used for experimental purposes.

Research Goals

It is the aim of this thesis to answer the following mechanistic questions: What is the reacting nucleophile? How can we control the reactivity of zinc thiolates? These questions will be addressed using model compounds because they are relatively easy to synthesize, are capable of systematic variation, and are less complicated than using a protein system. More specifically, there will be kinetic experiments using the synthesized heteroscorpionate model compounds in alkylation reactions, see Figure 6.

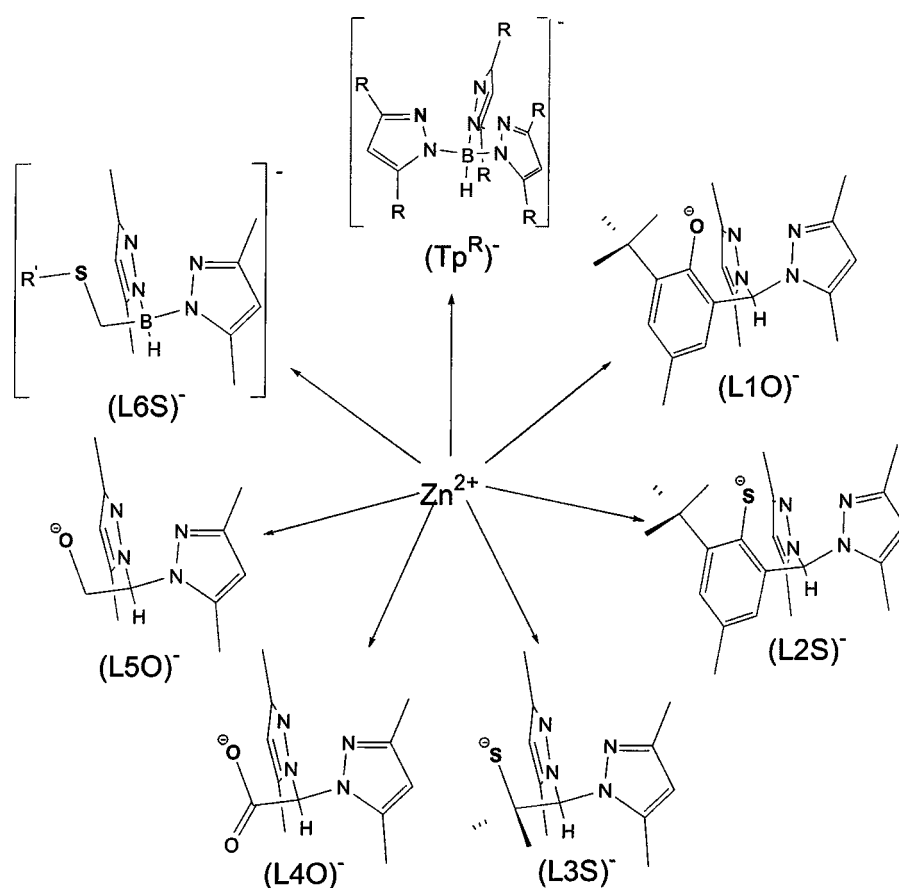


Figure 6. Family of ligands used for model compounds

The rates of alkylation are determined for the zinc thiolate model compounds. These compounds mimic all of the possible donor atoms that are viable in biological systems. Solvent effects will be used to answer the question of what is the reacting nucleophile, and hydrogen bonding will be used to answer the question of how the reactivity can be controlled. It is hypothesized that the use of hydrogen bonding will control the reactivity of the zinc thiolates. There will be corresponding hydrogen bonded and non-hydrogen-bonded compounds, and the rates of alkylation will be compared.

Applications

This thesis project is relevant to structure-based drug design of pharmaceuticals, for exploiting the reactivity of zinc thiolate proteins. Learning how to control the reactivity of zinc thiolates will allow for the synthesis of chemicals that can enhance or inhibit the reactivity of zinc thiolates. The insight into the mechanism for the nucleophiles will enhance other avenues of research.

CHAPTER II

MATERIALS

The reagents and solvents were purchased from commercial sources, and used as received unless otherwise noted. Dichloromethane was distilled under argon over CaH₂. The NMR solvents CDCl₃, CD₃CN, and CD₃OD were purchased from Aldrich, and used as received. The alkylating agents methyl iodide and trimethyloxonium tetrafluoroborate were purchased from Aldrich, and used as received. The heteroscorpionate model compounds were synthesized according to the literature methods², as described in the Methods chapter.

Model Compounds

The ligands for the model compounds are: [L1O] = (3-*tert*-butyl-2-hydroxy-5-methylphenyl)bis(3,5-dimethyl-1-pyrazolyl)methane; [L3S] = (2-methylethanethiol-bis-3,5-dimethylpyrazolyl)methane; [L4O] = bis(3,5-dimethyl-1-pyrazolyl)acetate.

The synthetic model compounds used for the experiments are:

[(L1O)Zn(SPh)], [(L1O)Zn(NAcSPh)], [(L3S)ZnI], [(L3S)Zn(NAcSPh)],

[(L4O)Zn(SPh)], **[(L4O)Zn(NAcSPh)]**, and **[(L1O)Zn(NCOCF₃SPh)]**. The (L1O) ligand offers N₂O as the ligand donor set, where the oxygen is donated by a phenol group. The [L4O] ligand is also a N₂O ligand donor set, however the donated oxygen is a carboxylate oxygen. The [L3S] ligand is unique in that the sulfur is chelated in the backbone of the ligand, with a N₂S as the donor set. The ligand for the [L4O] complexes was provided by Dr. Brian S. Hammes, St. Joseph's University, Philadelphia, Pennsylvania. The ligands for the [L1O] and [L3S] complexes were provided by Dr. Zahida Shirin, Southwest Texas State University, San Marcos, Texas. The **[(L3S)ZnI]** complex was previously synthesized by Dr. Carl J. Carrano, Southwest Texas State University, San Marcos, Texas. All other compounds, excluding the **[(L1O)Zn(SPh)]** and **[(L4O)Zn(SPh)]**, were synthesized by Dr. Zahida Shirin. The **[(L1O)Zn(SPh)]** was synthesized in lab by the author, and the **[(L4O)Zn(SPh)]** by Dr. Brian S. Hammes. All syntheses are described in the Methods chapter.

NMR Spectrometer

¹H NMR spectra were collected on a Varian Unity INOVA 400MHz NMR spectrometer. Chemical shifts are reported in ppm, relative to an internal standard of TMS. ¹H NMR spectra were collected for the characterizations of compounds and for the kinetic studies.

X-ray Crystallography

Crystal, data collection, and refinement parameters for **[(L3S)ZnI]**, **[(L3S)Zn(NAcSPh)]**, **[(L3SCH₃)Zn(NAcSPh)]**, **[(L1O)Zn(NAcSPh)]**, and **[(L4O)Zn(NAcSPh)]**, are given in Appendix C, and described in the Methods chapter. The structures were determined on a Siemens P4 diffractometer, with an X-ray source ($\lambda=0.71073\text{\AA}$) controlled via PC computer, or on a Nonius Kappa CCD diffractometer at the University of Texas, Austin, operated by Dr. Vincent Lynch.

IR Spectroscopy

IR spectra were recorded as KBr disks on a Perkin-Elmer Spectrum One FTIR spectrometer equipped with a Dell Optiplex PC. The spectra were used to characterize **[(L1O)Zn(NAcSPh)]**, **[(L1O)Zn(NCOCF₃SPh)]**, and **[(L4O)Zn(NAcSPh)]**, as described in the Methods chapter.

Elemental Analysis

The elemental analyses were obtained from Quantitative Technologies, Inc., Whitehouse, NJ. All samples were dried in vacuo prior to analysis. Details for the complexes **[(L1O)Zn(NAcSPh)]** and **[(L4O)Zn(NAcSPh)]** are described in the Methods chapter.

CHAPTER III

METHODS

Synthesis of (2-Methylethanethiol-bis-3,5-dimethylpyrazolyl)methane zinc iodide, [(L3S)ZnI]

This complex was synthesized by Dr. Carl Carrano in previous experiments.²⁰

A solution of L3SH (0.78 g, 2.8 mmol) in 30 mL of CH₃OH was treated with sodium methylate, NaOMe, (0.15 g, 2.8 mmol) under argon. After stirring the solution for 0.5 hour, solid ZnI₂ (0.89 g, 2.8 mmol) was added slowly. The resulting solution was stirred for 2 hours and filtered to give 0.90 g (69%) of [(L3S)ZnI] as a white solid.

Crystals for an X-ray diffraction study were grown by the slow diffusion of hexane into a CH₂Cl₂ solution of [(L3S)ZnI]. ¹HNMR (CDCl₃) δ 6.00 (s, 1 H, CH), 5.97 (s, 2 H, PzH), 2.51 (s, 6 H, Pz-CH₃), 2.40 (s, 6 H, Pz-CH₃), 1.37 (s, 6H, C(CH₃)₂). ¹³C NMR (CDCl₃) δ 150.42, 140.71, 106.75, 73.10, 48.32, 33.66, 13.84, 11.38.

Synthesis of [(3-*tert*-butyl-2-hydroxy-5-methylphenyl)bis(3,5-dimethylpyrazolyl)]methane zinc benzenethiol, [(L1O)Zn(SPh)]

This complex was synthesized by the author. A solution of (L1O) ligand (1.0829 g) and anhydrous toluene (30 mL) was mixed with a solution of 2M ZnMe₂ (3.65 mL) and stirred for 1 hour under argon, to produce [(L1O)ZnMe] (1.0412 g, 6.25 mmol). A solution of [(L1O)ZnMe] in CH₂Cl₂ was treated with a CH₂Cl₂ solution of thiophenol (0.66 mL, 6.5 mmol). The resulting solution was stirred for 1.5 hour, dried under reduced pressure, and crystallized by layering a CH₂Cl₂ solution of the complex with diisopropyl ether, yielding 60% complex. ¹H NMR (CDCl₃) δ 7.52 (d, 2H, *J*=8 Hz, S-ArH), 7.12 (d, 1H, *J*=2 Hz, ArH), 6.89 (t, 1H, *J*=8 Hz, S-ArH), 6.85 (s, 1H, -CH-), 6.64 (d, 1H, *J*=2 Hz, ArH), 5.87 (s, 1H, PzH), 2.60 (s, 6H, Pz-CH₃), 2.46 (s, 6H, Pz-CH₃), 2.43 (s, 6H, S-Ar(CH₃)₂), 2.16 (s, 3H, Ar-CH₃), 1.05 (s, 9H, -C(CH₃)₃). ¹³C NMR (CDCl₃) δ 163.02, 150.42, 142.62, 141.33, 140.22, 138.49, 129.98, 128.80, 127.06, 123.25, 119.99, 119.75, 106.65, 73.39, 35.10, 29.04, 24.63, 20.49, 13.15, 11.72.

Synthesis of [(3-*tert*-butyl-2-hydroxy-5-methylphenyl)bis(3,5-dimethylpyrazolyl)]methane zinc N-(2-mercaptophenyl)acetamide, [(L1O)Zn(NAcSPh)]

Solid NaBH₄ (0.02 g, 0.53 mmol) was added to a THF-ethanol (9:1, 25 ml) of 2,2'-Dithiobis(*N*-phenylacetamide) (0.17 g, 0.51 mmol). The mixture was stirred at room temperature for about 2 hours to give a clear solution, to which [(L1O)ZnCH₃]

(0.40, 0.89 mmol) was added. The resulting solution was stirred overnight, solvents were removed, and the solid was dried under reduced pressure. The resulting solid was redissolved in CH_2Cl_2 , filtered through celite, and crystallized by layering with hexane. Yield: 0.37 g (69%). Anal. Calcd. for $\text{C}_{30}\text{H}_{37}\text{N}_5\text{O}_2\text{S}_1\text{Zn}(\text{CH}_2\text{Cl}_2)_{0.12}$: C, 59.57; H, 6.18; N, 11.53. Found: C, 59.59; H, 6.27; N, 11.43. FTIR (KBr), cm^{-1} : ν_{NH} 3324. FTIR (in CH_2Cl_2): ν_{NH} 3327. ^1H NMR (CDCl_3) δ 8.85 (s, 1H, *NH*), 8.33 (d, 1H, $J=7.6$ Hz, *S-ArH*), 7.80 (d, 1H, $J=7.4$ Hz, *S-ArH*), 7.06 (d, 1H, $J=2.4$ Hz, *ArH*), 7.02 (t, 1H, $J=7.8$ Hz, *S-ArH*), 6.90 (s, 1H, *-CH-*), 6.78 (t, 1H, $J=7.8$ Hz, *S-ArH*), 6.68 (d, 1H, $J=2$ Hz, *ArH*), 5.91 (s, 2H, *PzH*), 2.46 (s, 6H, *Pz-CH*₃), 2.22 (s, 3H, *S-ArCH*₃), 2.20 (s, 6H, *Pz-CH*₃), 2.19 (s, 3H, *ArCH*₃), 1.35 (s, 9H, *-C(CH*₃)₃). ^{13}C NMR (CDCl_3) δ 168.40, 163.02, 150.39, 142.69, 140.68, 138.43, 134.29, 130.34, 129.06, 124.57, 123.28, 120.66, 119.78, 119.19, 106.81, 73.50, 35.40, 29.33, 25.04, 20.40, 12.79, 11.62,

Synthesis of bis-(3,5-dimethylpyrazolyl)acetyl zinc N-(2-mercaptoacetamide,

[(L₄O)Zn(NAcSPh)]

The complex was synthesized by the same method as described for [(L₁O)Zn(NAcSPh)]. Colorless crystals were obtained from CH_2Cl_2 / diisopropyl ether solution in 60% yield. Anal. Calcd. for $\text{C}_{26}\text{H}_{35}\text{N}_5\text{O}_3\text{SZn}(\text{CH}_2\text{Cl}_2)_{0.1}$: C, 54.85; H, 6.21; N, 12.25. Found: C, 54.91; H, 6.16; N, 11.98. FTIR (KBr), cm^{-1} : ν_{NH} 3307. FTIR (in CH_2Cl_2): ν_{NH} 3341. ^1H NMR (CDCl_3) δ 8.85 (s, 1H, *NH*), 8.26 (d, 1H, $J=7.6$ Hz, *S-ArH*), 7.72 (d, 1H, $J=8$ Hz, *S-ArH*), 7.03 (t, 1H, $J=8$ Hz, *S-ArH*), 6.84 (t,

1H, J= 7.6 Hz, S-ArH), 6.60 (s, 1H, -CH-), 6.05 (s, 2H, PzH), 2.45(s, 6H, Pz-CH₃), 2.26 (s, 3H, S-ArCH₃), 1.27 (s, 18H, Pz-(CH₃)₃). ¹³C NMR (CDCl₃) δ , 164.72, 141.53, 135.49, 125.85, 123.47, 119.66, 104.84, 67.68, 31.96, 30.23, 25.12, 11.25.

Synthesis of [(3-*tert*-butyl-2-hydroxy-5-methylphenyl)bis(3,5-dimethylpyrazolyl)]methane zinc 2,2,2-trifluoro-N-(2-mercaptophenyl)acetamide, [(L₁O)Zn(NCOCF₃SPh)]

Solid NaBH₄ (0.02 g, 0.53 mmol) was added to a THF-ethanol (9:1, 25 ml) of 2,2'-Dithio-bis(*N*-phenyl-2,2,2-trifluoroacetamide) (0.17 g, 0.51 mmol). The mixture was stirred at room temperature for about 2 hours to give a clear solution, to which [(L₁O)ZnCH₃] (0.40, 0.89 mmol) was added. The resulting solution was stirred overnight, solvents removed, and the solid was dried under reduced pressure. The resulting solid was redissolved in CH₂Cl₂ , filtered through celite, and crystallized by layering with hexane. Yield 0.29 g (66%). FTIR (KBr), cm⁻¹: ν_{NH} 3247. FTIR (in CH₂Cl₂): ν_{NH} 3264. ¹H NMR (CDCl₃) δ 10.00 (s, 1H, NH), 8.34 (d, 1H, J= 8 Hz, S-ArH), 7.89 (d, 1H, J= 8 Hz, S-ArH), 7.10 (t, 1H, J= 7.8 Hz, S-ArH), 7.05(d, 1H, J= 2.4 Hz, ArH), 6.94 (t, 1H, J= 7.6 Hz, S-ArH), 6.90 (s, 1H, -CH-), 6.68 (d, 1H, J= 2.0 Hz, ArH), 5.93 (s, 2H, PzH), 2.46 (s, 6H, Pz-CH₃), 2.29 (s, 6H, Pz-CH₃), 2.18 (s, 3H, ArCH₃) 1.26 (s, 9H, -C(CH₃)₃),). ¹³C NMR (CDCl₃) δ 162.93, 150.37, 142.69, 140.78, 134.98, 130.40, 129.15, 125.28, 125.05, 120.81, 119.75, 119.46, 106.87, 73.53, 35.36, 29.20, 20.43, 12.92, 11.66

Synthesis of (2-Methylethanethiol-bis-3,5-dimethylpyrazolyl)methane zinc N-(2-mercaptophenyl)acetamide, [(L3S)Zn(NAcSPh)]

Solid NaBH₄ (0.02 g, 0.53 mmol) was added to a THF-ethanol (9:1, 25 ml) of 2,2'-Dithiobis(*N*-phenylacetamide) (0.17 g, 0.51 mmol). The mixture was stirred at room temperature for about 2 hours to give a clear solution, to which [(L₃S)ZnCH₃] (0.40, 0.89 mmol) was added. The resulting solution was stirred overnight, solvents removed, and the solid was dried under reduced pressure. The resulting mass was redissolved in CH₂Cl₂ , filtered through celite, and crystallized by layering with hexane. Yield: 0.37 g (69%).

Synthesis of (2-Methyl-2methanethiol-bis-3,5-dimethylpyrazolyl)methane zinc N-(2-mercaptophenyl)acetamide, [(L3SCH₃)Zn(NAcSPh)]

This compound was synthesized in the same manner as the [(L1O)Zn(NAcSPh)] complex, using the [L3S] ligand. The white colored product was reacted in equimolar ratio with trimethyloxonium tetrafluoroborate, in acetonitrile. The product was characterized using ¹H NMR.

X-ray Crystallography

Crystals of five complexes were sealed in thin-walled quartz capillaries, and mounted on a Siemens P4 diffractometer. The structures were solved using direct

methods or via the Patterson function, completed by subsequent difference Fourier syntheses, and refined by full-matrix least-squares procedures on F². All non-hydrogen atoms were refined with anisotropic displacement coefficients and treated as idealized contributions using a riding model except where noted. All software and sources of the scattering factors are contained in the SHELXTL 5.0 program library (G. Sheldrick, Siemens XRD, Madison, WI). Selected bond angles and bond lengths for the complexes are shown in Appendix C. The ORTEP diagram for [(L3S)ZnI] is shown in Figure 7; for [(L1O)Zn(NAcSPh)] is shown in Figure 8; for [(L4O)Zn(NAcSPh)] is shown in Figure 9; for [(L3S)Zn(NAcSPh)] is shown in Figure 10; for [(L3SCH3)Zn(NAcSPh)] is shown in Figure 11. These figures contain the thermal ellipsoid diagrams at appropriate probability.

Kinetic Experiments

All experiments were performed under pseudo-first-order conditions with the alkylating agent in large excess. In a typical experiment, 1.8×10^{-5} moles of the metal complex was dissolved in 1 mL of solvent to give an 18 mM solution. Due to solubility problems, some reactions were run at 5 mM or 10 mM, as shown in Table 1. The solution was transferred to a NMR tube, and the alkylating agent, methyl iodide or trimethyloxonium tetrafluoroborate, was added in excess, via a gas-tight syringe. The methyl iodide was added in excess of ten equivalents, while the trimethyloxonium tetrafluoroborate was added in a five equivalent excess because of the solubility problems. The tube was then sealed with a septum. The reactions were

monitored by ^1H NMR spectroscopy at 25°C . The concentrations of product and reactant compound were measured relative to each other. Typical ^1H NMR parameters for the kinetics reactions included four to eight scans per spectrum, and twelve spectra per reaction. Acquisitions were taken throughout the course of each reaction. The length of time between acquisitions varied greatly, depending on the complex, methylating agent, and the solvent. The fastest reactions had a delay time between acquisitions of thirty seconds, while the longest reactions had acquisitions taken twice daily. All other parameters were set as standard values.

		[Zn] in reactions using MeI	[Zn] in reactions using $(\text{CH}_3)_3\text{OBF}_4$
Chloroform	[L3SZnI]	18mM	10mM
	[(L1O)Zn(SPh)]	18mM	10mM
	[(L1O)Zn(NAcSPh)]	18mM	10mM
	[(L1O)Zn(NCOCF ₃ SPh)	18mM	10mM
	[(L4O)Zn(SPh)]	18mM	10mM
	[(L4O)Zn(NAcSPh)]	18mM	10mM
Acetonitrile	[L3SZnI]	18mM	10mM
	[(L1O)Zn(SPh)]	18mM	10mM
	[(L1O)Zn(NAcSPh)]	18mM	10mM
	[(L1O)Zn(NCOCF ₃ SPh)	18mM	10mM
	[(L4O)Zn(SPh)]	18mM	10mM
	[(L4O)Zn(NAcSPh)]	18mM	10mM
Methanol	[L3SZnI]	18mM	10mM
	[(L1O)Zn(SPh)]	5mM	5mM
	[(L1O)Zn(NAcSPh)]	5mM	5mM
	[(L1O)Zn(NCOCF ₃ SPh)	5mM	5mM
	[(L4O)Zn(SPh)]	N/a	N/a
	[(L4O)Zn(NAcSPh)]	N/a	N/a

Table 1. Concentrations for each reaction

Kinetic Data Analysis

The kinetic data was plotted as percent of product formed versus time, or as percent of unreacted complex versus time. A least squares fit to a single exponential was used to determine the pseudo-first order rate constant. The equation for the exponential rise is:

$$f=a[1-\exp(-bx)]+c$$

where **a** is the amplitude of the exponential (=100), **b** is the rate constant, and **c** is the zero intercept (=0). The equation for the decay exponential is:

$$f=a \exp(-bx)+c \exp(-dx)$$

where **a** is the first exponential amplitude, **b** is the first exponential rate constant, **c** is the second exponential amplitude, and **d** is the second exponential rate constant. Data analysis was performed using Sigmaplot (Jandel Scientific, v1.02, 1994) software on a Gateway 2000 PC. Pseudo-first-order rate constants were calculated for each reaction. The kinetic data tables and ¹H NMR spectra are shown in Appendices A-C.

CHAPTER IV

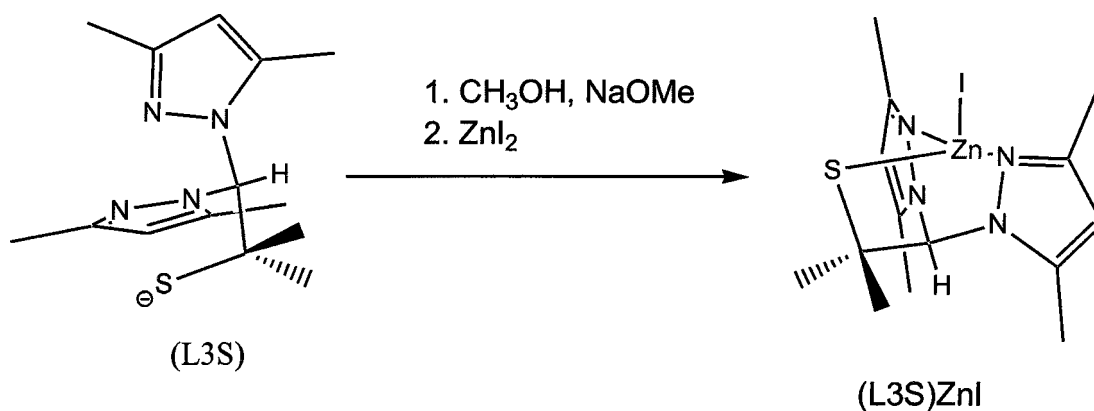
RESULTS

Synthesis and Crystallography.

1. Synthesis of (2-Methylethanethiol-bis-3,5-dimethylpyrazolyl) zinc iodide,

[(L3S)ZnI]

The complex, [(L3S)ZnI], was synthesized by reaction of the deprotonated [L3S] ligand with zinc iodide, details are described in the Methods section. The product was isolated in 69% yield. The synthetic pathway is shown in Scheme 1.



Scheme 1: Synthesis of [(L3S)ZnI]

Colorless crystals of **[(L3S)ZnI]** were formed by slow diffusion of hexane into a dichloromethane solution, as represented in Figure 7. The zinc has pseudotetrahedral geometry, coordinated to two pyrazolyl nitrogen donors, the sulfur donor, and the iodide.

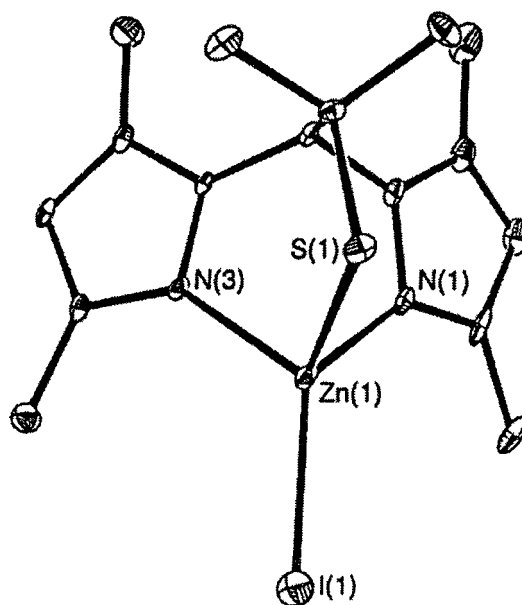
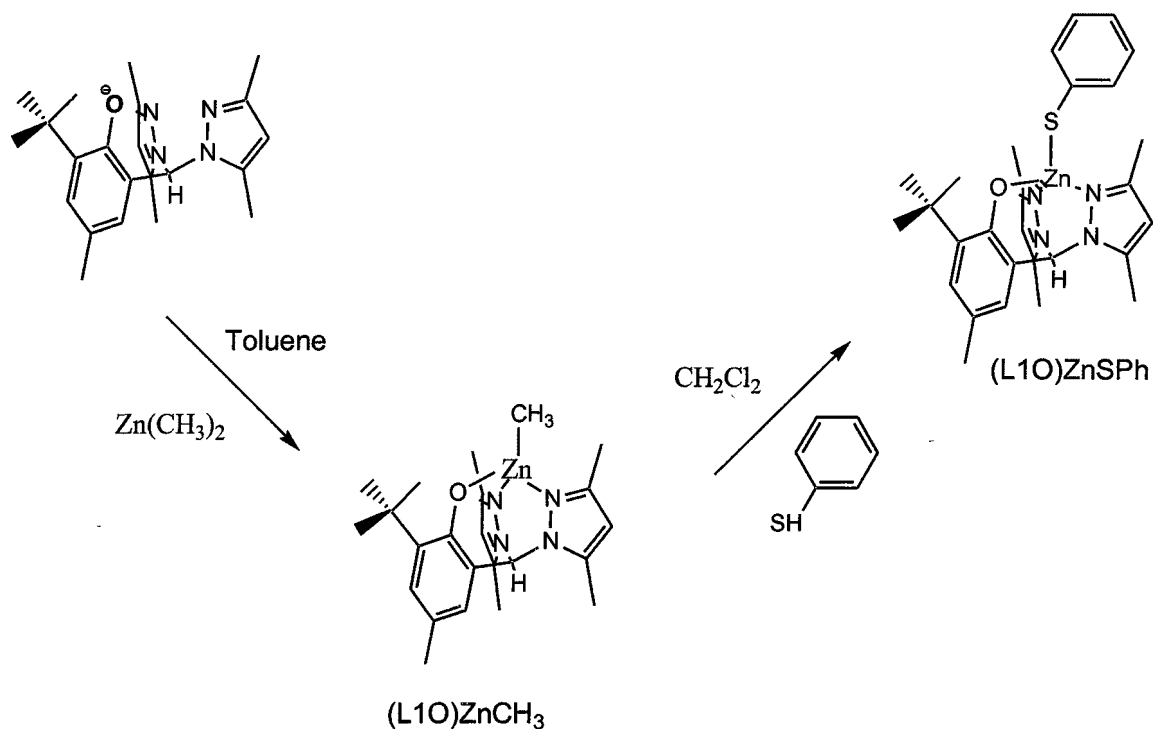


Figure 7. ORTEP diagram with 30% thermal ellipsoids for **[(L3S)ZnI]** showing atomic labeling for the coordination sphere only. Hydrogen atoms are omitted for clarity.²⁰

2. Synthesis of (3-*tert*-butyl-2-hydroxy-5-methylphenyl)bis(3,5-dimethylpyrazolyl) zinc benzenethiol, [(L1O)Zn(SPh)]

The complex, **[(L1O)Zn(SPh)]**, was synthesized by reaction of the [L1O] ligand with dimethyl zinc, and then treated with a dichloromethane solution of

thiophenol, details are described in the Methods section. The product was isolated in 69% yield. The synthetic pathway is shown in Scheme 2.

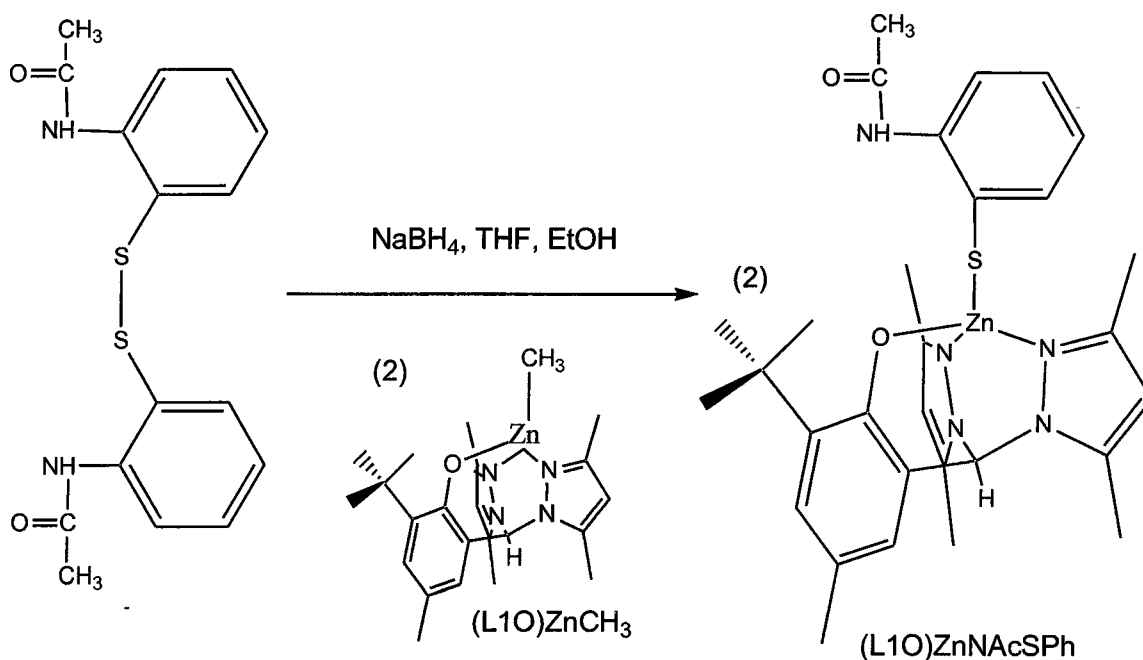


Scheme 2: Synthesis of [(L1O)Zn(SPh)]

Colorless crystals of [(L1O)Zn(SPh)] were formed by slow diffusion of diisopropyl ether into a dichloromethane solution. The zinc has pseudotetrahedral geometry, coordinated to two pyrazolyl nitrogen donors, the phenolic oxygen, and the sulfur donor².

3. Synthesis of (3-*tert*-butyl-2-hydroxy-5-methylphenyl)bis(3,5-dimethylpyrazolyl) zinc N-(2-mercaptophenyl)acetamide, [(L1O)Zn(NAcSPh)]

The complex, [(L1O)Zn(NAcSPh)], was prepared by reaction of (L1O)ZnMe with a solution of 2,2'-dithiobis(*N*-phenylacetamide), reduced with NaBH₄ to generate the free thiol. The reaction proceeded in 69% yield, with details described in the Methods section. The synthetic pathway is shown in Scheme 3.



Scheme 3: Synthesis of [(L1O)Zn(NAcSPh)]

Colorless crystals of [(L1O)Zn(NAcSPh)] were formed by slow diffusion of hexane into a dichloromethane solution of the complex. The zinc has pseudotetrahedral geometry, coordinated to two pyrazolyl nitrogen donors, the phenolic oxygen, and the sulfur donor. The X-ray structure of [(L1O)Zn(NAcSPh)] is shown in Figure 8. The

internal hydrogen bonding is observed between the hydrogen on the nitrogen of the acetamide and the thiolate sulfur. These parameters are shown in Appendix C.

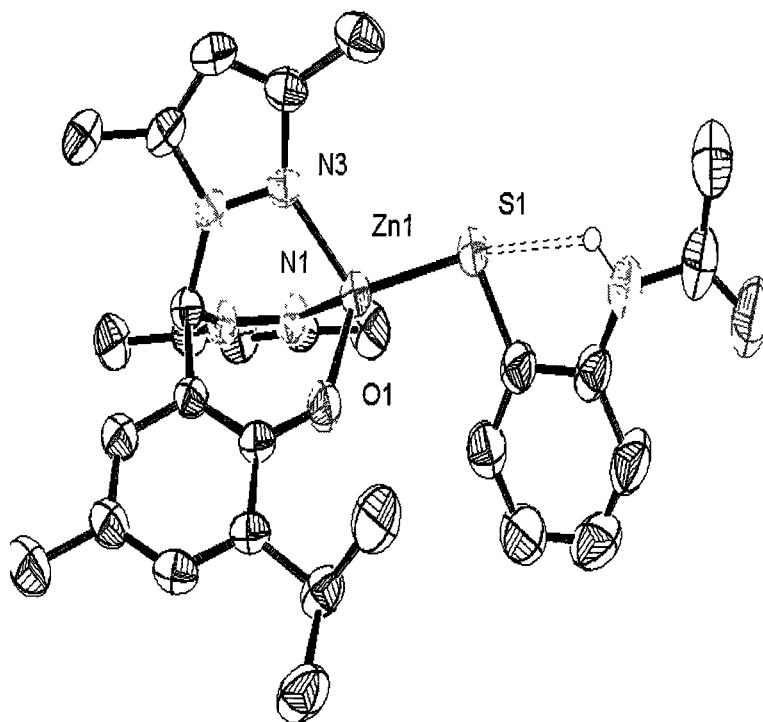
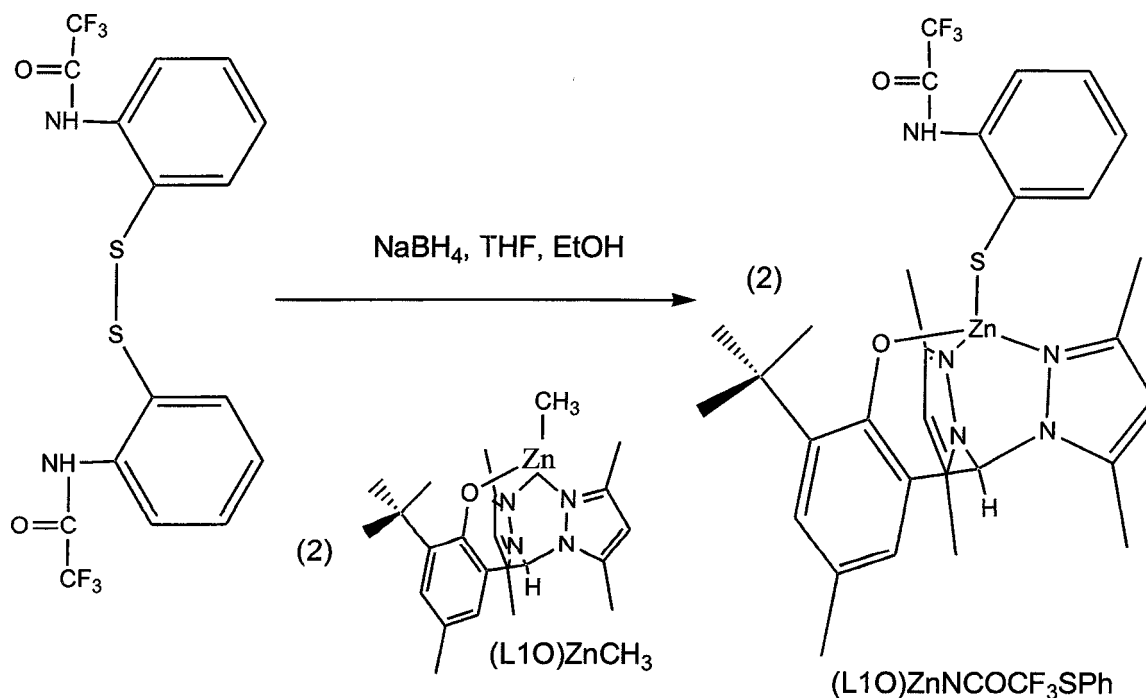


Figure 8. ORTEP diagram with 30% thermal ellipsoids for $[(L1O)Zn(NAcSPh)]$ showing atomic labeling for the coordination sphere only. The hydrogen atom involved in hydrogen bonding is the only hydrogen shown.

Colorless crystals of $[(L1O)Zn(NAcSPh)]$ were produced via slow diffusion of hexane into a dichloromethane solution. The zinc has pseudotetrahedral geometry, coordinated to two pyrazolyl nitrogen donors, the phenolic oxygen, and the sulfur donor. The X-ray structure of $[(L1O)Zn(NAcSPh)]$ is shown in Figure 8. The internal hydrogen bonding is observed between the hydrogen on the nitrogen of the acetamide and the thiolate sulfur, as described in Appendix C.

4. Synthesis of (3-*tert*-butyl-2-hydroxy-5-methylphenyl)bis(3,5-dimethylpyrazolyl) zinc 2,2,2-trifluoro-*N*-(2-mercaptophenyl)acetamide, [(L1O)Zn(NCOCF₃SPh)]

The complex, [(L1O)Zn(NCOCF₃SPh)], was synthesized by reaction of (L1O)ZnMe and 2,2'-dithio-bis(*N*-phenyl-2,2,2-trifluoroacetamide) in a solution of NaBH₄ to generate free thiol groups, as described in the Methods section. The product was isolated in 66% yield. The synthetic pathway is shown in Scheme 4.



Scheme 4: Synthesis of [(L1O)Zn(NCOCF₃SPh)]

Colorless crystals of [(L1O)Zn(NCOCF₃SPh)] were collected via slow diffusion of hexane into a dichloromethane solution. The X-ray structure of

$[(L1O)Zn(NCOCF_3SPh)]$ is shown in Figure 9. The zinc has pseudotetrahedral geometry, coordinated to two pyrazolyl nitrogen donors, the phenolic oxygen, and the sulfur donor. Appendix C depicts the bond parameters.

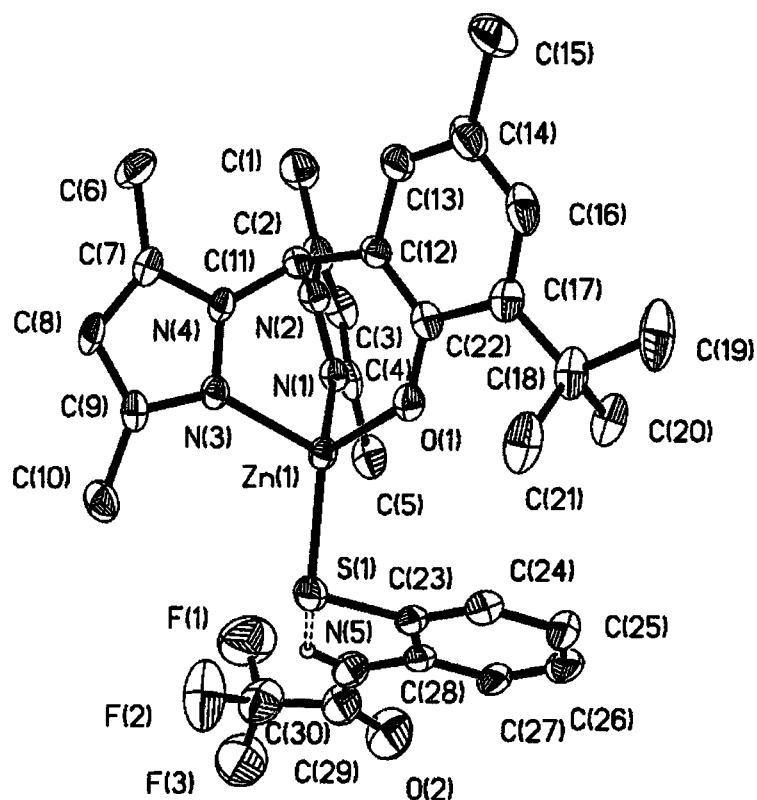


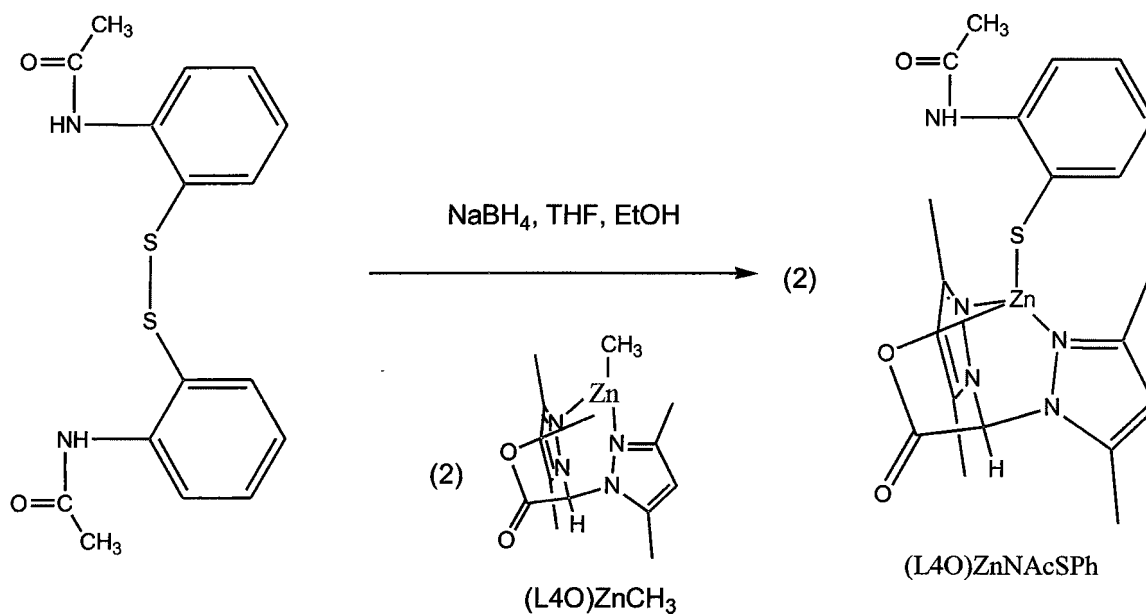
Figure 9. ORTEP diagram with 30% thermal ellipsoids for $[(L1O)Zn(NCOCF_3SPh)]$ showing atomic labeling. The hydrogen atom involved in hydrogen bonding is the only hydrogen shown.

5. Synthesis of bis(3,5-dimethylpyrazolyl)acetyl zinc N-(2-mercaptophenyl)acetamide, $[(L4O)Zn(NAcSPh)]$

The complex, $[(L4O)Zn(NAcSPh)]$, was synthesized by reaction of $(L4O)ZnMe$ with 2,2'-dithiobis(*N*-phenylacetamide) in solution with $NaBH_4$ in order to free thiophenol groups. The mixture was stirred until the reaction was complete,

details are described in the Methods section. The product was isolated in 60% yield.

The synthetic pathway is shown in Scheme 5.



Scheme 5: Synthesis of [(L4O)Zn(NAcSPh)]

Colorless crystals of [(L4O)Zn(NAcSPh)] were created by way of slow diffusion of diisopropyl ether into a dichloromethane solution. The zinc has pseudotetrahedral geometry, coordinated to two pyrazolyl nitrogen donors, the carboxylate oxygen, and the sulfur donor. The X-ray structure of [(L4O)Zn(NAcSPh)] is shown in Figure 10. The internal hydrogen bonding is observed between the hydrogen on the nitrogen of the acetamide and the carboxylate oxygen, as depicted in Figure 10.

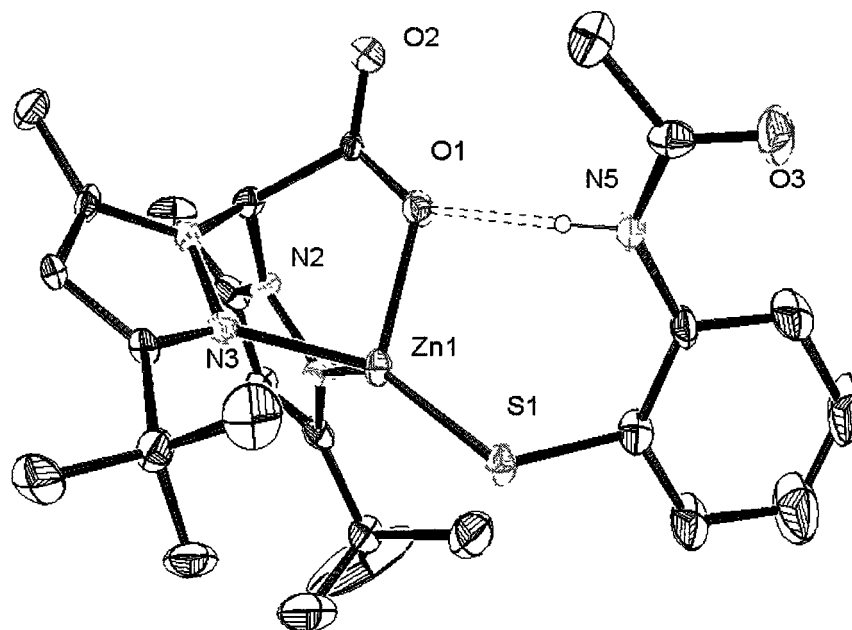
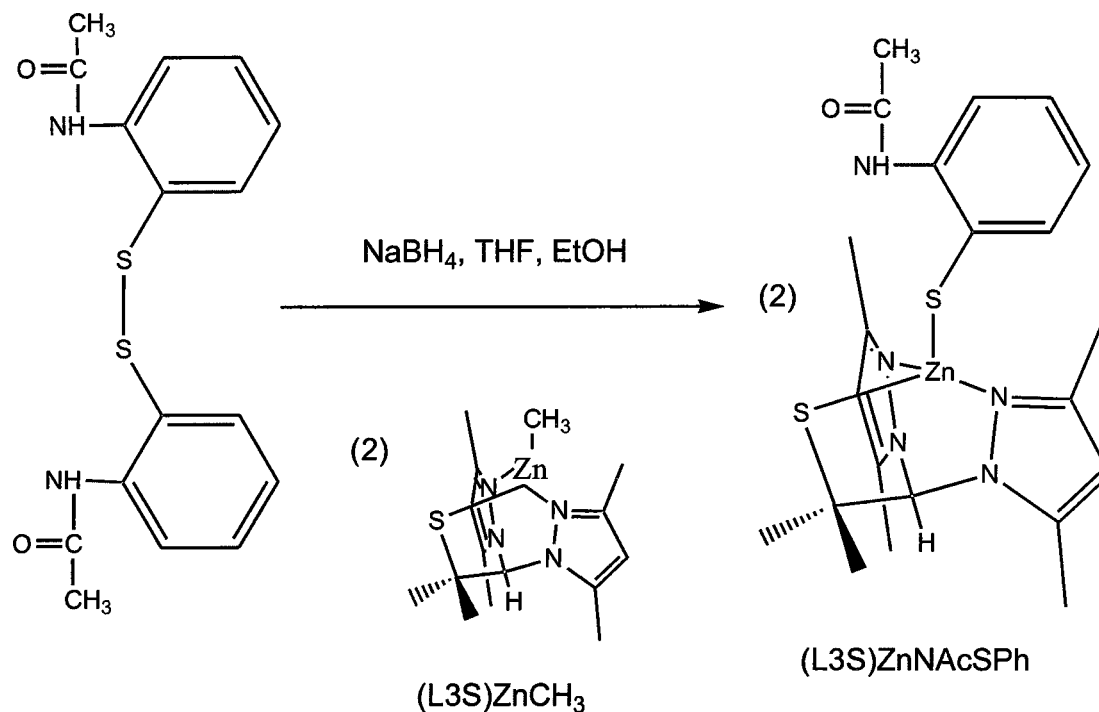


Figure 10. ORTEP diagram with 30% thermal ellipsoids for $[(L4O)Zn(NAcSPh)]$ showing atomic labeling for the coordination sphere only. The hydrogen atom shown is the only hydrogen atom involved in hydrogen bonding.

6. Synthesis of (2-Methylethanethiol-bis-3,5-dimethylpyrazolyl) zinc N-(2-mercaptophenyl)acetamide, $[(L3S)Zn(NAcSPh)]$

The complex, $[(L3S)Zn(NAcSPh)]$, was synthesized by reaction of 2,2'-dithiobis(*N*-phenylacetamide) and a solution of $NaBH_4$, to make free thiophenol groups. Next, $(L3S)ZnMe$ was added and the mixture was stirred until the reaction was complete, details are described in the Methods section. The product was isolated in 69% yield. The synthetic pathway is shown in Scheme 6.



Scheme 6: Synthesis of $[(\text{L3S})\text{Zn}(\text{NAcSPh})]$

Colorless crystals of $[(\text{L3S})\text{Zn}(\text{NAcSPh})]$ were collected by slow diffusion of hexane into a dichloromethane solution. The zinc has pseudotetrahedral geometry, coordinated to two pyrazolyl nitrogen donors, the thioalkyl sulfur, and the thiophenolic sulfur donor, as shown in Figure 11. The internal hydrogen bonding is observed between the hydrogen on the nitrogen of the acetamide and the thiophenolic sulfur. Crystallographic parameters are shown in Appendix C.

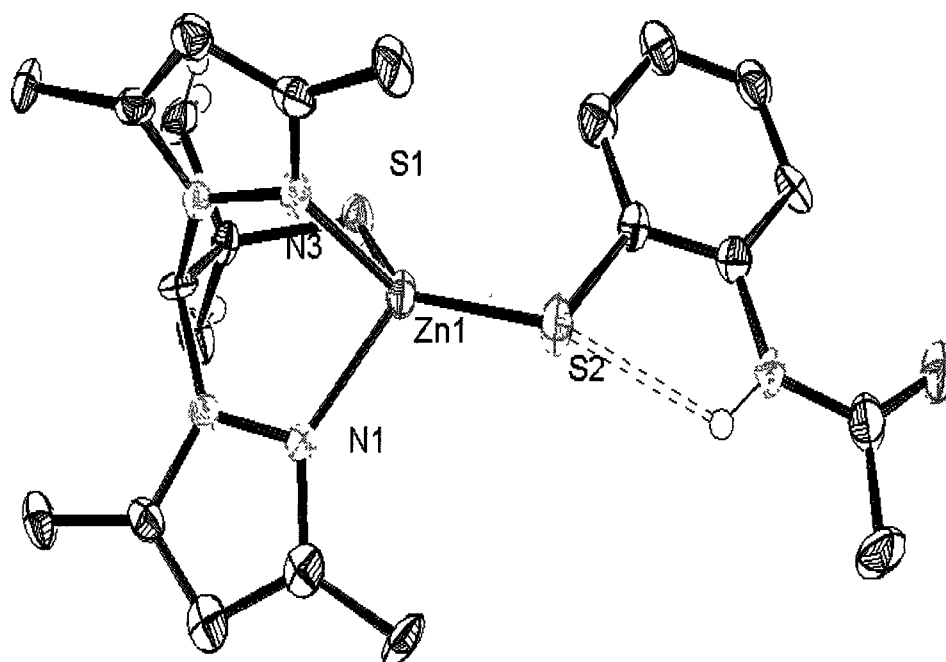


Figure 11. ORTEP diagram with 30% thermal ellipsoids for $[(L3S)Zn(NAcSPh)]$ showing atomic labeling for the coordination sphere only. The hydrogen atom shown is the hydrogen involved in hydrogen bonding.

7. Synthesis of $[(L3SCH_3)Zn(NAcSPh)]$

The complex, $[(L3SCH_3)Zn(NAcSPh)]$, was synthesized from $[(L3S)Zn(NAcSPh)]$ in an acetonitrile solution using trimethyloxonium tetrafluoroborate as the alkylating agent, as described in the Methods chapter. No kinetic studies were performed for this model compound because only the product

was of interest. The alkylating agent was added in an equimolar ratio and reacted at room temperature, 25°C. The only product formed was $[(L3SCH_3)Zn(NAcSPh)]$.

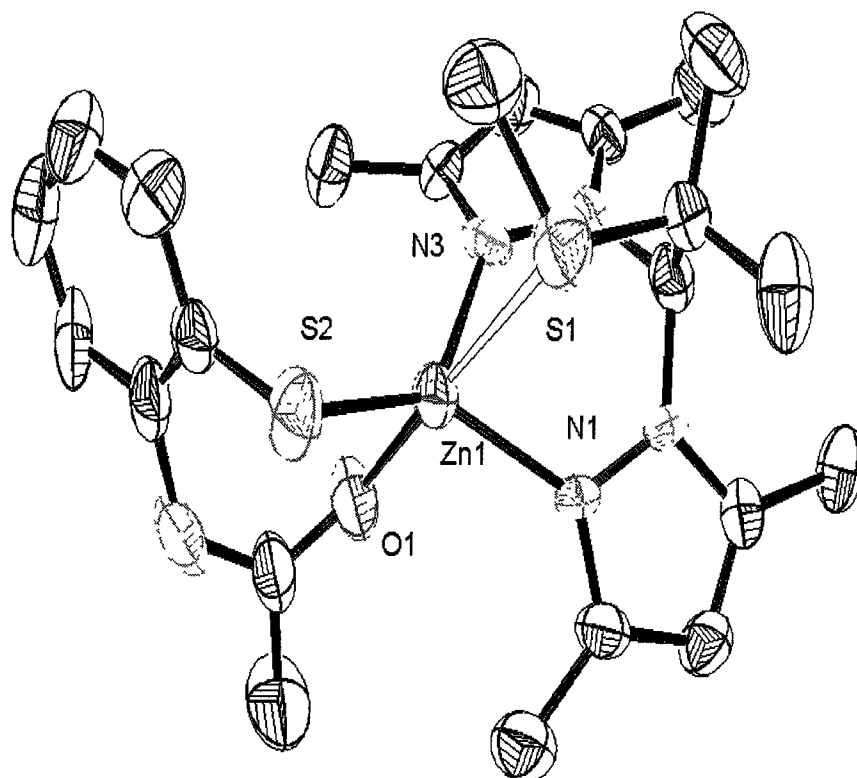


Figure 12. ORTEP diagram with 30% thermal ellipsoids for $[(L3SCH_3)Zn(NAcSPh)]$ showing atomic labeling for the coordination sphere only. The hydrogen atom involved in hydrogen bonding is the only hydrogen shown.

It is clear from the crystal structures in Figure 12, that the chelated sulfur of the $[L3S]$ ligand was the only sulfur to be alkylated. The thiophenol sulfur was not involved in the alkylation reaction. When the S1 sulfur becomes methylated, it remains bound to the zinc albeit with a long (2.773\AA) bond length. As a result, the O1 of the N-acetyl group is a viable donor to the zinc and gives a pseudopentacoordinate structure.

Reactivity

1. Methylation of [(L3S)ZnI]

The [(L3S)ZnI] complex was methylated with excess iodomethane and with trimethyloxonium tetrafluoroborate. The rate of methylation was followed by ^1H NMR methods.

The ^1H NMR spectra for the reaction of [(L3S)ZnI] with methyl iodide, as given in Appendix B, show the formation of product at 1.33 ppm and 1.69 ppm. The peak at 1.33 ppm corresponds to the new methyl on the complex from the iodomethane. The pyrazole peak at 2.51 ppm also shifts slightly downfield. The peak at 2.17 ppm corresponds to the methyl iodide. The peak at 6.08 ppm, corresponding to the bridgehead proton, shifts to 6.25 ppm in the product. The kinetic results are based on the peaks at 6.25 ppm and 6.08 ppm. These peaks were chosen because they most clearly show the product formation.

The ^1H NMR spectra for the reaction of [(L3S)ZnI] with trimethyloxonium tetrafluoroborate, as given in Appendix B, illustrates the new methyl group addition. There is a shift in the 6.18 ppm peak of the bridgehead, and the assignment of a new methyl peak at 1.75 ppm. The kinetic results are based on the peaks at 4.37 ppm and 3.23 ppm. These peaks were chosen for integration because they most clearly show the use of the reactants, i.e. they refer to the presence of the unreacted $(\text{CH}_3)_3\text{O}^+$, and the reacted $(\text{CH}_3)_2\text{O}$, alkylating agent.

In both the iodomethane and trimethyloxonium tetrafluoroborate reactions, the zinc complex reacted relatively quickly at room temperature. Each reaction was completed within minutes to hours upon addition of the methylating agent. The kinetic data are given in Appendix A. The methylated product is **[(L3SCH₃)ZnI]**.

2. Methylation of **[(L1O)Zn(SPh)]**

The **[(L1O)Zn(SPh)]** complex was methylated with excess iodomethane and with trimethyloxonium tetrafluoroborate. The rate of methylation was followed by ¹H NMR methods. This complex has minimal solubility in methanol, necessitating the use of lower concentrations (5mM), as shown in Table 1.

The ¹H NMR spectra for the reaction of **[(L1O)Zn(SPh)]** with methyl iodide, as given in Appendix B, show the formation of product at 1.32 ppm. The peak at 1.32 ppm corresponds to the thioether methyl. The presence of the product is also illustrated in the shift of aromatic peaks at 7.30 ppm, 7.40 ppm, 7.25 ppm, and 7.15 ppm. The peak at 2.17 ppm corresponds to the methyl iodide. The kinetic results are based on the peaks at 7.25 ppm and 7.30 ppm because they are clearly shown to increase and decrease in intensity as the reaction goes to completion.

The ¹H NMR spectra for the reaction of **[(L1O)Zn(SPh)]** with trimethyloxonium tetrafluoroborate, as given in Appendix B, illustrates the new methyl group addition. The peak at 1.40 ppm is assigned to the new methyl group on the thiophenol. The kinetic results are based on the peaks at 7.90 ppm and 7.15 ppm, for ease of integration, which correspond to aromatic peaks.

Alkylation occurred rapidly for this complex in both alkylating reagents.

These reactions were on the order of minutes to hours. The kinetic data are shown in Appendix A. The products are $[(L1O)ZnI] + [CH_3SPh]$, where the iodide, a stronger electrophile, bound to the zinc, forces the thioether to disassociate into solution.

3. Methylation of $[(L1O)Zn(NAcSPh)]$

The $[(L1O)Zn(NAcSPh)]$ complex was methylated with excess iodomethane or with trimethyloxonium tetrafluoroborate. The rate of methylation was followed by 1H NMR methods. This complex was also minimally soluble in methanol, as seen in Table 1.

The 1H NMR spectra for the reaction of $[(L1O)Zn(NAcSPh)]$ with methyl iodide, as given in Appendix B, show the formation of a product with a peak at 1.27 ppm, which corresponds to the thioether methyl from the iodomethane. The pyrazole peak at 2.48 ppm and the t-butyl peak at 2.16 ppm shift slightly downfield. The peak at 2.17 ppm corresponds to the methyl iodide. The peak at 6.08 ppm corresponds to the bridgehead protons. The aromatic peaks at 7.23 ppm, 7.45 ppm, and 7.85 ppm are also shifted with the addition of a methyl group. The kinetic results are based on the peaks at 6.80 ppm and 7.23 ppm, which are aromatic hydrogens. These peaks were chosen because they most clearly show the product formation.

The 1H NMR spectra for the reaction of $[(L1O)Zn(NAcSPh)]$ with trimethyloxonium tetrafluoroborate, as given in Appendix B, illustrates the new methyl group addition. There is a shift in the aromatic peaks due to the presence of a

thioether. The new methyl peak appears at 1.40 ppm, while the other aliphatic peaks are shifted to slightly higher values. The kinetic results are based on the peaks at 7.79 ppm and 7.60 ppm, which are aromatic hydrogens, for ease of integration.

The reactions with methyl iodide took days to complete, while with trimethyloxonium tetrafluoroborate they took only hours. The kinetic data, shown in Appendix A, clearly show that this hydrogen-bonded compound was significantly slower to react than the non-hydrogen-bonded compound. The results are supported for all three solvents, although methanol showed only a modest decrease in the rate constant. This is most likely due to hydrogen bonding of the complex to the methanol. The methylated products formed were **[(L1O)ZnI] + [NAcCH₃SPh]** and **[(L1O)Zn(NAcCH₃SPh)]**, respectively.

4. Methylation of [(L1O)Zn(NCOCF₃SPh)]

The **[(L1O)Zn(NCOCF₃SPh)]** complex was methylated with excess iodomethane or trimethyloxonium tetrafluoroborate. The rate of methylation was followed by ¹H NMR methods. This complex was also minimally soluble in methanol, as seen Table 1.

The ¹H NMR spectra for the reaction of **[(L1O) Zn(NCOCF₃SPh)]** with methyl iodide, as given in Appendix B, show the formation of a thioether product at 1.32 ppm, which corresponds to the thioether methyl from the iodomethane. The peak at 2.17 ppm is consistent with the methyl iodide. The kinetic results are based on the aromatic peaks at 7.16 ppm and 7.33 ppm because they clearly increase and decrease

in intensity as the reaction proceeds to completion. The aromatic peaks at 7.33 ppm, 7.50 ppm, and 7.68 ppm are shifted with the addition of a methyl group. The highly deshielded proton at 10 ppm is the proton on the nitrogen of acetamide.

The ^1H NMR spectra for the reaction of $[(\text{L1O})\text{Zn}(\text{NCOCF}_3\text{SPh})]$ with trimethyloxonium tetrafluoroborate, as given in Appendix B, illustrates the new methyl group addition. There is a shift in the aromatic peaks due to the presence of a thioether. The thioether methyl peak is at 1.40 ppm, while the other aliphatic peaks are shifted to slightly higher ppm values. The aromatic shifts occur at 7.80 ppm, 7.70 ppm, 7.45 ppm, and 7.33 ppm. The bridgehead peak is shifted to 6.35 ppm. The proton on the acetamide nitrogen has a peak at 9.8 ppm. The kinetic results are based on the peaks at 1.40 ppm and 2.31 ppm for ease of integration.

The reactions using iodomethane ran in the range of hours to a week before completion. However with the cationic electrophile, the reactions ran between minutes to hours. The kinetic data is shown in Appendix A. The products formed were $[(\text{L1O})\text{ZnI}] + [\text{NCOCF}_3\text{CH}_3\text{SPh}]$.

5. Methylation of $[(\text{L4O})\text{Zn}(\text{SPh})]$

The $[(\text{L4O})\text{Zn}(\text{SPh})]$ complex was methylated with excess iodomethane or trimethyloxonium tetrafluoroborate. The rate of methylation was followed by ^1H NMR methods. This compound was completely insoluble in methanol, therefore those reactions were omitted, as seen Table 1.

The ^1H NMR spectra for the reaction of **[(L1O)Zn(SPh)]** with methyl iodide, as given in Appendix B, show the formation of a thioether product at 1.40 ppm, which corresponds to the new methyl from the iodomethane onto the thiophenol. The pyrazole protons are at 2.76 ppm, and the *t*-butyl protons are at 2.22 ppm. The presence of the new thioether methyl is also illustrated in the shift of aromatic peaks at 7.9 ppm, 7.71 ppm, 7.30 ppm, and 7.25 ppm. The peak at 2.17 ppm corresponds to the methyl iodide. The kinetic results are based on the aromatic peaks at 7.25 ppm and 7.49 ppm. These peaks were chosen because they most clearly show the product formation.

The ^1H NMR spectra for the reaction of **[(L1O)Zn(SPh)]** with trimethyloxonium tetrafluoroborate, as given in Appendix B, illustrates the new methyl group addition. The peak at 2.35 ppm designates the new thioether methyl group, which is highly deshielded. The aromatic shifts at 7.72 ppm, 7.81 ppm, 7.92 ppm indicate a shift in the frequency absorbed due to the methylation. The kinetic results are based on the peaks at 7.43 ppm and 7.63 ppm, which were chosen for clarity of integration.

This complex took an extraordinarily long time to react. The reactions ranged from days in acetonitrile to weeks in chloroform. This range is seen in Appendix A, with the rate constants quite slow in every solvent and with each alkylating agent. The products made were **[(L4O)ZnI] + [CH₃SPh]**.

6. Methylation of [(L4O)Zn(NAcSPh)]

The [(L4O)Zn(NAcSPh)] complex was methylated with excess iodomethane or trimethyloxonium tetrafluoroborate. The rate of methylation was followed by ^1H NMR methods. This compound was completely insoluble in methanol therefore those reactions were omitted, as seen Table 1.

The ^1H NMR spectra for the reaction of [(L4O)Zn(NAcSPh)] with methyl iodide, as given in Appendix B, show the formation of thioether product at 1.41 ppm, which matches to the thioether methyl. The pyrazole protons are at 2.47 ppm, and the *t*-butyl protons are at 2.40 ppm. The bridgehead protons have peaks assigned at 6.7 ppm and 6.2 ppm. The aromatic peaks at 7.85 ppm, 7.45 ppm, and 7.15 ppm are seen to shift because the thiophenol has become methylated. The peak at 2.17 ppm corresponds to the methyl iodide. The kinetic results are based on the aliphatic peaks at 1.41 ppm and 1.30 ppm. These peaks were chosen because they most clearly show the product formation.

The ^1H NMR spectra for the reaction of [(L4O)Zn(NAcSPh)] with trimethyloxonium tetrafluoroborate, as given in Appendix B, illustrates the new methyl group addition. The peak at 2.31 ppm designates the new methyl group on the thioether, which is highly deshielded. The bridgehead shifts are assigned at 6.32 ppm and 6.17 ppm. The kinetic results are based on the aromatic peaks at 8.00 ppm and 7.23 ppm because they clearly show the shift from product formation.

The reactions with methyl iodide in chloroform were on the order of weeks, and in acetonitrile on the order of hours. When switching to the cationic agent, the reactions were on the order of hours for both solvents, although acetonitrile still

reacted faster. The reaction products were $[(\mathbf{L4O})\mathbf{ZnI}] + [\mathbf{NAcCH}_3\mathbf{SPh}]$. Appendix A shows the kinetic data, and it is clear that the rate constants for $[(\mathbf{L4O})\mathbf{Zn}(\mathbf{NAcSPh})]$ are not drastically slower than for its non-hydrogen bonded analog. This data is surprising in that it does not follow the trend that was seen in the $[\mathbf{L1O}]$ complexes.

CHAPTER V

DISCUSSION

Kinetics: Solvent Effects

The rate constants for the reactions were compared by tabulation of the data, as seen in Tables 2-7. A reaction was arbitrarily assigned a rate of 1, and the other rates were assigned relative to the rate of 1. This was used for ease of comparison between the compounds and the solvents.

The data collected from the kinetic reactions proved to be of use in supporting the hypothesis. As seen in Table 2, it is clear that the reaction rates are affected by solvent choice.

	Chloroform	Acetonitrile	Methanol
[(L3S)ZnI]	0.88	7.60	0.45
[(L4O)Zn(SPh)]	0.0079	0.04	N/A
[(L1O)Zn(SPh)]	1	4	0.37

Table 2. Relative Rate Constant Comparisons for each ligand in methyl iodide.

Chloroform, acetonitrile, and methanol were used for the experiments and were chosen because of their relative polarities: nonpolar, polar aprotic, and polar protic.

The use of three types of solvent will aid in determining a theoretical mechanism of alkylation for the model compounds. In iodomethane, the $[(L1O)Zn(SPh)]$ has a rate that is similar to that of the $[(L3S)ZnI]$, in both methanol and chloroform. However, $[(L3S)ZnI]$ reacts twice as fast in acetonitrile.

A comparison of $[(L3S)ZnI]$ complex to the $[(L1O)Zn(SPh)]$ complex shows that the $[L1O]$ ligand reacts faster with the trimethyloxonium tetrafluoroborate than the $[(L3S)ZnI]$ complex, as seen in Table 3. The trend is followed in all three solvents. When compared to the $[(L4O)Zn(SPh)]$ complex, these complexes are significantly faster by orders of magnitude, see Table 3. The same trend is seen in both alkylating agents, with respect to the $[(L4O)Zn(SPh)]$ complex. Both $[(L1O)Zn(SPh)]$ and $[(L3S)ZnI]$ complexes are significantly faster in chloroform and acetonitrile, see Tables 2 and 3.

	Chloroform	Acetonitrile	Methanol
$[(L3S)ZnI]$	0.55	11.85	0.27
$[(L4O)Zn(SPh)]$	0.10	3.63	N/A
$[(L1O)Zn(SPh)]$	1	32.50	11.09

Table 3. Relative Rate Constant Comparisons for each ligand in $(CH_3)_3OBF_4$.

This information is interesting because it indicates that the sulfur that is targeted for alkylation reacts similarly whether it is chelating, as in the $[(L3S)ZnI]$, or monodentate, as in the $[(L1O)Zn(SPh)]$. If a dissociative route was operative, then one would assume that the chelating sulfur would be relatively less reactive because it is far less likely to dissociate from the zinc, even transiently, as this would be thermodynamically unfavorable. However, the data clearly show that either

conformation is accessible for alkylation. The indication is that the thiolate is not dissociating from the zinc in order to react, since the chelated structure is also equally reactive. Thus, this is a further piece of evidence to support the zinc-bound thiolate as the reactive nucleophile theory.

It is worthy of note that the **[(L4O)Zn(SPh)]**, with the carboxylate oxygen donor, consistently reacted much slower than the **[(L1O)Zn(SPh)]** and the **[(L3S)ZnI]** complexes. To date it is unclear as to why this occurs.

It is clear that the effects of solvation can be powerful. While there are various analyses that are utilized to determine mechanism, one that is commonly used is the Ingold Analysis, see Figure 13.

1. $RX + S^- \rightarrow [S^{\delta-} R X^{\delta-}]$	RX= Neutral electrophile
2. $RX + Zn-S \rightarrow [Zn-S^{\delta+} R X^{\delta-}]$	RX= Neutral electrophile
3. $RX^+ + S^- \rightarrow [S^{\delta-} R X^{\delta-}]$	RX^+ = Cationic electrophile
4. $RX^+ + Zn-S \rightarrow [Zn-S^{\delta+} R X^{\delta-}]$	RX^+ = Cationic electrophile

Figure 13. Ingold Analysis for nucleophile determination

The analysis enables one to determine the effects of solvent on the mechanism of a nucleophilic reaction. Reactions 1 and 2, of Figure 13, assume a neutral electrophile, such as methyl iodide, while reactions 3 and 4 consider a cationic electrophile, such as trimethyloxonium tetrafluoroborate. In reaction 1, the anionic sulfur is the nucleophile to the RX electrophile, where in the transition state, the charge becomes dispersed. Thus in a polar solvent, there should be a decrease in the rate of the reaction, as compared to a nonpolar solvent. In reaction 2, an uncharged zinc-bound thiolate is the presumed nucleophile. This results in an increase in the

charge during the transition state, and thus there will be a large increase in the rate of reaction in a polar solvent because the polar solvent will stabilize this increase in charge.

Continuing the use of the Ingold Analysis, reaction 3 describes the reaction between a cationic electrophile and an anionic thiolate. Here, the charges are expected to be greatly decreased in the transition state and therefore a large decrease will be seen in the rate upon switching from nonpolar to polar environments. Conversely, if the neutral thiolate is the nucleophile, the charge is dispersed in the transition state, and a small decrease in the rate is expected. Our data show that there is a relatively small change in the rate going between nonpolar to polar solvent using trimethyloxonium tetrafluoroborate as the electrophile. The rate constants differed by a range of one to ten times faster in the nonpolar chloroform solvent, as seen in Table 3. The results are similar for the iodomethane. Thus it is concluded that the zinc-bound thiolate is the reacting nucleophile for both electrophiles. This conclusion is contrary to the generally accepted mechanism of thiolate dissociation²⁶. The data suggest that a generalized pathway is not acceptable and that zinc thiolate proteins may operate by a variety of individual mechanisms.

Kinetics: Hydrogen Bonding in [(L1O)Zn(NAcSPh)] and [(L4O)Zn(NAcSPh)]

It is important to compare one set of hydrogen-bonded analogs at a time. First, looking at the [L1O] pair of analogs, [(L1O)Zn(SPh)] with not hydrogen bonding, and [(L1O)Zn(NAcSPh)] containing a hydrogen bond, it is clear that in all solvents the presence of hydrogen bonding has a strong influence on the rate of

alkylation, as shown in Table 4. The hydrogen-bonded analogs had a significantly slower rate than their counterparts. Using methyl iodide as the alkylating agent, the **[(L1O)Zn(NAcSPh)]** is slower by a factor of about 200 in chloroform and about 30 in acetonitrile.

	Chloroform	Acetonitrile	Methanol
[(L1O)Zn(SPh)]	1	4	0.37
[(L1O)Zn(NAcSPh)]	0.0048	0.12	0.03
[(L1O)Zn(NCOCF₃SPh)]	0.0074	0.37	0.68

Table 4. Relative Rate Comparisons between the **[L1O]** analogs in CH₃I.

This is supportive evidence for the hypothesis that hydrogen bonding can control the reactivity of zinc thiolates. Even reactions in methanol, which showed a much narrower difference, corresponded to the trend. This is because there is a slight amount of hydrogen bonding to the solvent instead of internal hydrogen bonding within the complex. When using the trimethyloxonium salt, a similar trend of hydrogen bonds reducing the rate of reaction, was observed for acetonitrile and methanol, but not for chloroform, see Table 5.

	Chloroform	Acetonitrile	Methanol
[(L1O)Zn(SPh)]	1	32.50	11.09
[(L1O)Zn(NAcSPh)]	1.72	13.77	2.49
[(L1O)Zn(NOCF₃SPh)]	0.27	5.93	2.68

Table 5. Relative Rate Comparison between the **[L1O]** analogs in (CH₃)₃OBF₄.

The data from the **[L4O]** pair does not correlate with that of the **[L1O]** pair. When using methyl iodide as the electrophile, **[(L4O)Zn(NAcSPh)]** is only about

two times slower than the **[(L4O)Zn(SPh)]** non-hydrogen bonded analog in acetonitrile, and only seven times slower in chloroform, see Table 6.

	Chloroform	Acetonitrile
[(L4O)Zn(SPh)]	1	5
[(L4O)Zn(NAcSPh)]	0.14	2.11

Table 6. Relative Rate Comparison between the **[L4O]** analogs in CH₃I.

With the cationic alkylating agent, the rates again differ by factors of only ten and four, see Table 7. This surprising data does not appear to support the hypothesis that hydrogen bonding greatly decreases the rate of alkylation.

	Chloroform	Acetonitrile
[(L4O)Zn(SPh)]	1	34.55
[(L4O)Zn(NAcSPh)]	0.25	3.09

Table 7. Relative Rate Comparison between the **[L4O]** analogs in (CH₃)₃OBF₄.

In order to understand this discrepancy, an x-ray structure was determined for both the **[(L1O)Zn(NAcSPh)]** and **[(L4O)Zn(NAcSPh)]**, see Figures 8 and 10. The results show that **[(L4O)Zn(NAcSPh)]** has an internal hydrogen bond between the N-acetyl group and the carboxylate oxygen donor atom, rather than the sulfur. The sulfur is therefore not involved in any hydrogen bonding interactions. From this, it is clear that the kinetic data is valid; the compound should not have been as affected because the nucleophile is not inhibited by the hydrogen bond. This data now conclusively supports the hypothesis that the presence of hydrogen bonding to the thiol is a means of controlling thiolate reactivity.

Hydrogen Bonding: [(L3S)Zn(NAcSPh)]

To further test the effectiveness of the hydrogen bonding, a compound was synthesized containing two sulfur donor atoms. Since the heteroscorpionate thiolate sulfur reacted as rapidly as the thiophenol sulfur, a **[L3S]** ligand was affixed to the N-acetyl thiophenol, producing two viable alkylation sites, only one of which is involved in hydrogen bonding, shown in Figure 11. The **[(L3S)Zn(NAcSPh)]** was reacted with the strong and indiscriminant alkylating agent, trimethyloxonium tetrafluoroborate. This reaction yielded only a single product, **[(L3SCH₃)Zn(NAcSPh)]**, shown in Figure 12. The chelating sulfur was the only atom to become alkylated, indicating that the N-acetyl thiophenol was completely protected by the hydrogen bonding. In comparison to the **[(L1O)Zn(SPh)]** and the **[(L3S)ZnI]**, which had similar reactivities, the alkylating agent did not methylate indiscriminately. This product appears to be the kinetically and thermodynamically more stable product. This is more evidence to support the hypothesis that hydrogen bonding controls the reactivity of zinc thiolates.

In addition, the reaction between trimethyloxonium tetrafluoroborate and **[(L3S)Zn(NAcSPh)]** demonstrates how hydrogen bonding generates specificity for alkylation reactions. It has been established that the Ada protein has four sulfur donor atoms, yet only one becomes alkylated. It is likely that the other atoms are involved with hydrogen bonding and/or are sterically unable to react, thus validating the structure/function relationship, which is the premise of this thesis research. Our conclusions have been supported by recent research¹⁵. The specificity is vital to the

protein because only a certain thiolate should be targeted for alkylation in order for the protein to perform its proper functions. In conjunction with this notion, it is known that zinc finger proteins tend to have a significant hydrogen-bonding network throughout the protein. From the data gathered, it can be deduced that hydrogen bonding is protecting the zinc thiolates of zinc fingers from reaction with electrophiles. This provides an explanation of the previously discussed paradox of why Ada and GATA have different reactivities but the same coordination structures.

Kinetics: Hydrogen Bonding in [(L1O)Zn(NAcSPh)] and [(L1O)Zn(NCOCF₃SPh)]

Thus far, the data has shown a positive result for the effectiveness of hydrogen bonding to control the reactivity of the model compounds. In addition to the previous hydrogen-bonding experiments, it was necessary to test the strength of the conclusions. The use of an additional model compound where one can increase the strength of the hydrogen bond was needed, i.e. a stronger bond should further slow the reaction. [(L1O)Zn(NCOCF₃SPh)] was synthesized for this purpose. The fluorine atoms of the fluoro-acetyl group are very electronegative, thus by an inductive effect they create a stronger hydrogen bond to the sulfur atom. The compound is identical to [(L1O)Zn(NAcSPh)] in all other aspects. Indeed, the stronger bond slowed the alkylation by factors ranging from two to 5, when using the cationic electrophile, shown in Table 5.

However, with methyl iodide, the $[(\mathbf{L1O})\mathbf{Zn}(\mathbf{NCOCF}_3\mathbf{SPh})]$ did not react slower than the $[(\mathbf{L1O})\mathbf{Zn}(\mathbf{NAcSPh})]$, as shown in Table 4. To date, this cannot be explained, however it suggests that the strength of the hydrogen bond will not radically affect the rate of reaction. In addition, the rates from the use of both methylating agents are consistent with the proposed zinc-bound thiolate as the nucleophile. This experiment solidifies the research performed.

Conclusions

In conclusion, the synthesis of model compounds to mimic the reactive sites of zinc thiolate proteins allows for experimentation in the control of their alkylation. The kinetic experiments performed in this research project allow the distinguishing characteristics of the donor atoms to be seen and for a mechanism of reaction to be proposed. The chelated thiolate was shown to react similarly to the thiophenol sulfur in the non-hydrogen-bonded compounds, while $[\mathbf{L4O}]$ ligand, with the carboxylate oxygen, reacted slowly. From the use of the Ingold Analysis, a mechanism was projected to follow the associated pathway, i.e. the thiolate did not dissociate as an anion before reacting. The comparison of two alkylating agents, one neutral and the other cationic, allowed for this mechanistic determination. All reactions utilize the $\text{S}_{\text{N}}2$ pathway. This data is contrary to a previously accepted generalized theory of dissociation.

In addition, the research demonstrated that the use of hydrogen bonding is effective in controlling the reactivity of zinc thiolates. By taking the theory one step

further, it was established that hydrogen bonding not only allows control of reactivity, but it provides a means of superb selectivity. This was demonstrated in the reaction of [(L3S)Zn(NAcSPh)] with trimethyloxonium tetrafluoroborate to produce a single methylated product. The product contained a thioether that was coordinated to the [L3S] ligand, and not to the N-acetylthiophenol. The generated selectivity is observed in reactive biomolecules, with precise distinguishing reactivities.

Another experiment was performed to increase the strength of the hydrogen bond to further decrease the reactivity of the zinc thiolate model compound. The kinetic data indicated that a stronger hydrogen bond does not necessarily affect the rate of methylation. This experimental data correlates to the stated hypothesis that hydrogen bonding does reduce zinc thiolate reactivity, but it does not support the notion that the strength of the bond is the key factor.

Future Research

The research presented is by no means an end to this realm of study. It is clear that this examination of model compounds is useful for a variety of future research endeavors. One set of experiments that could be immediately embarked upon is to synthesize more model compounds that correlate to those used in this thesis. For example, one could use [(L3S)Zn(NAcSPh)], [(L3S)Zn(NCOCF₃SPh)], and [(L4O)Zn(NCOCF₃SPh)] in a series of kinetic experiments, as outlined in this thesis.

A second endeavor would be to use small peptide sequences that utilize the same donor atoms as those in the model compounds for alkylation reactions. These peptides would be analogs of those seen in living organisms. Once the methylation mechanism of the small peptides is established and characterized, the reaction of entire proteins could be studied. In addition, perhaps an alkylating agent that more closely resembles a biomolecule could be employed.

Analogous studies can be performed for many types of pathogenic microorganisms. For instance, research could be performed on the NCp7 protein of HIV, by attempting to alkylate the zinc-bound thiolate. A pharmaceutical reagent will need to be synthesized to selectively target the zinc fingers in the NCp7 protein for methylation, and not to alkylate the vital zinc fingers in the host proteins.

REFERENCES

1. McCall, K.; Huang, C.; Fierke, C. "Function and Mechanism of Zinc Metalloenzymes" *J. Nutrition* **2000** *130* 1437S-1446S.
2. Warthen, C.R.; Hammes, B.S.; Carrano, C.J.; Crans, D.C. "Methylation of neutral pseudotetrahedral zinc thiolate complexes: model reactions for alkyl group transfer to sulfur by zinc-containing enzymes" *J. Biol. Inorg. Chem.* **2001** *6*:82-90.
3. Brand, U.; Rombach, M.; Seebacher, J.; Vahrenkamp, H. "Functional modeling of cobalamine-independent Methionine Synthase with pyrazolylborate-zinc-thiolate complexes" *Inorg. Chem.* **2001** *40* 6151-6157.
4. Bombarda, E.; Morellet, N.; Cherradi, H.; Spiess, B.; Bouaziz, S.; Grell, E.; Roques, B.; Mély, Y. "Determination of the pK_a of the four Zn²⁺-coordinating residues of the distal finger motif of the HIV-1 nucleocapsid protein: consequences on the binding of Zn²⁺" *J. Mol. Biol.* **2001** *310* 659-672.
5. Ohneda, K; Yamamoto, M "Roles of hematopoietic transcription factors GATA-1 and GATA-2 in the development of red blood cell lineage" *Acta Haematol* **2002** *108(4)* 237-245.
6. www.uth.tmc.edu/apstracts/2000/gastro/October/227g.html Visited on 12/28/02.
7. www.stanford.edu/~ewilhelm/secondary/Luteal/GATA4.htm Visited on 12/28/02.

8. Lowry, J.; Atchley, W. *J. of Mol. Evol.* **2000** 50 103-115.
9. Hammes, B.S.; Carrano, C.J. "Structure and physical properties of several pseudotetrahedral zinc complexes containing a new alkyl thiolate heteroscorpionate ligand." *J. Chem. Soc., Dalton Trans.* **2000** 3304-3309.
10. Bertola, F.; Manigand, C.; Picard, P.; Belghazi, M.; Precigoux, G. "Human T-lymphotrophic virus type I nucleocapsid protein NCp15: structural study and stability of the n-terminal zinc-finger" *Biochem. J.* **2000** 352 293-300.
11. McDonnell, N.; De Guzman, R.; Rice, W.; Turpin, J.; Summers, M. "Zinc ejection as a new rationale for the use of Cystamine and related disulfide-containing antiviral agents in the treatment of AIDS" *J. Med. Chem.* **1997** 40 1969-1976.
12. www-lecb.ncifcrf.gov/~maynarda/NCp7.html. Visited on 9/7/02.
13. Loo, J.A.; Holler, T.P.; Sanchez, J.; Gogliotti, R.; Maloney, L.; Reily, M. "Biophysical characterization of zinc ejection from HIV nucleocapsid protein by anti-HIV 2,2'-dithiobis[benzamides] and benzisothiazolones" *J. Med. Chem.* **1996** 39 4313-4320.
14. Outten, C.; Tobin, D.; Penner-Hahn, J.; O'Halloran, T. "Characterization of the metal receptor sites in *E. coli* Zur, an ultrasensitive zinc(II) metalloregulatory protein" *Biochemistry* **2001** 40 110417-10423.
15. He, C.; Wei, H.; Verdine, G. L. "Converting the Sacrificial DNA Repair Protein N-Ada into a Catalytic Methyl Phosphotriester Repair Enzyme" *J. Am. Chem. Soc.* **2003** 125(6) 1450-1451.

16. Wilker, J.J.; Lippard, S.J. "Modeling the DNA methylphosphotriester repair site in *E. coli* Ada. Why zinc and for Cysteines?" *J. Am. Chem. Soc.* **1995** *117* 8682-8683.
17. Wilker, J.J.; Wetterhahn, K.E.; Lippard, S.J. "Methyl transfer to Mercury thiolates: effects of coordination number and ligand dissociation" *Inorg. Chem.* **1997** *36* 2079-2083.
18. Chiou, S.; Innocent, J.; Riordan, C.; Lam, K.; Liable-Sands, L.; Rheingold, A. "Synthetic models for the zinc sites in the methionine synthases" *Inorg. Chem.* **2000** *39* 4347-4353.
19. Harris, C.; Derdowski, A.; Poulter, C. "Modulation of the zinc(II) center in protein farnesyltransferase by mutagenesis of the zinc(II) ligands" *Biochemistry* **2002** *41* 10554-10562.
20. Hammes, B.; Carrano, C. "Methylation of (2-Methylethanethiol-bis-3,5-dimethylpyrazolyl)methane Zinc Complexes and Coordination of the Resulting Thioether: Relevance to Zinc-Containing Alkyl Transfer Enzymes" *Inorg. Chem.* **2001** *40(5)* 919-927.
21. Ueyama, N.; Okamura, T.; Nakamura, A. "Structure and Properties of Molybdenum (IV,V) Arenethiolates with a Neighboring Amide Group. Significant Contribution of NH...S Hydrogen Bond to Positive Shift of Redox Potential of Mo (V)/Mo(IV)." *J. Am. Chem. Soc.* **1992** *114(21)* 8129-8137.
22. Krizek, B.A.; Amann, B.T.; Kilfoil, V.J.; Merkle, D.L.; Berg, J.M. "A consensus zinc finger peptide: design, high-affinity metal binding, a pH-dependent structure, and a His to Cys sequence variant" *J. Am. Chem. Soc.* **1991** *113* 4518-4523.

23. Krizek, B.A.; Merkle, D.L.; Berg, J.M. "Ligand variation and metal ion binding specificity in zinc finger peptides" *Inorg. Chem.* **1993** *32* 937-940.
24. Hafnann, J.P.; Whittaker, S.B-M.; Hemmings, A.M.; James, R.; Kleanthous, C.; Moore, G.R. "NMR studies of metal ion binding to the zn-finger-like HNH motif of colicin E9" *JIB* **2000** *79* 365-370.
25. Schmiedeskamp, M.; Klevit, R. "Paramagnetic cobalt as a probe of the orientation of an accessory DNA-binding region of the yeast ADR1 zinc-finger protein" *Biochemistry* **1997** *36* 14003-14011.
26. Wilker, J; Lippard, S. "Alkyl transfer to metal thiolates: kinetics, active species identification, and relevance to the DNA methyl phosphotriester repair center of *E. coli* Ada" *Inorg. Chem.* **1997** *36* 969-978.
27. Chiou, S.; Riordan, C.; Rheingold, A. "Synthetic Modeling of Zinc Thiolates: Quantitative Assessment of Hydrogen-Bonding in Modulating Sulfur Alkylation Rates"

APPENDIX A: KINETIC DATA

KINETIC DATA

[(L3S)ZnI] + MeI		
<u>Chloroform</u>		
	Run #	Rate (sec-1)
[Zn]=18mM	2	3.03E-04
[Zn]=18mM	3	3.20E-04
Average =		3.12E-04
Stdev =		8.50E-06
<u>Acetonitrile</u>		
	Run #	Rate (sec-1)
[Zn]=18mM	1	2.09E-03
[Zn]=18mM	2	3.33E-03
Average =		2.71E-03
Stdev =		6.20E-04
<u>Methanol</u>		
	Run #	Rate (sec-1)
[Zn]=18mM	1	1.65E-04
[Zn]=18mM	2	1.64E-04
Average =		1.65E-04
Stdev =		5.00E-07

[(L3S)ZnI] + (CH₃)₃OBF₄		
<u>Chloroform</u>		
	Run #	Rate (sec-1)
[Zn]=10mM	5	3.18E-04
[Zn]=10mM	6	2.60E-04
Average =		2.89E-04
Stdev =		2.90E-05
<u>Acetonitrile</u>		
	Run #	Rate (sec-1)
[Zn]=10mM	2	6.50E-03
[Zn]=10mM	3	5.90E-03
Average =		6.20E-03
Stdev =		3.00E-04
<u>Methanol</u>		
	Run #	Rate (sec-1)
[Zn]=10mM	1	1.57E-04
[Zn]=10mM	2	1.26E-04
Average =		1.42E-04
Stdev =		1.55E-05

Chart 1. [(L3S)ZnI] + MeI → [(L3SCH₃)ZnI],
 [(L3S)ZnI] + (CH₃)₃OBF₄ → [(L3SCH₃)ZnI] + (CH₃)₂OBF₄,
 reactions at 25°C.

KINETIC DATA

[(L1O)Zn(SPh)] + MeI			[(L1O)Zn(SPh)] + (CH ₃) ₃ OBF ₄		
<u>Chloroform</u>			<u>Chloroform</u>		
	Run #	Rate (sec-1)		Run #	Rate (sec-1)
[Zn]=18mM	1	3.58E-04	[Zn]=10mM	1	5.20E-04
[Zn]=18mM	2	3.47E-04	[Zn]=10mM	2	5.26E-04
Average =		3.53E-04	Average =		5.23E-04
Stdev =		5.50E-06	Stdev =		3.00E-06
<u>Acetonitrile</u>			<u>Acetonitrile</u>		
	Run #	Rate (sec-1)		Run #	Rate (sec-1)
[Zn]=18mM	1	1.45E-03	[Zn]=10mM	1	1.39E-02
[Zn]=18mM	2	1.39E-03	[Zn]=10mM	2	2.00E-02
Average =		1.42E-03	[Zn]=10mM	3	1.93E-02
Stdev =		3.00E-05	Average =		1.77E-02
Stdev =		3.00E-05	Stdev =		2.56E-03
<u>Methanol</u>			<u>Methanol</u>		
	Run #	Rate (sec-1)		Run #	Rate (sec-1)
[Zn]=5mM	1	1.47E-04	[Zn]=5mM	1	5.87E-03
[Zn]=5mM	3	1.16E-04	[Zn]=5mM	2	5.89E-03
Average =		1.32E-04	Average =		5.88E-03
Stdev =		1.55E-05	Stdev =		1.00E-05

Chart 2. [(L1O)Zn(SPh)] + MeI → [(L1O)ZnI] + [CH₃SPh],
 [(L1O)Zn(SPh)] + (CH₃)₃OBF₄ → [(L1O)Zn(SCH₃Ph)] + (CH₃)₂OBF₄,
 reactions at 25°C.

KINETIC DATA

[(L1O)Zn(NacSPh)] + MeI		
<u>Chloroform</u>		
	Run #	Rate (sec-1)
[Zn]=18mM	2	1.50E-06
[Zn]=18mM	3	1.89E-06
[Zn]=18mM	4	1.62E-06
Average =		1.67E-06
Stdev =		1.47E-07
<u>Acetonitrile</u>		
	Run #	Rate (sec-1)
[Zn]=18mM	1	4.15E-05
[Zn]=18mM	3	4.14E-05
Average =		4.15E-05
Stdev =		5.00E-08
<u>Methanol</u>		
	Run #	Rate (sec-1)
[Zn]=5mM	1	8.27E-06
[Zn]=5mM	2	1.30E-05
[Zn]=5mM	3	1.22E-05
Average =		1.12E-05
Stdev =		1.92E-06

[(L1O)Zn(NacSPh)] + (CH₃)₃OBF₄		
<u>Chloroform</u>		
	Run #	Rate (sec-1)
[Zn]=10mM	1	9.69E-04
[Zn]=10mM	2	8.38E-04
Average =		9.04E-04
Stdev =		6.55E-05
<u>Acetonitrile</u>		
	Run #	Rate (sec-1)
[Zn]=10mM	1	6.60E-03
[Zn]=10mM	2	7.80E-03
Average =		7.20E-03
Stdev =		6.00E-04
<u>Methanol</u>		
	Run #	Rate (sec-1)
[Zn]=5mM	1	9.18E-04
[Zn]=5mM	2	1.80E-03
Average =		1.36E-03
Stdev =		4.41E-04

Chart 3. [(L1O)Zn(NAcSPh)] + MeI → (L1O)ZnI + [NAcSCH₃Ph],
 [(L1O)Zn(NAcSPh)] + (CH₃)₃OBF₄ → [(L1O)Z(NAcSCH₃Ph)] +
 (CH₃)₂OBF₄, reactions at 25°C.

KINETIC DATA

[(L1O)Zn(NCOCF ₃ SPh)] + MeI			[(L1O)Zn(NCOCF ₃ SPh)] + (CH ₃) ₃ OBf ₄		
<u>Chloroform</u>			<u>Chloroform</u>		
	Run #	Rate (sec-1)		Run #	Rate (sec-1)
[Zn]=18mM	1	2.43E-06	[Zn]=10mM	1	1.50E-04
[Zn]=18mM	2	2.84E-06	[Zn]=10mM	2	1.31E-04
Average =		2.64E-06	Average =		1.41E-04
Stdev =		2.05E-07	Stdev =		9.50E-06
<u>Acetonitrile</u>			<u>Acetonitrile</u>		
	Run #	Rate (sec-1)		Run #	Rate (sec-1)
[Zn]=18mM	1	9.10E-05	[Zn]=10mM	1	2.40E-03
[Zn]=18mM	2	1.70E-04	[Zn]=10mM	2	3.80E-03
Average =		1.31E-04	Average =		3.10E-03
Stdev =		3.95E-05	Stdev =		7.00E-04
<u>Methanol</u>			<u>Methanol</u>		
	Run #	Rate (sec-1)		Run #	Rate (sec-1)
[Zn]=5mM	1	2.48E-04	[Zn]=5mM	1	1.49E-03
[Zn]=5mM	2	2.27E-04	[Zn]=5mM	2	1.34E-03
Average =		2.38E-04	Average =		1.42E-03
Stdev =		1.05E-05	Stdev =		7.50E-05

Chart 4. [(L1O)Zn(NCOCF₃SPh)] + MeI → [(L1O)ZnI] + [(NCOCF₃SCH₃Ph)],
 [(L1O)Zn(NCOCF₃SPh)] + (CH₃)₃OBf₄ →
 [(L1O)Zn(NCOCF₃SCH₃Ph)] + (CH₃)₂OBf₄, reactions at 25°C.

KINETIC DATA

[(L4O)Zn(SPh)] + MeI			[(L4O)Zn(SPh)] + (CH ₃) ₃ OBF ₄		
<u>Chloroform</u>			<u>Chloroform</u>		
	Run #	Rate (sec-1)		Run #	Rate (sec-1)
[Zn]=18mM	1	3.05E-06	[Zn]=10mM	1	5.93E-05
[Zn]=18mM	2	2.70E-06	[Zn]=10mM	2	5.05E-05
Average =		2.88E-06	Average =		5.49E-05
Stdev =		1.75E-07	Stdev =		4.40E-06
<u>Acetonitrile</u>			<u>Acetonitrile</u>		
	Run #	Rate (sec-1)		Run #	Rate (sec-1)
[Zn]=18mM	2	1.85E-05	[Zn]=10mM	1	1.33E-03
[Zn]=18mM	3	1.02E-05	[Zn]=10mM	2	2.76E-03
Average =		1.44E-05	[Zn]=10mM	3	1.73E-03
Stdev =		4.15E-06	Average =		1.94E-03
			Stdev =		5.47E-04

Chart 5. [(L4O)Zn(SPh)] + MeI → [(L4O)ZnI] + [SCH₃Ph],
 [(L4O)Zn(SPh)] + (CH₃)₃OBF₄ → [(L4O)Zn(SCH₃Ph)] + (CH₃)₂OBF₄,
 reactions at 25°C.

KINETIC DATA

[(L4O)Zn(NacSPh)] + MeI			[(L4O)Zn(NacSPh)] + (CH ₃) ₃ OBF ₄		
<u>Chloroform</u>			<u>Chloroform</u>		
	Run #	Rate (sec-1)		Run #	Rate (sec-1)
[Zn]=18mM	2	4.47E-07	[Zn]=10mM	1	1.35E-05
[Zn]=18mM	3	3.63E-07	[Zn]=10mM	2	1.57E-05
Average =		4.05E-07	Average =		1.46E-05
Stdev =		4.20E-08	Stdev =		1.10E-06
<u>Acetonitrile</u>			<u>Acetonitrile</u>		
	Run #	Rate (sec-1)		Run #	Rate (sec-1)
[Zn]=18mM	1	5.78E-06	[Zn]=10mM	1	1.10E-04
[Zn]=18mM	2	6.15E-06	[Zn]=10mM	2	2.40E-04
Average =		5.97E-06	Average =		1.75E-04
Stdev =		1.85E-07	Stdev =		6.50E-05

Chart 6. [(L4O)Zn(NAcSPh)] + MeI → [(L4O)ZnI] + [NAcSCH₃Ph],
 [(L4O)Zn(NAcSPh)] + (CH₃)₃OBF₄ → [(L4O)Zn(NAcSCH₃Ph)] +
 (CH₃)₂OBF₄, reactions at 25°C.

COMPARATIVE KINETIC CHARTS

Compound	Chloroform	Acetonitrile	Methanol
	ave. rate (x10⁻⁴)	Ave. rate (x10⁻⁴)	ave. rate (x10⁻⁴)
[(L3S)ZnI]	3.12(8)	27(6)	1.650(5)
[(L1O)Zn(SPh)]	3.53(5)	14.2(3)	1.3(1)
[(L1O)Zn(NAcSPh)]	0.017(1)	0.4150(5)	0.11(2)
[(L1O)Zn(NCOF ₃ SPh)]	0.026(2)	1.3(4)	2.4(1)
[(L4O)Zn(SPh)]	0.028(2)	0.14(4)	N/A
[(L4O)Zn(NAcSPh)]	0.0040(4)	0.059(1)	N/A

Chart 7. Average Kinetic Results using methyl iodide

Compound	Chloroform	Acetonitrile	Methanol
	ave. rate (x10⁻⁴)	Ave. rate (x10⁻⁴)	ave. rate (x10⁻⁴)
[(L3S)ZnI]	2.9(2)	0.62(3)	1.4(1)
[(L1O)Zn(SPh)]	5.23(3)	0.017(2)	0.588(1)
[(L1O)Zn(NAcSPh)]	9.0(6)	0.72(6)	0.13(4)
[(L1O)Zn(NCOCF ₃ SPh)]	1.41(9)	0.31(7)	0.142(7)
[(L4O)Zn(SPh)]	0.55(4)	0.19(5)	N/A
[(L4O)Zn(NacSPh)]	0.14(1)	1.7(6)	N/A

Chart 8. Average Kinetic Results using trimethyloxonium tetrafluoroborate

COMPARATIVE KINETIC CHARTS

Compound	Chloroform	Acetonitrile	Methanol
	ave. rate ($\times 10^{-4}$)	Ave. rate ($\times 10^{-4}$)	ave. rate ($\times 10^{-4}$)
[(L1O)Zn(SPh)]	3.53(5)	14.2(3)	1.3(1)
[(L1O)Zn(NAcSPh)]	0.017(1)	0.4150(5)	0.11(2)
[(L1O)Zn(NCOF ₃ SPh)]	0.026(2)	1.3(4)	2.4(1)
[(L4O)Zn(SPh)]	0.028(2)	0.14(4)	N/A
[(L4O)Zn(NacSPh)]	0.0040(4)	0.059(1)	N/A

Chart 9. Average Kinetic Results of the hydrogen bonded pairs using methyl iodide

Compound	Chloroform	Acetonitrile	Methanol
	ave. rate ($\times 10^{-4}$)	Ave. rate ($\times 10^{-4}$)	ave. rate ($\times 10^{-4}$)
[(L1O)Zn(SPh)]	5.23(3)	170(2)	58.8(1)
[(L1O)Zn(NAcSPh)]	9.0(6)	72(6)	13(4)
[(L1O)Zn(NCOCF ₃ SPh)]	1.41(9)	31(7)	14.2(7)
[(L4O)Zn(SPh)]	0.55(4)	19(5)	N/A
[(L4O)Zn(NAcSPh)]	0.14(1)	1.7(6)	N/A

Chart 10. Average Kinetic Results of the hydrogen bonded pairs using trimethyloxonium tetrafluoroborate

COMPARATIVE KINETIC CHARTS

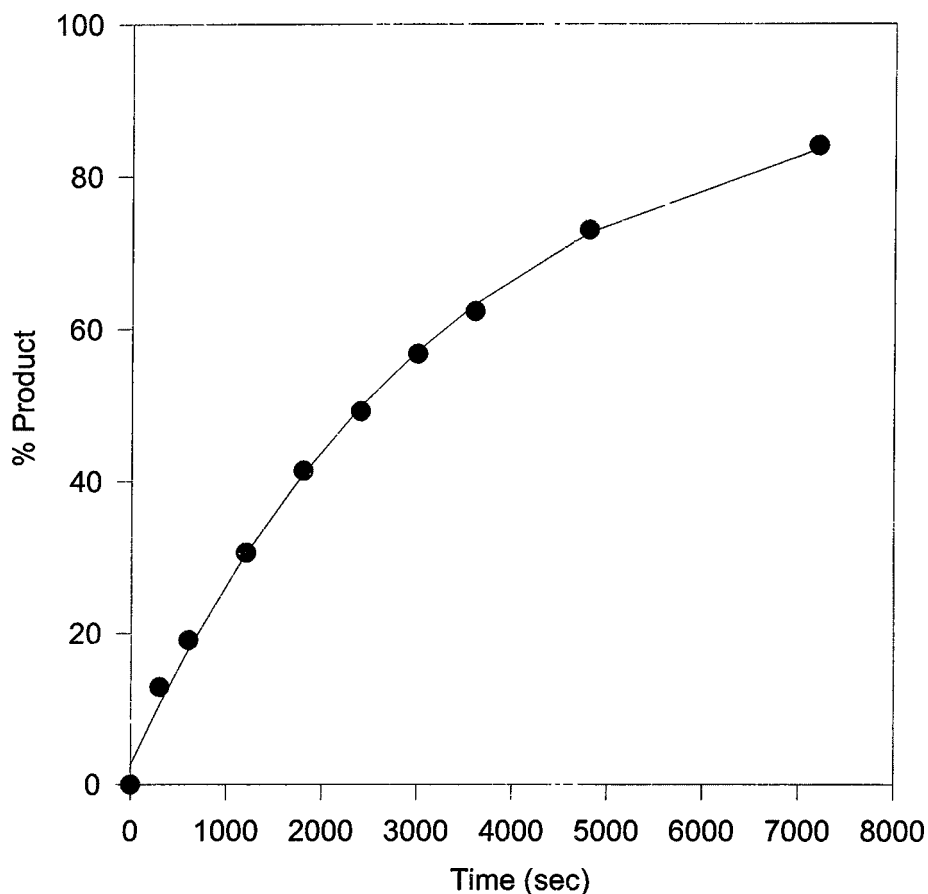
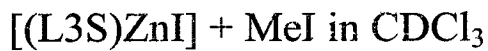
Compound	Chloroform	Acetonitrile	Methanol
	ave. rate ($\times 10^{-4}$)	ave. rate ($\times 10^{-4}$)	ave. rate ($\times 10^{-4}$)
[(L3S)ZnI]	3.12(8)	27(6)	1.650(5)
[(L1O)Zn(SPh)]	3.53(5)	14.2(3)	1.3(1)
[(L4O)Zn(SPh)]	0.028(2)	0.14(4)	N/A

Chart 11. Average Kinetic Results for ligand comparison using methyl iodide

Compound	Chloroform	Acetonitrile	Methanol
	ave. rate ($\times 10^{-4}$)	ave. rate ($\times 10^{-4}$)	ave. rate ($\times 10^{-4}$)
[(L3S)ZnI]	2.9(2)	62(3)	1.4(1)
[(L1O)Zn(SPh)]	5.23(3)	170(2)	58.8(1)
[(L4O)Zn(SPh)]	0.55(4)	19(5)	N/A

Chart 12. Average Kinetic Results for ligand comparison using trimethyloxonium tetrafluoroborate

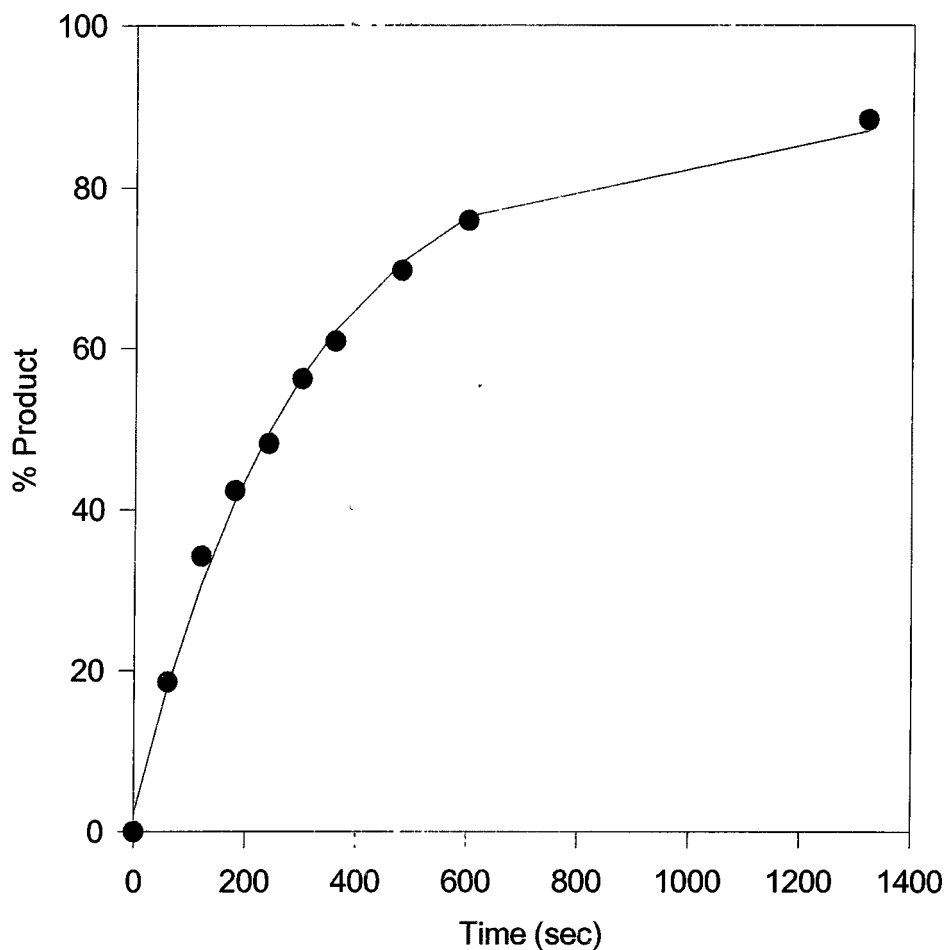
APPENDIX B: GRAPHS AND ^1H NMR SPECTRA



Time (sec)	% Product			Plot Values
0.0000	0.0000	Amplitude:	91.1940	2.6848
300.0000	12.8700	Rate const.:	3.0337e-4	10.6180
600.0000	19.1000	Zero Intercept	2.6848	17.8610
1200.0000	30.6100			30.5115
1800.0000	41.3900			41.0569
2400.0000	49.2400			49.8473
3000.0000	56.7300			57.1748
3600.0000	62.3200			63.2830
4800.0000	72.9700			72.6189
7200.0000	84.0400			83.6138

Graph 1. Exponential curve of the reaction as it goes to 100% completion. This reaction was run at 18mM with an excess of 10 equivalents of the MeI. The peaks at 5.96ppm and 6.17ppm were monitored for the data collection. Curve-fitting and rate determination was performed using SigmaPlot software.

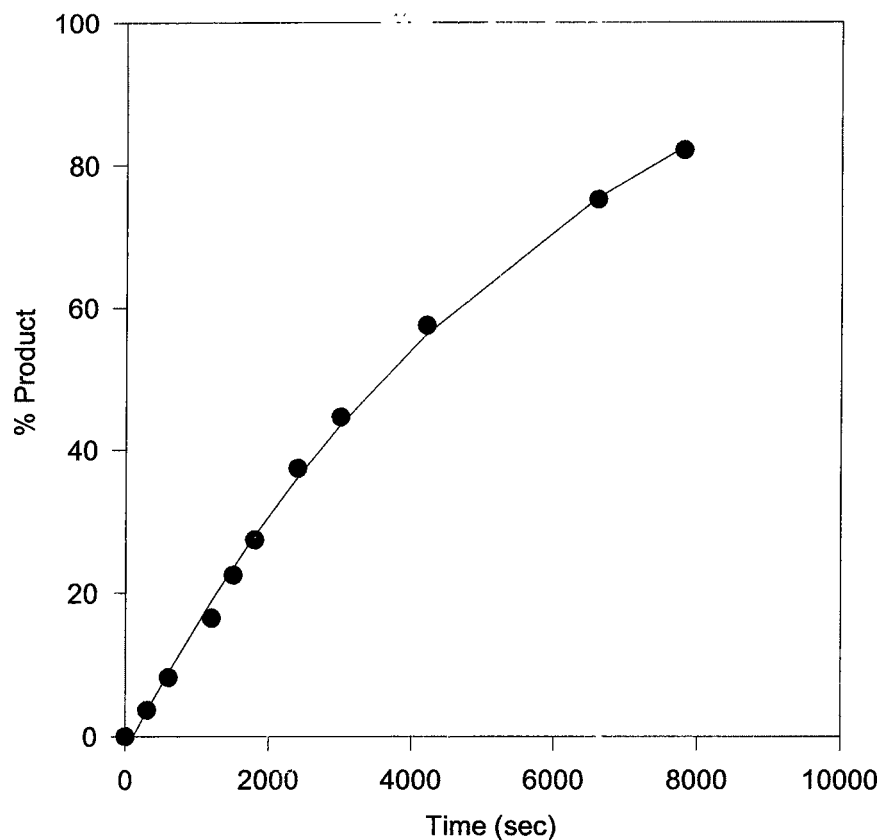
[(L3S)ZnI] + MeI in CD₃CN



Time (sec)	% Product			Plot values
0	0	Amplitude.	85 715	2.323
60	18.53	Rate Constant.	3 332E-03	17.857
120	34.23	Zero Intercept.	2 323	30.575
180	42.33			40.989
240	48.18			49.515
300	56.18			56.497
360	60.84			62.213
480	69.62			70.725
600	75.86			76.431
1320	88.34			86.985

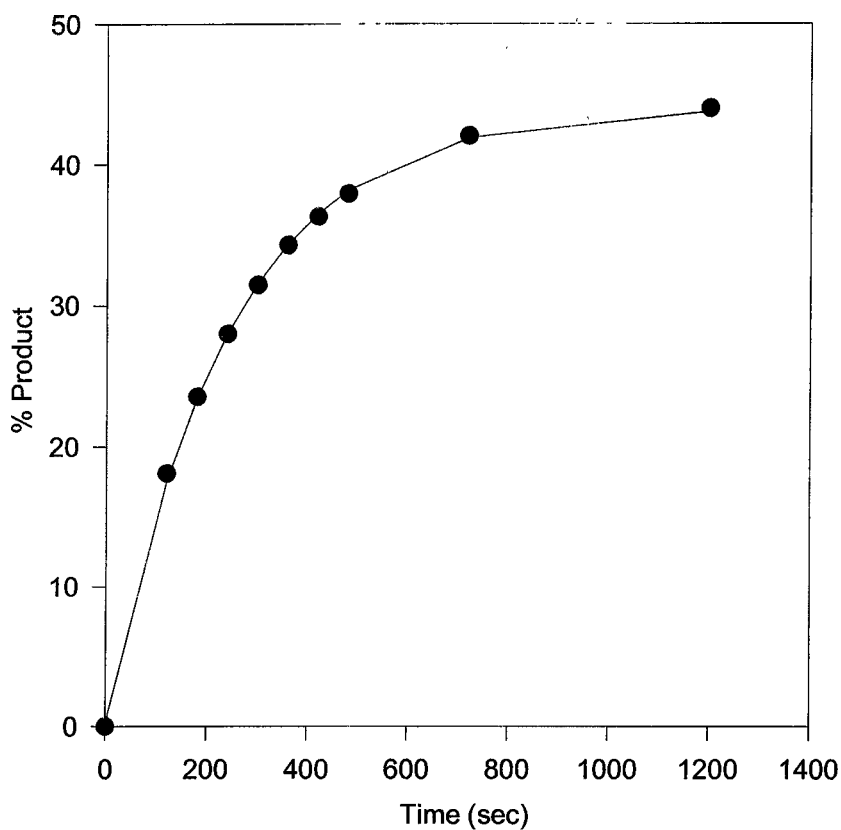
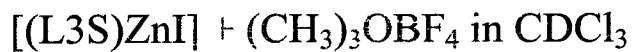
Graph 2. Exponential curve of the reaction as it goes to 100% completion. This reaction was run at 18mM with an excess of 10 equivalents of the MeI. The peaks at 6.0ppm and 6.40ppm were monitored for the data collection. Curve-fitting and rate determination was performed using SigmaPlot software.

[(L3S)ZnI] + MeI in CD₃OD



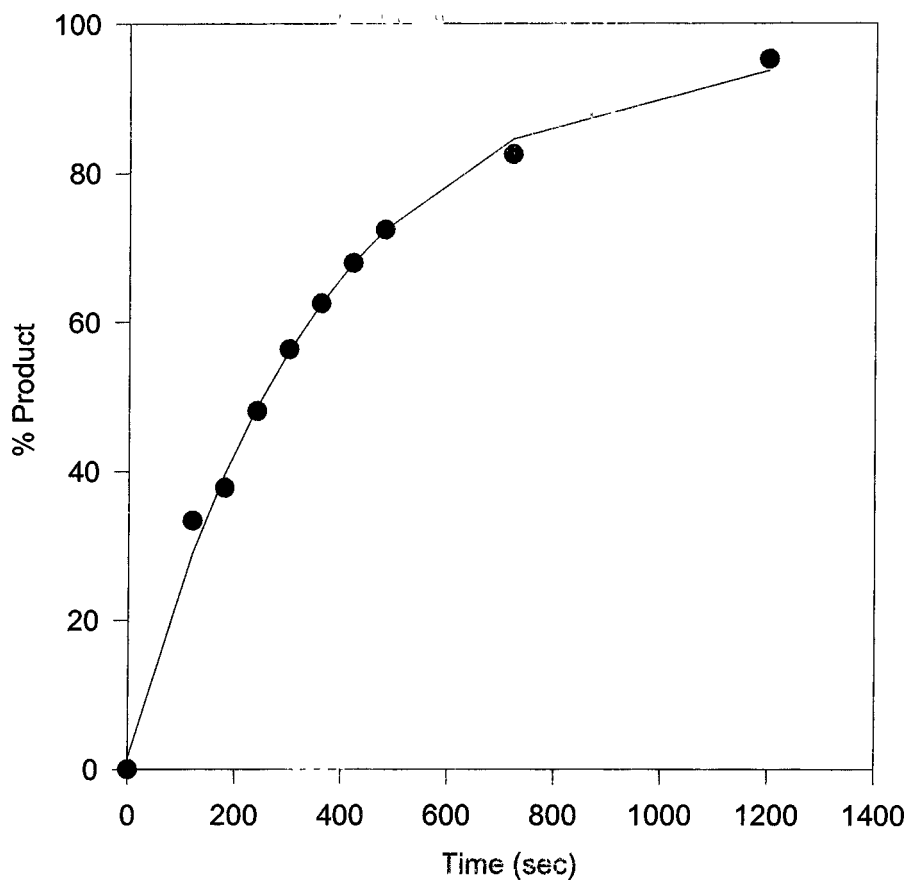
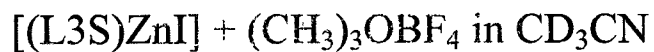
Time (sec)	% Product			Plot Values
0	0	Amplitude:	116.633	-2.010
300	3.69	Rate Constant:	1.651E-04	3.625
600	8.26	Zero Intercept:	-2.010	8.988
1200	16.52			18.948
1500	22.49			23.571
1800	27.38			27.970
2400	37.39			36.140
3000	44.61			43.541
4200	57.51			56.314
6600	75.08			75.386
7800	81.98			82.437

Graph 3. Exponential curve of the reaction as it goes to 100% completion. This reaction was run at 18mM with an excess of 10 equivalents of the MeI. The peaks at 6.1ppm and 6.40ppm were monitored for the data collection. Curve-fitting and rate determination was performed using SigmaPlot software.



Time (sec)	% Product			Plot Values
0	0	Amplitude:	43.800	0.238
120	18.08	Rate Costant:	4.192E-03	17.551
180	23.55	Zero Intercept:	0.238	23.441
240	27.99			28.021
300	31.46			31.583
360	34.26			34.352
420	36.28			36.506
480	37.92			38.181
720	42.02			41.896
1200	43.96			43.751

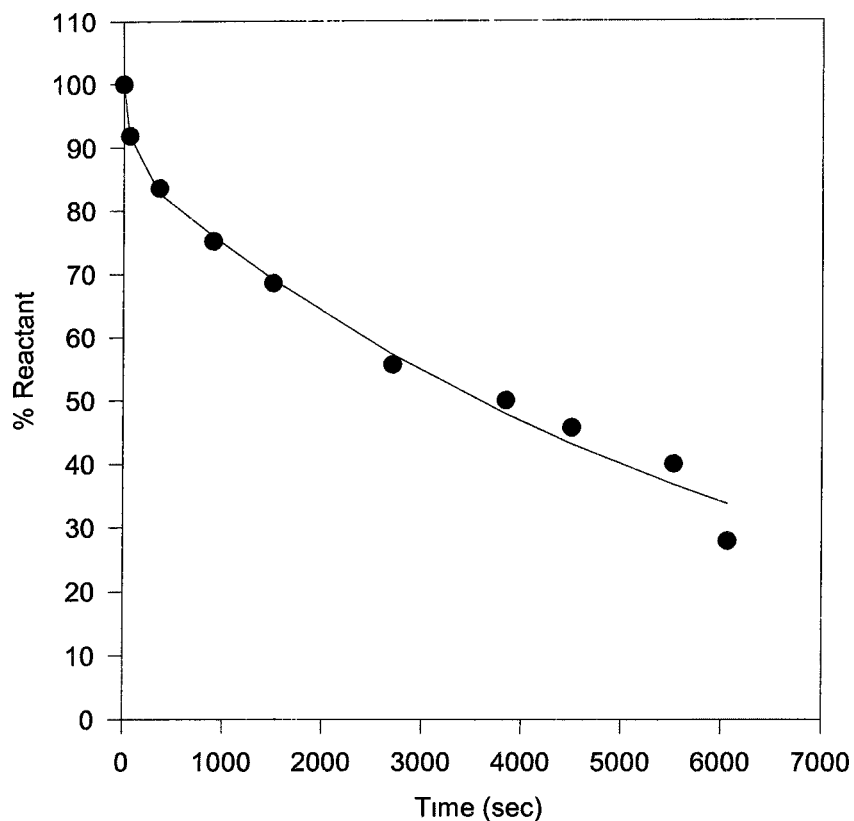
Graph 4. Exponential curve of the reaction as it goes to 100% completion. This reaction was run at 10mM with an excess of 5 equivalents of the $(CH_3)_3OBF_4$. The peaks at 1.64ppm and 1.7ppm were monitored for the data collection. Curve-fitting and rate determination was performed using SigmaPlot software.



Time (sec)	% Product			Plot Values
0	0	Amplitude	95.294	1.592
120	33.41	Rate Constant:	2.832E-03	29.051
180	37.8	Zero Intercept.	1.592	39.653
240	48.08			48.598
300	56.33			56.144
360	62.51			62.512
420	67.92			67.884
480	72.39			72.417
720	82.43			84.487
1200	95.17			93.703
7800	81.98			82.437

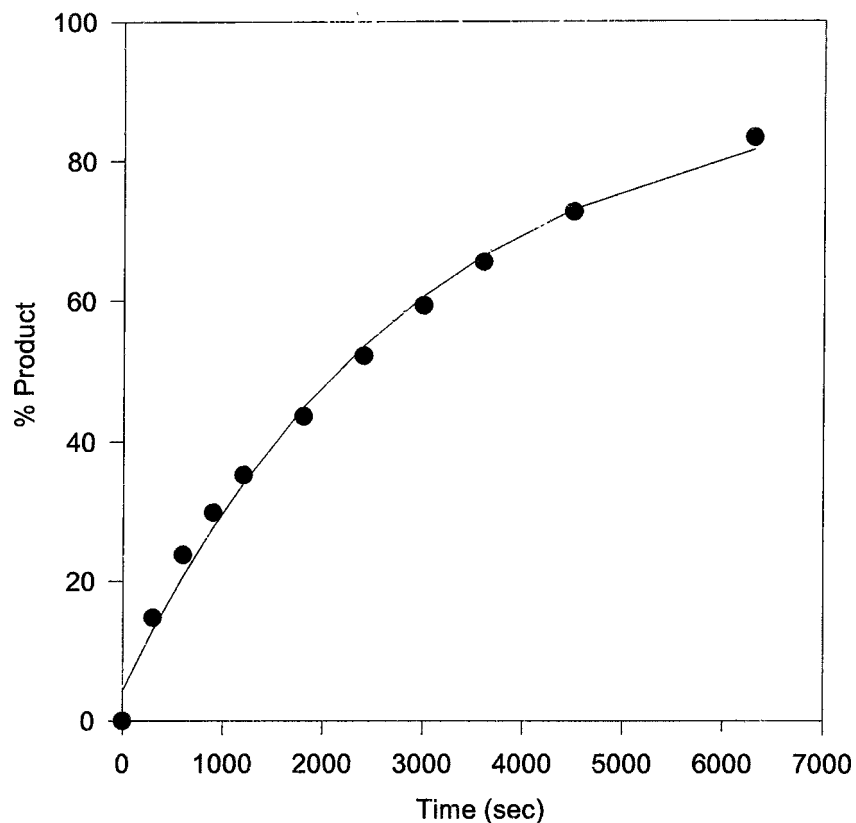
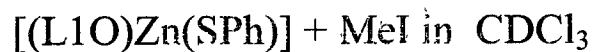
Graph 5. Exponential curve of the reaction as it goes to 100% completion. This reaction was run at 10mM with an excess of 5 equivalents of the $(CH_3)_3OBF_4$. The peaks at 3.25ppm and 4.43ppm were monitored for the data collection. Curve-fitting and rate determination was performed using SigmaPlot software.

[(L3S)ZnI] + (CH₃)₃OBF₄ in CD₃OD



Time (sec)	% Product			Plot Values
0	0		12.445	99.978
60	8.15		1.454E-02	91.912
360	16.44	Amplitude:	87.533	82.780
900	24.82	Rate Constant	1.573E-04	75.978
1500	31.46			69.135
2700	44.36			57.243
3840	50.02			47.845
4500	54.34			43.127
5520	60.02			36.734
6060	72.13			33.743
7800	81.98			28.437

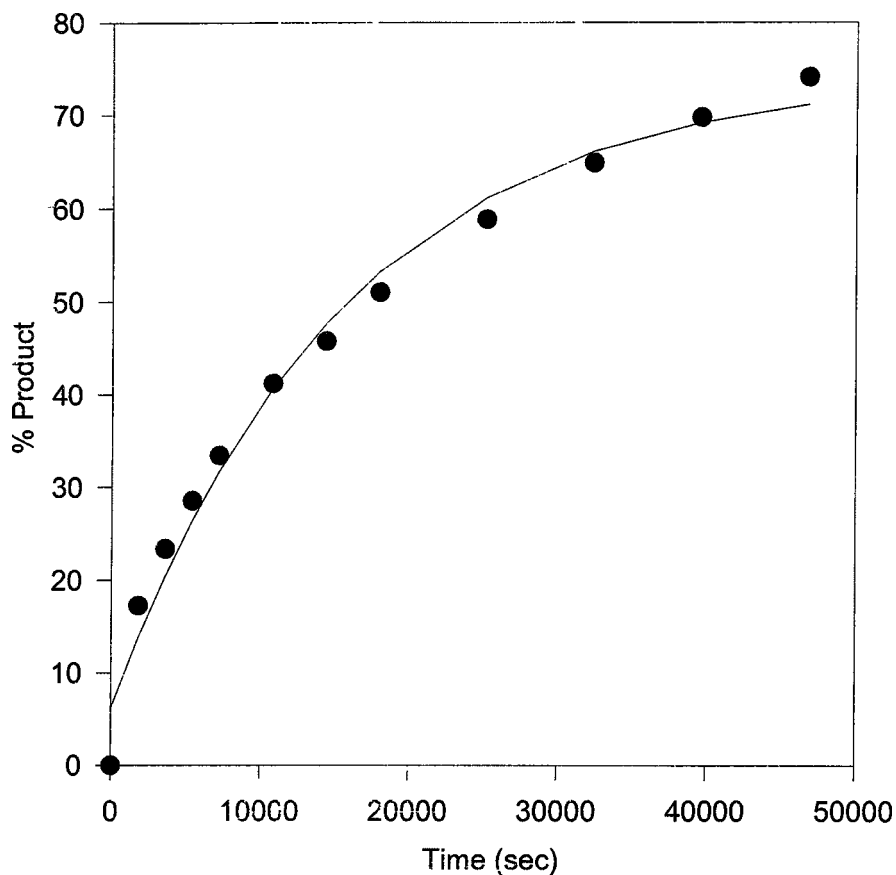
Graph 6. Exponential curve of the reaction as it goes to 100% completion. This reaction was run at 10mM with an excess of 5 equivalents of the (CH₃)₃OBF₄. The peaks at 1.44ppm and 1.35ppm were monitored for the data collection. Curve-fitting and rate determination was performed using SigmaPlot software.



Time (sec)	% Product			Plot Values
0	0	Amplitude:	86.941	4.385
300	14.73	Rate Constant:	3.478E-04	13.000
600	23.78	Zero Intercept:	4.385	20.762
900	29.86			27.754
1200	35.21			34.053
1800	43.58			44.841
2400	52.19			53.597
3000	59.32			60.704
3600	65.54			66.472
4500	72.76			73.153
6300	83.36			81.609

Graph 7. Exponential curve of the reaction as it goes to 100% completion. This reaction was run at 18mM with an excess of 10 equivalents of the MeI. The peaks at 7.31ppm and 7.23ppm were monitored for the data collection. Curve-fitting and rate determination was performed using SigmaPlot software.

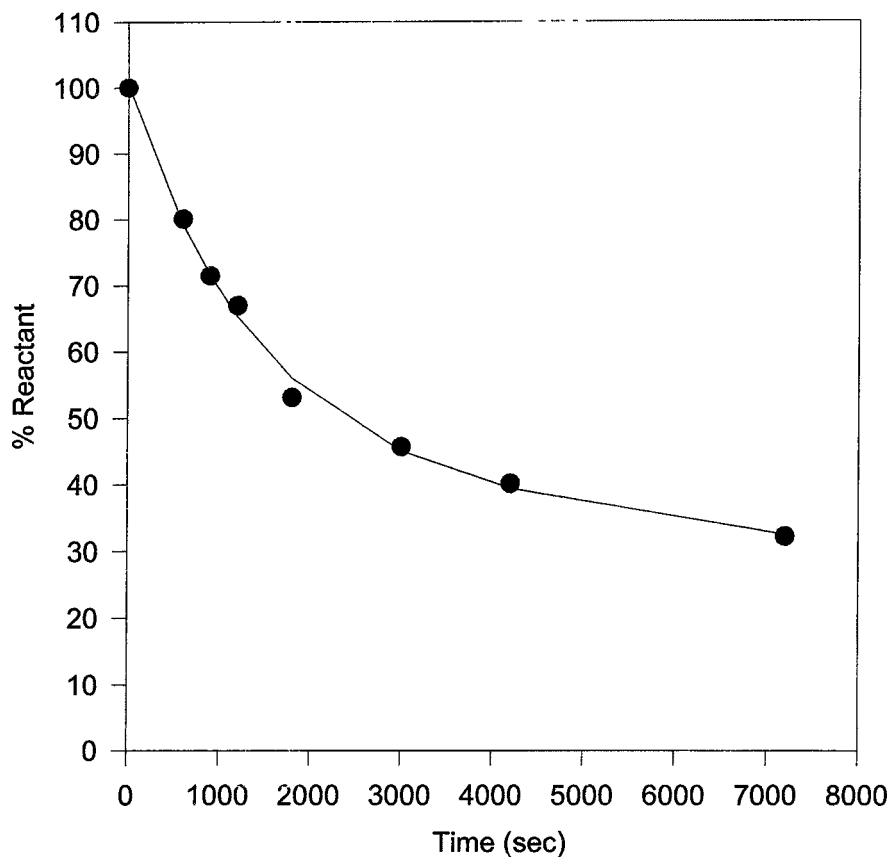
[(L1O)Zn(SPh)] + MeI in CD₃CN



Time (sec)	% Product			Plot Values
0	0	Amplitude:	68.109	6 226
1800	17.22	Rate Constant:	6.525E-05	13 774
3600	23.37	Zero Intercept:	6.226	20.486
5400	28.53			26 453
7200	33.44			31 760
10800	41.2			40 674
14400	45.79			47.721
18000	51.01			53.293
25200	58.82			61.182
32400	64.88			66.113
39600	69.71			69.196
46800	74.03			71 123

Graph 8. Exponential curve of the reaction as it goes to 100% completion. This reaction was run at 18mM with an excess of 10 equivalents of the MeI. The peaks at 7.3ppm and 7.2ppm were monitored for the data collection. Curve-fitting and rate determination was performed using SigmaPlot software.

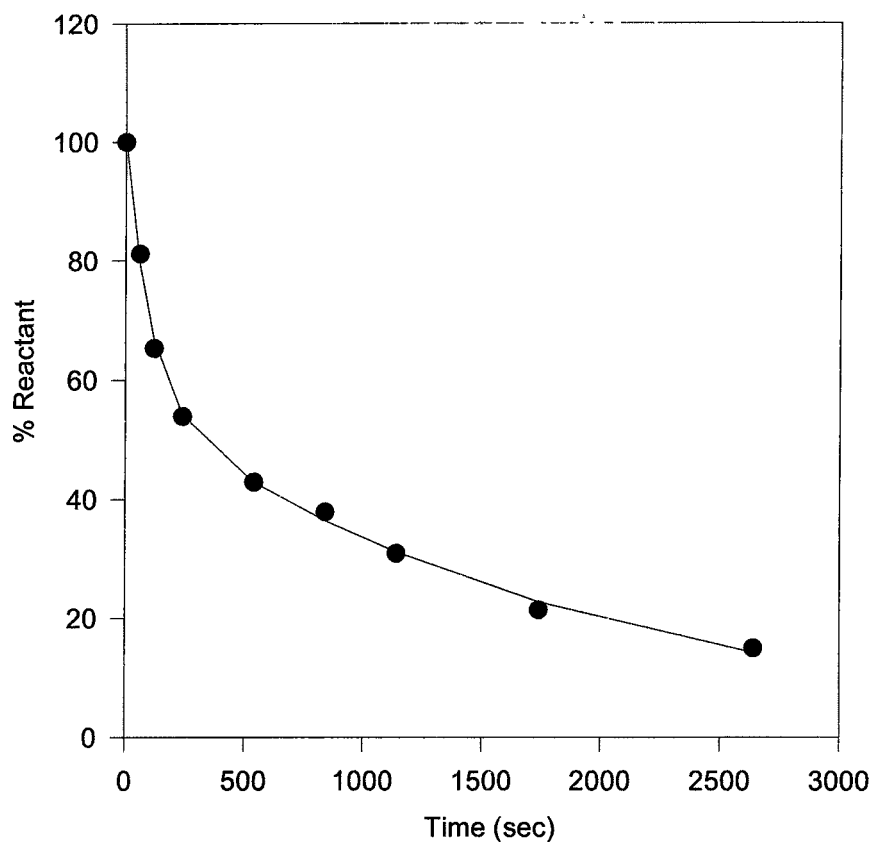
[(L1O)Zn(SPh)] + MeI in CD₃OD



Time (sec)	% Product			Plot Values
0	0		55.737	100.445
600	19.89		7.375E-04	79.312
900	28.54	Amplitude.	44.708	71.615
1200	33.01	Rate Constant:	4.551E-05	65.336
1800	46.93			55.971
3000	54.28			45.103
4200	59.83			39.448
7200	67.8			32.493

Graph 9. Exponential curve of the reaction as it goes to 100% completion. This reaction was run at 5mM with an excess of 10 equivalents of the MeI. The peaks at 6.54ppm and 6.34ppm were monitored for the data collection. Curve-fitting and rate determination was performed using SigmaPlot software.

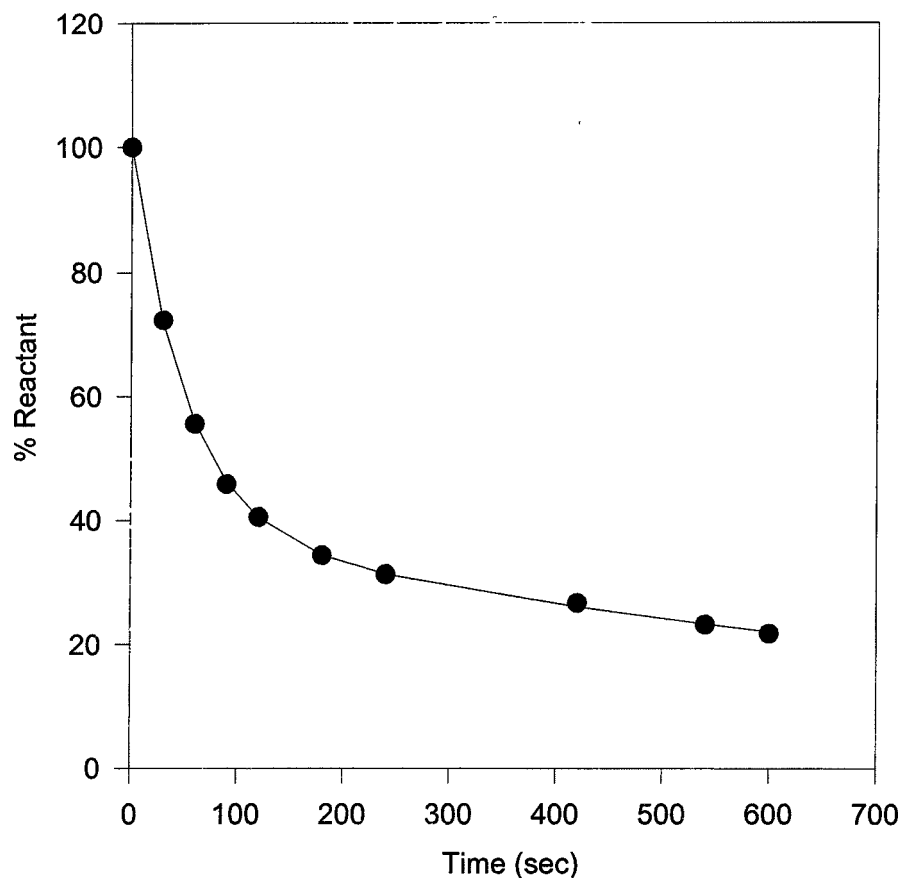
[(L1O)Zn(SPh)]+ (CH₃)₃OBF₄ in CDCl₃



Time (sec)	% Product			Plot Values
0	0		43.900	100.530
60	18.88		9.770E-03	79.297
120	34.73	Amplitude:	56.630	66.760
240	46.12	Rate Constant:	5.250E-04	54.133
540	57.12			42.880
840	62.15			36.455
1140	69.13			31.135
1740	78.65			22.725
2640	85.09			14.172

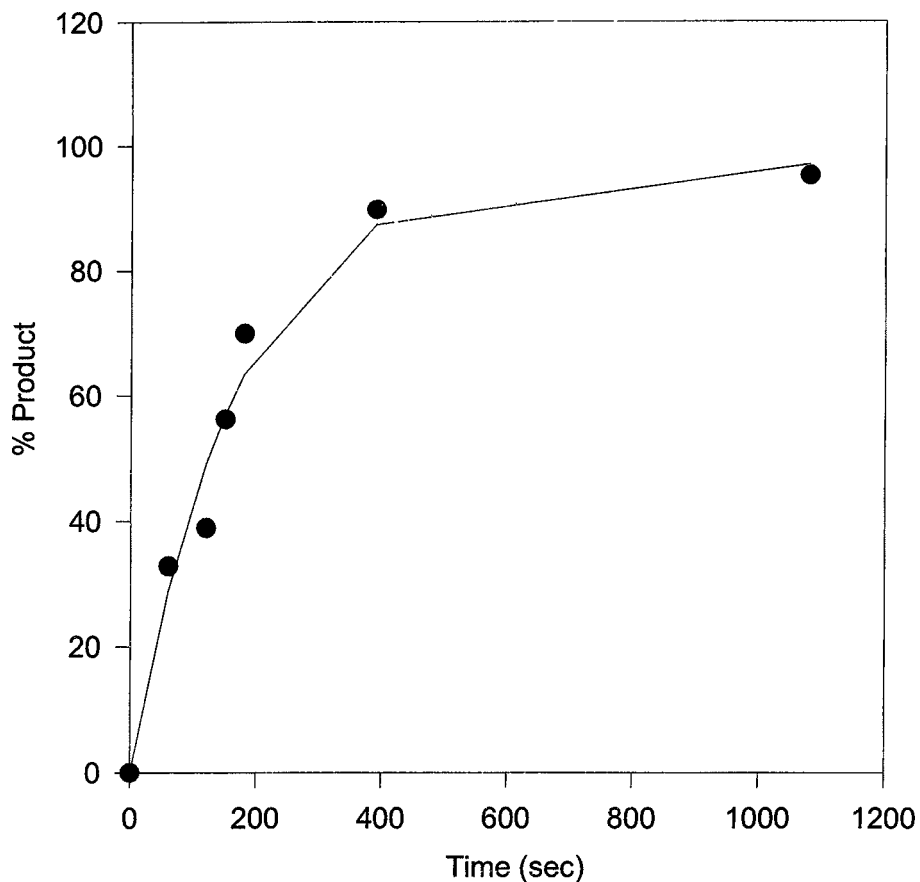
Graph 10. Exponential curve of the reaction as it goes to 100% completion. This reaction was run at 10mM with an excess of 5 equivalents of the (CH₃)₃OBF₄. The peaks at 6.15ppm and 5.9ppm were monitored for the data collection. Curve-fitting and rate determination was performed using SigmaPlot software.

$[(L1O)Zn(SPh)]^+ (CH_3)_3OBF_4$ in CD_3CN



Time (sec)	% Product			Plot Values
0	0	Amplitude:	61.766	100 131
30	27.7	Rate Constant:	1.932E-02	71.919
60	44.41		38.365	55.685
90	54.16		9.209E-04	46.171
120	59.49			40.433
180	65.62			34.413
240	68.72			31.356
420	73.3			26.078
540	76.77			23.334
600	78.24			22.079

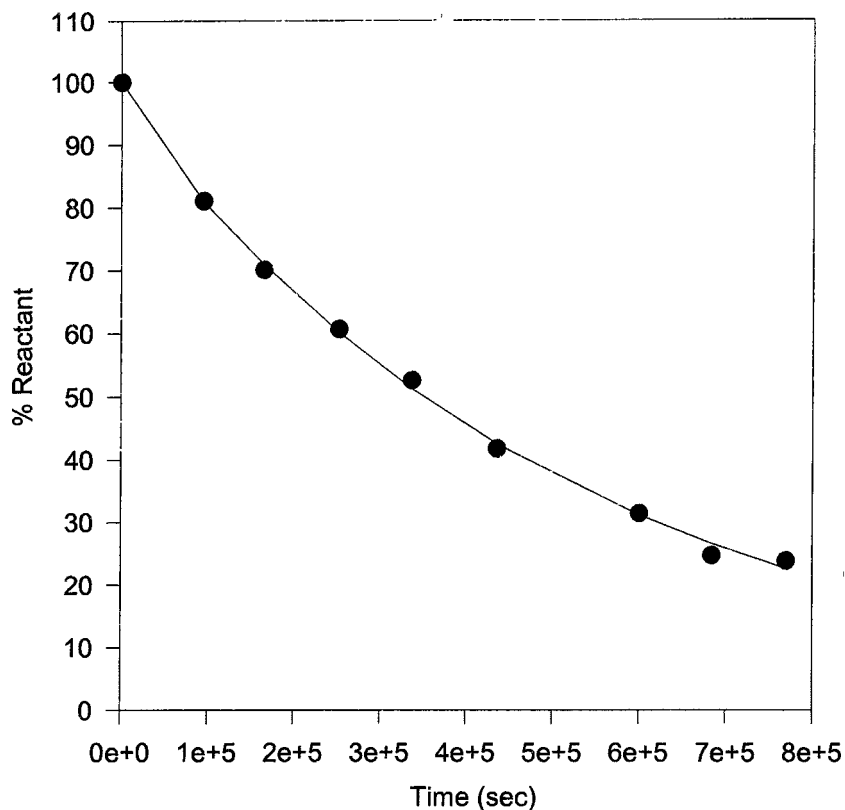
Graph 11. Exponential curve of the reaction as it goes to 100% completion. This reaction was run at 10mM with an excess of 5 equivalents of the $(CH_3)_3OBF_4$. The peaks at 7.91ppm and 7.14ppm were monitored for the data collection. Curve-fitting and rate determination was performed using SigmaPlot software.



Time (sec)	% Product			Plot Values
0	0	Amplitude	97.361	-0.153
60	32.8	Rate Constant:	5.891E-03	28.838
120	38.89	Zero Intercept:	-0.153	49.196
150	56.2			56.974
180	69.94			63.492
390	89.78			87.424
1080	95.2			97.040

Graph 12. Exponential curve of the reaction as it goes to 100% completion. This reaction was run at 5mM with an excess of 5 equivalents of the $(CH_3)_3OBF_4$. The peaks at 1.66ppm and 1.45ppm were monitored for the data collection. Curve-fitting and rate determination was performed using SigmaPlot software.

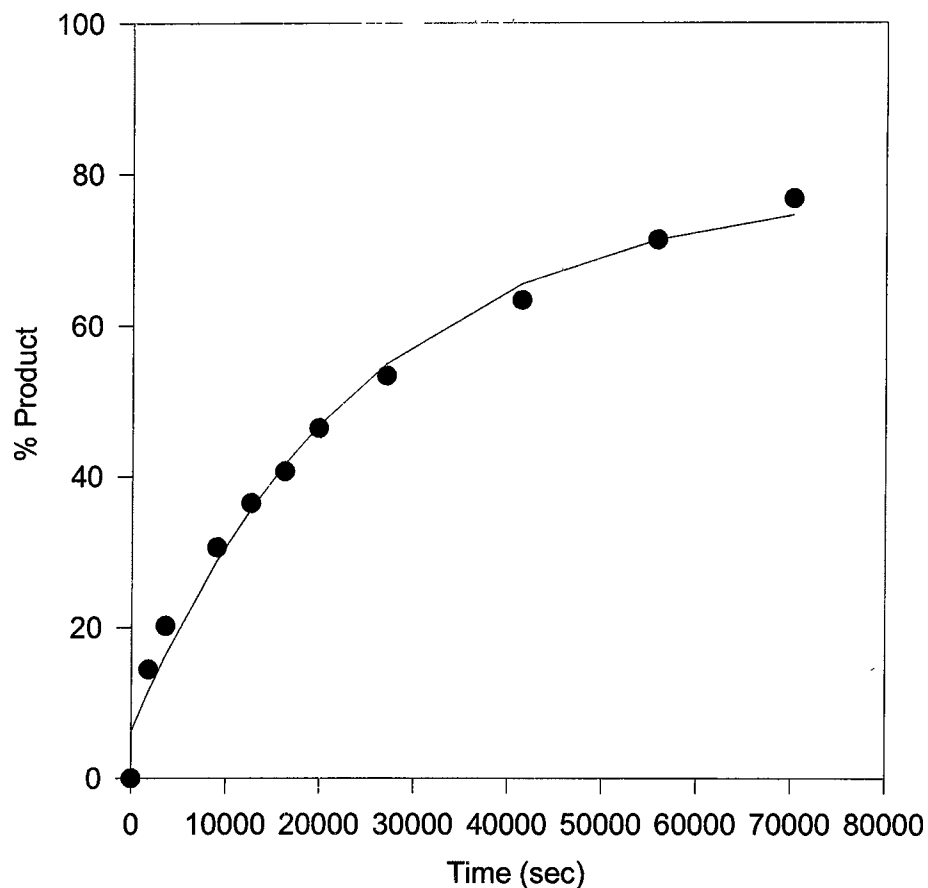
[(L1O)Zn(NAcSPh)] + MeI in CDCl₃



Time (sec)	% Product			Plot Values
0	0		3.036	100.000
95100	18.93		1.000E-03	81.002
165300	29.92	Amplitude:	96.964	70.930
252600	39.34	Rate Constant:	1.891E-06	60.134
337200	47.41			51.243
435900	58.23			42.517
600600	68.6			31.137
684300	75.31			26.578
769800	76.16			22.610

Graph 13. Exponential curve of the reaction as it goes to 100% completion. This reaction was run at 18mM with an excess of 10 equivalents of the MeI. The peaks at 1.39ppm and 1.35ppm were monitored for the data collection. Curve-fitting and rate determination was performed using SigmaPlot software.

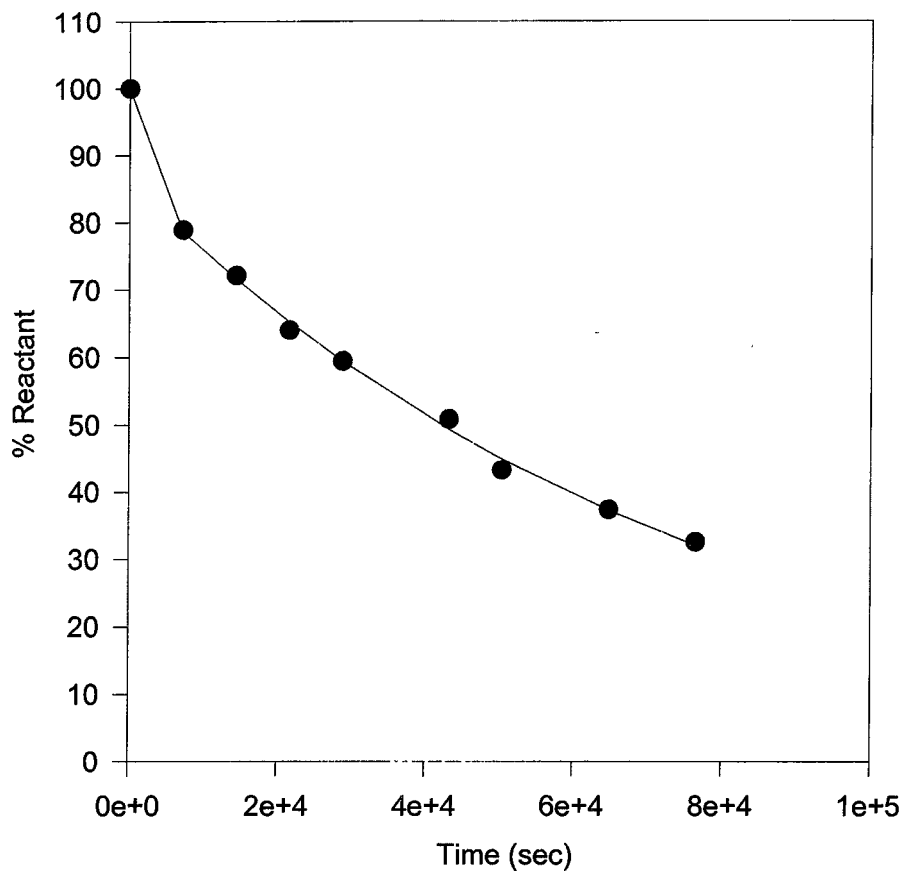
[(L1O)Zn(NAcSPh)] + MeI in CD₃CN



Time (sec)	% Product			Plot Values
0	0	Amplitude:	72.308	6.300
1800	14.41	Rate Constant:	4.139E-05	11.492
3600	20.2	Zero Intercept:	6.300	16.310
9000	30.57			28.789
12600	36.47			35.686
16200	40.68			41.628
19800	46.4			46.748
27000	53.35			54.959
41400	63.37			65.578
55800	71.38			71.429
70200	76.74			74.653

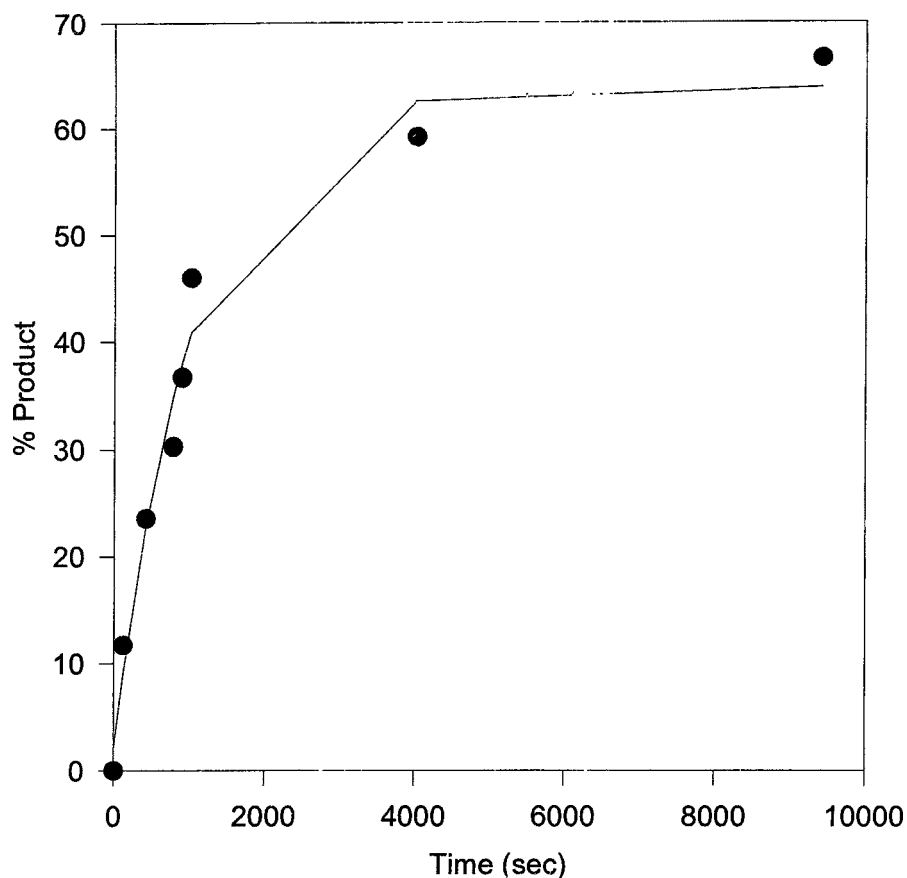
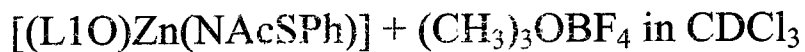
Graph 14. Exponential curve of the reaction as it goes to 100% completion. This reaction was run at 18mM with an excess of 10 equivalents of the MeI. The peaks at 7.23ppm and 6.80ppm were monitored for the data collection. Curve-fitting and rate determination was performed using SigmaPlot software.

[(L1O)Zn(NAcSPh)] + MeI in CD₃OD



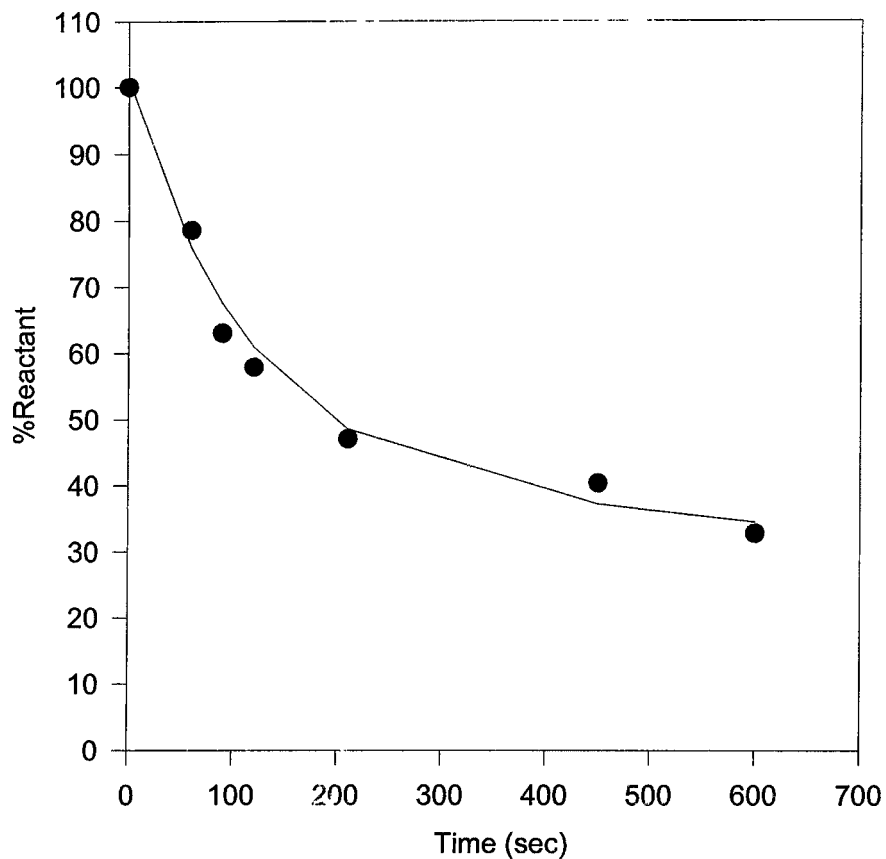
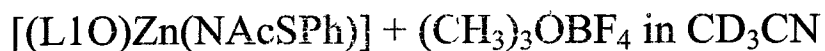
Time (sec)	% Product			Plot Values
0	0		13.704	100 000
7200	21.1		1.400E-01	78.610
14400	27.9	Amplitude:	86.296	71.609
21600	35.99	Rate Constant	1.296E-05	65.231
28800	40.57			59.421
43200	49.21			49.308
50400	56.71			44.917
64800	62.6			37.272
76500	67.46			32.030

Graph 15. Exponential curve of the reaction as it goes to 100% completion. This reaction was run at 5mM with an excess of 10 equivalents of the MeI. The peaks at 0.57ppm and 0.53ppm were monitored for the data collection. Curve-fitting and rate determination was performed using SigmaPlot software.



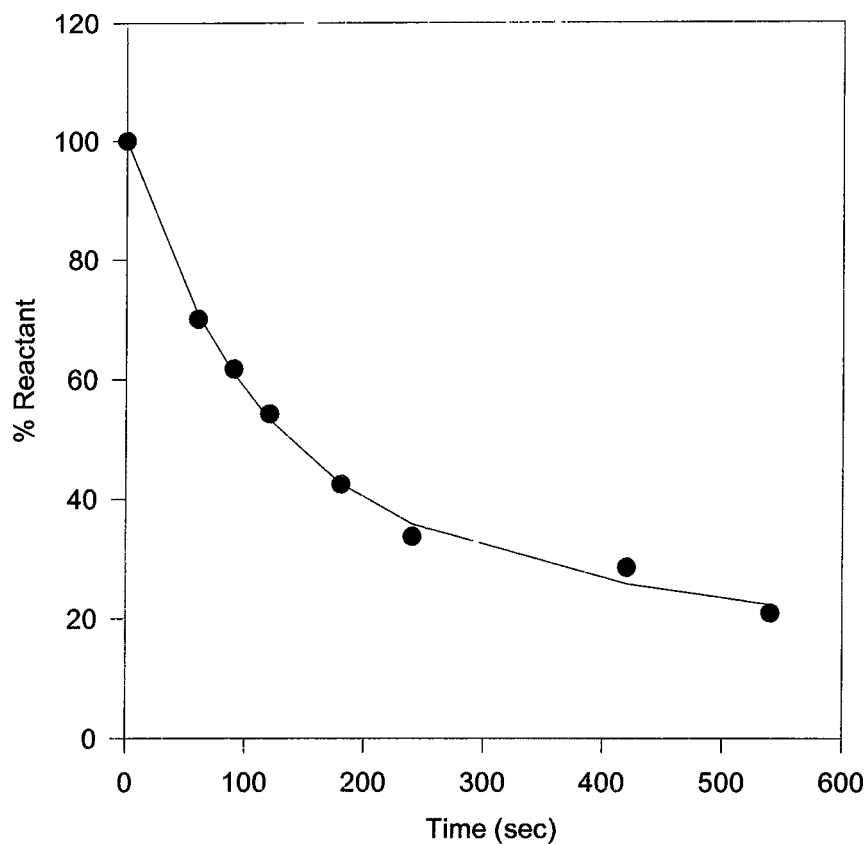
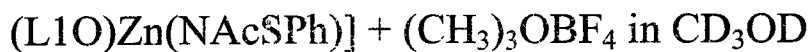
Time (sec)	% Product			Plot Values
0	0	Amplitude:	61.730	2.130
120	11.7	Rate Constant:	9.688E-04	8.905
420	23.55	Zero Intercept:	2.130	22.765
780	30.28			34.865
900	36.7			38.047
1020	46			40.880
4020	59.2			62.603
9420	66.62			63.853

Graph 16. Exponential curve of the reaction as it goes to 100% completion. This reaction was run at 10mM with an excess of 5 equivalents of the $(CH_3)_3OBF_4$. The peaks at 7.38ppm and 7.50ppm were monitored for the data collection. Curve-fitting and rate determination was performed using SigmaPlot software.



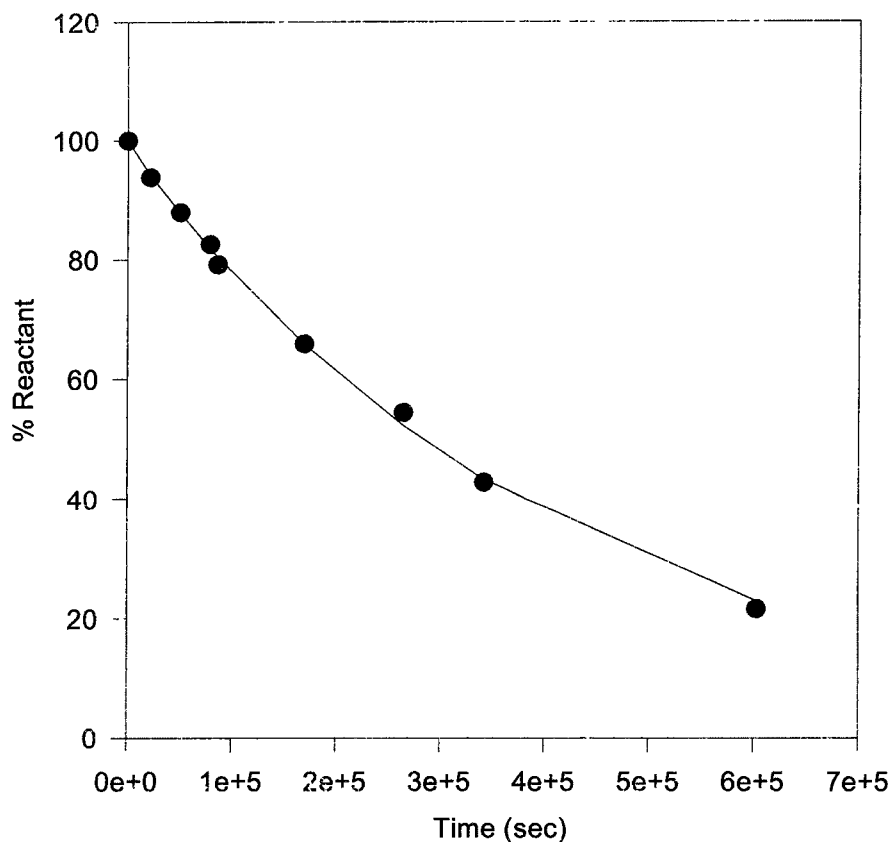
Time (sec)	% Product			Plot Values
0	0	Amplitude:	58.290	100.988
60	21.43	Rate Constant:	7.880E-03	75.965
90	36.97		42.669	67.501
120	42.12		3.707E-04	60.913
210	52.98			48.523
450	59.66			37.208
600	67.28			34.465

Graph 17. Exponential curve of the reaction as it goes to 100% completion. This reaction was run at 10mM with an excess of 5 equivalents of the $(CH_3)_3OBF_4$. The peaks at 7.66ppm and 7.79ppm were monitored for the data collection. Curve-fitting and rate determination was performed using SigmaPlot software.



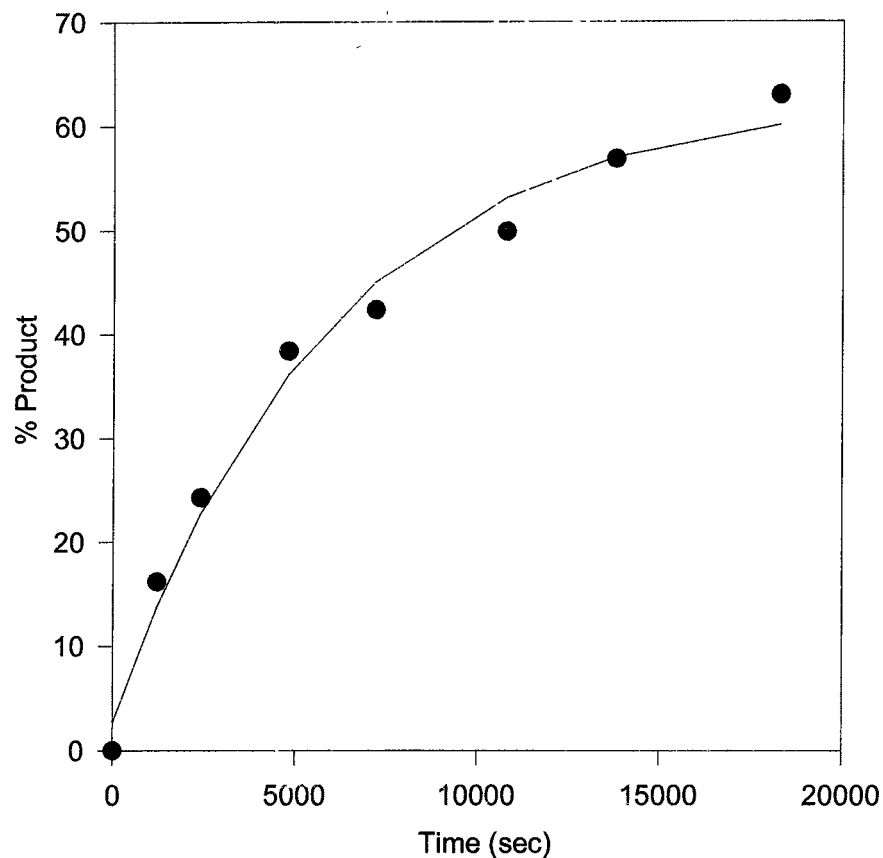
Time (sec)	% Product			Plot Values
0	0	Amplitude.	64.00960056	100.014421
60	29.93		9.269E-03	70.77972892
90	38.31		36.0048204	60.94409775
120	45.77	Rate Constant.	9.178E-04	53.29664495
180	57.55			42.5906324
240	66.31			35.80716349
420	71.48			25.7930741
540	79.07			22.36364838

Graph 18. Exponential curve of the reaction as it goes to 100% completion. This reaction was run at 5mM with an excess of 5 equivalents of the $(\text{CH}_3)_3\text{OBF}_4$. The peaks at 0.66ppm and 0.56ppm were monitored for the data collection. Curve-fitting and rate determination was performed using SigmaPlot software.



Time (sec)	% Product			Plot Values
0	0		0.792	100.000
21600	6.16		1.194E-02	94.138
50400	12.09	Amplitude	99.208	87.779
79200	17.45	Rate Constant:	2.428E-06	81.850
86400	20.85			80.431
169200	34.21			65.781
264600	45.65			52.178
342000	57.24			43.237
603000	78.41			22.940

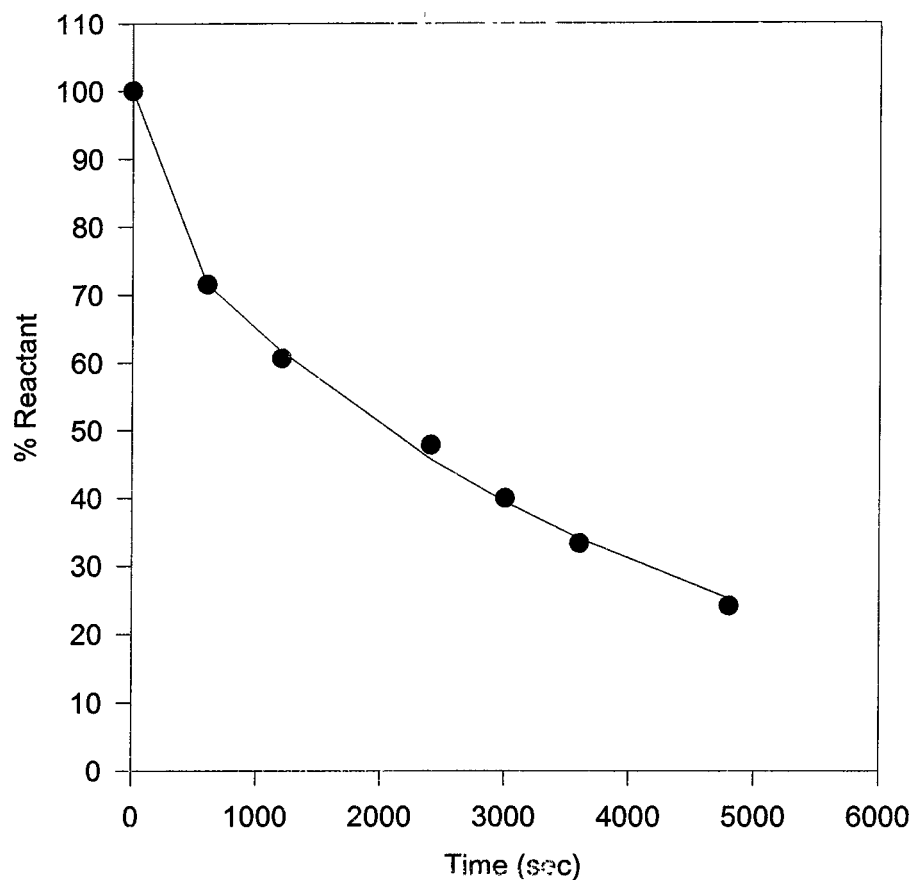
Graph 19. Exponential curve of the reaction as it goes to 100% completion. This reaction was run at 18mM with an excess of 10 equivalents of the MeI. The peaks at 7.58ppm and 7.37ppm were monitored for the data collection. Curve-fitting and rate determination was performed using SigmaPlot software.



Time (sec)	% Product			Plot Values
0	0	Amplitude	60.116	2.715
1200	16.2	Rate Constant:	1.695E-04	13.781
2400	24.29	Zero Intercept:	2.715	22.809
4800	38.4			36.187
7200	42.36			45.093
10800	49.91			53.196
13800	56.85			57.037
18300	62.94			60.129

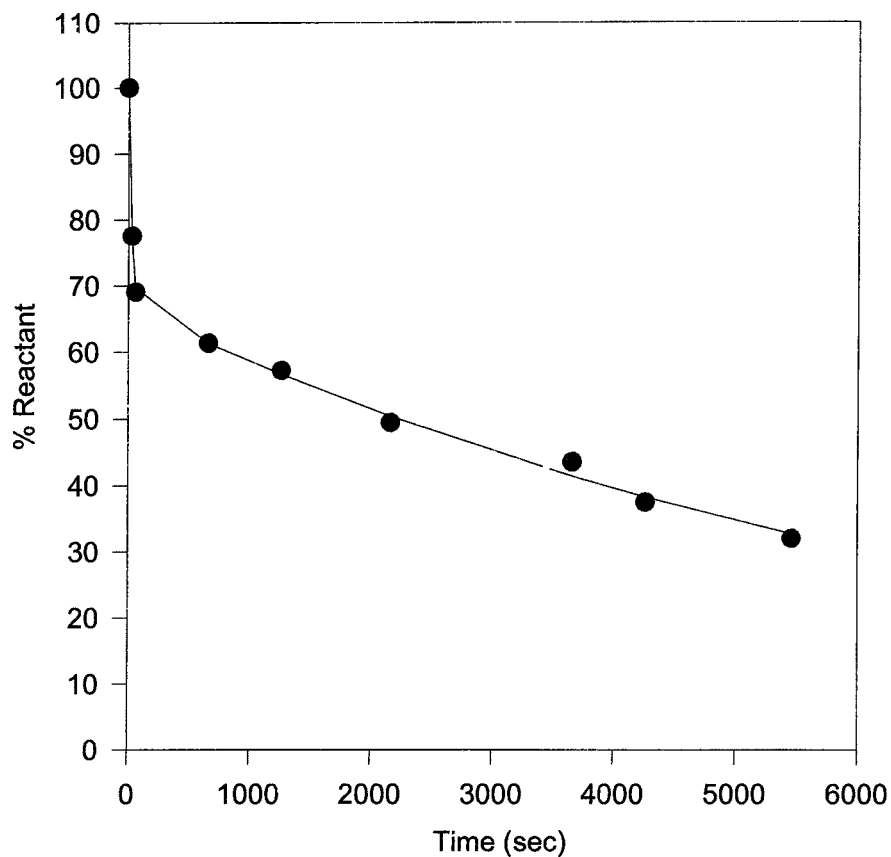
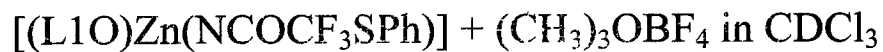
Graph 20. Exponential curve of the reaction as it goes to 100% completion. This reaction was run at 18mM with an excess of 10 equivalents of the MeI. The peaks at 7.33ppm and 7.14ppm were monitored for the data collection. Curve-fitting and rate determination was performed using SigmaPlot software.

[(L1O)Zn(NCOCF₃SPh)] + MeI in CD₃OD



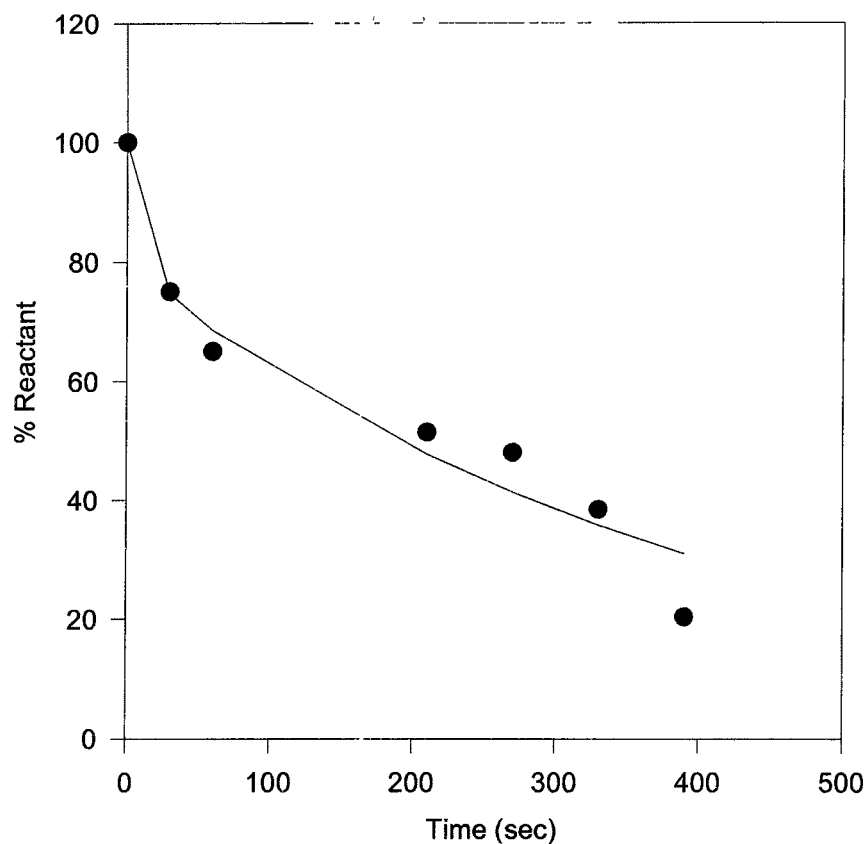
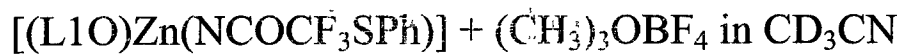
Time (sec)	% Product			Plot Values
0	0		16.954	100.000
600	28.48		4.853E+00	71.559
1200	39.35	Amplitude:	83.046	61.660
2400	52.17	Rate Constant:	2.481E-04	45.781
3000	60.02			39.449
3600	66.67			33.992
4800	75.84			25.238

Graph 21. Exponential curve of the reaction as it goes to 100% completion. This reaction was run at 5mM with an excess of 10 equivalents of the MeI. The peaks at 1.77ppm and 1.87ppm were monitored for the data collection. Curve-fitting and rate determination was performed using SigmaPlot software.



Time (sec)	% Product			Plot Values
0	0		33.227	100.064
30	22.42		3.807E-02	77.1791
60	30.93	Amplitude:	66.837	69.69769
660	38.67	Rate Constant:	1.311E-04	61.29658
1260	42.77			56.65946
2160	50.63			50.35315
3660	56.51			41.36348
4260	62.58			38.23431
5460	68.02			32.66823

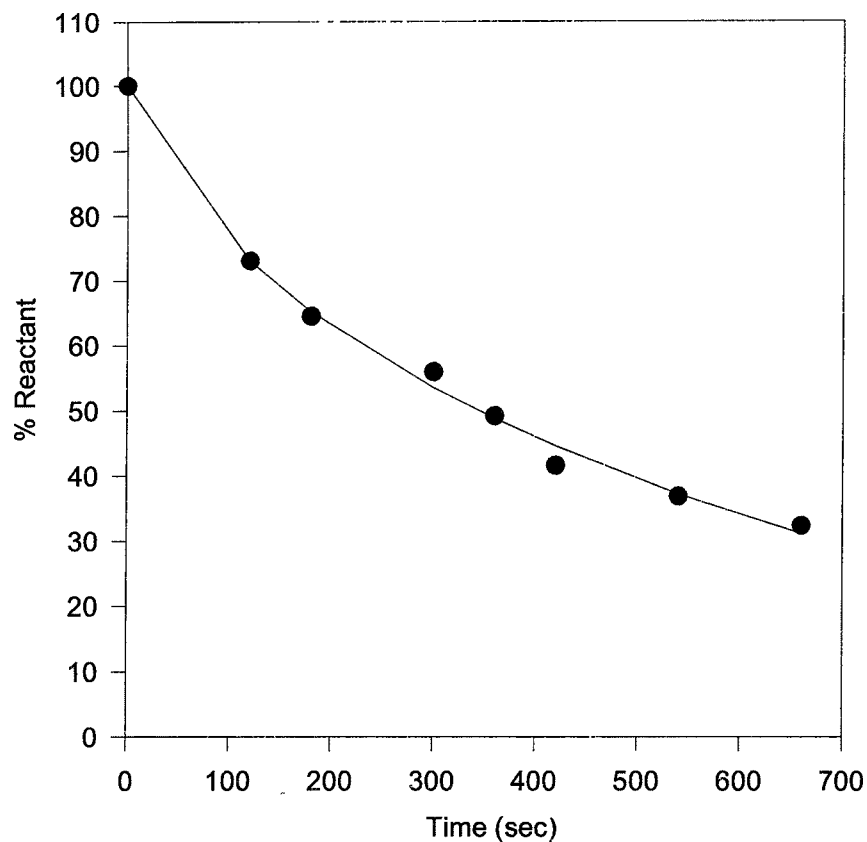
Graph 22. Exponential curve of the reaction as it goes to 100% completion. This reaction was run at 10mM with an excess of 5 equivalents of the $(CH_3)_3OBF_4$. The peaks at 6.75ppm and 6.70ppm were monitored for the data collection. Curve-fitting and rate determination was performed using SigmaPlot software.



Time (sec)	% Product			Plot Values
0	0		20.928	100.0079
30	24.96		9.831E-02	74.67311
60	35.01	Amplitude	79.080	68.51434
210	48.61	Rate Constant.	2.404E-03	47.73078
270	52.04			41.31911
330	61.6			35.76872
390	79.35			30.96392

Graph 23. Exponential curve of the reaction as it goes to 100% completion. This reaction was run at 10mM with an excess of 5 equivalents of the $(CH_3)_3OBF_4$. The peaks at 1.35ppm and 2.30ppm were monitored for the data collection. Curve-fitting and rate determination was performed using SigmaPlot software.

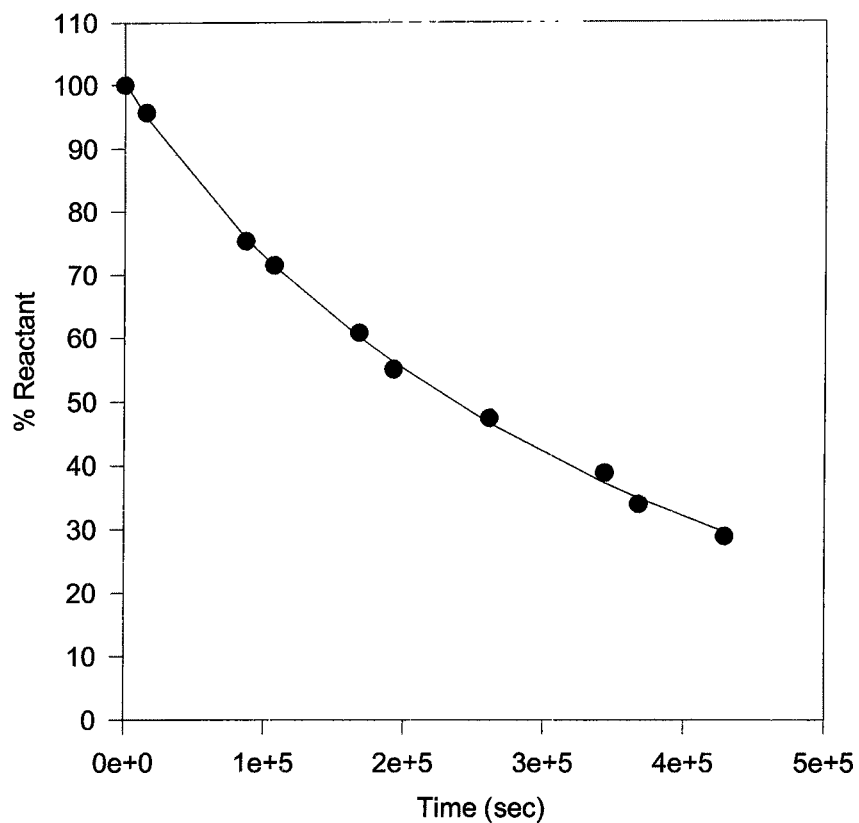
$[(L1O)Zn(NCOCF_3SPh)] + (CH_3)_3OBF_4$ in CD_3OD



Time (sec)	% Product			Plot Values
0	0		16.652	99.98567504
120	26.97		1.348E-02	72.98152253
180	35.48	Amplitude.	83.334	65.18614774
300	44.04	Rate Constant	1.491E-03	53.56735785
360	50.79			48.84580379
420	58.39			44.60423162
540	63.1			37.25883385
660	67.6			31.14656384

Graph 24. Exponential curve of the reaction as it goes to 100% completion. This reaction was run at 5mM with an excess of 5 equivalents of the $(CH_3)_3OBF_4$. The peaks at 1.63ppm and 1.60ppm were monitored for the data collection. Curve-fitting and rate determination was performed using SigmaPlot software.

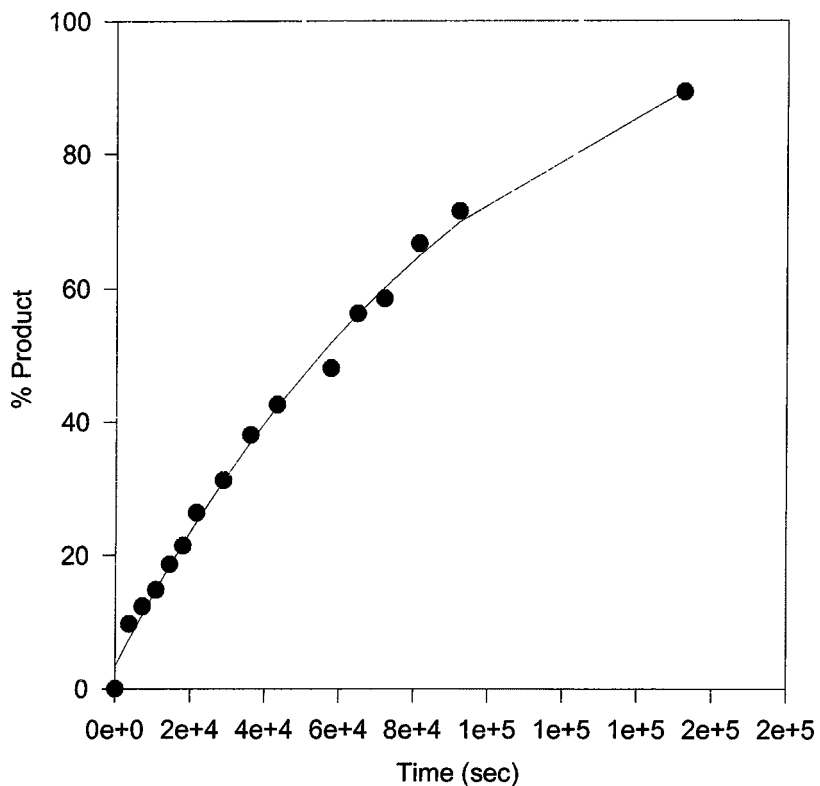
[(L4O)Zn(SPh)] + MeI in CDCl₃



Time (sec)	% Product			Plot Values
0	0	Amplitude:	94 106	100 3859
15300	4 35	Rate Constant:	2 697E-06	95.0203
86400	24.71		6.280	75.79652
106800	28.5		1.869E-05	71 41041
167700	39 25			60 145
192300	44 97			56 20149
261000	52 62			46 60182
343500	61.16			37.27865
367800	66.04			34 91113
429000	71 11			29.5966

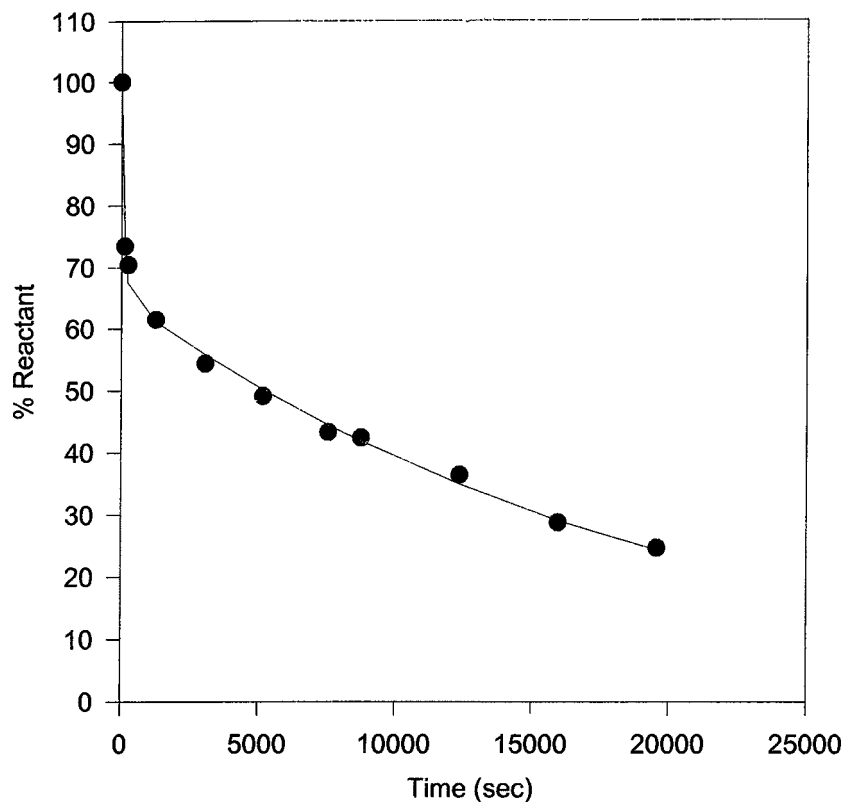
Graph 25. Exponential curve of the reaction as it goes to 100% completion. This reaction was run at 18mM with an excess of 10 equivalents of the MeI. The peaks at 1.44ppm and 1.32ppm were monitored for the data collection. Curve-fitting and rate determination was performed using SigmaPlot software.

[(L4O)Zn(SPh)] + MeI in CD₃CN



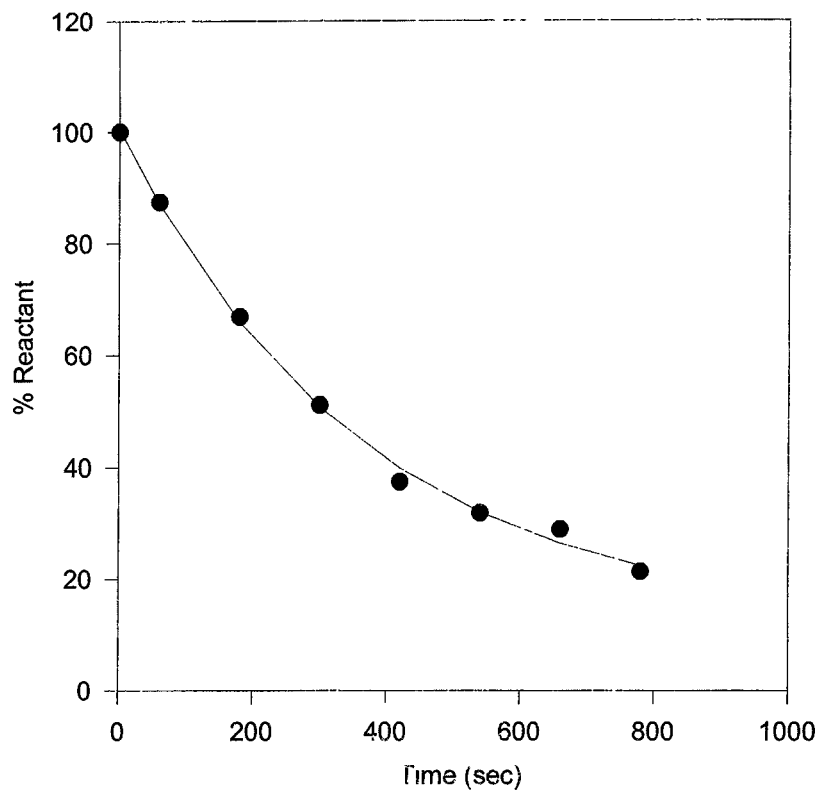
Time (sec)	% Product			Plot Values
0	0	Amplitude:	108.741	3.498605377
3600	9.73	Rate Constant:	1.022E-05	7.425398487
7200	12.33	Zero Intercept:	3.499	11.21038953
10800	14.81			14.85869918
14400	18.62			18.37526319
18000	21.43			21.76483909
21600	26.37			25.0320126
28800	31.22			31.21667331
36000	37.99			36.9627253
43200	42.57			42.30127417
57600	47.97			51.86941155
64800	56.18			56.15079609
72000	58.46			60.12854997
81300	66.63			64.85188368
92100	71.37			69.80244705
152400	89.09			89.32061636

Graph 26. Exponential curve of the reaction as it goes to 100% completion. This reaction was run at 18mM with an excess of 10 equivalents of the MeI. The peaks at 1.41ppm and 1.31ppm were monitored for the data collection. Curve-fitting and rate determination was performed using SigmaPlot software.



Time (sec)	% Product			Plot Values
0	0		34.576	99.736
120	26.56		9.995E-03	75.187
240	29.59	Amplitude:	65.160	67.516
1260	38.47	Rate Constant:	5.048E-05	61.145
3060	45.63			55.834
5160	50.87			50.218
7560	56.66			44.488
8760	57.58			41.873
12360	63.61			34.914
15960	71.24			29.112
19560	75.34			24.274

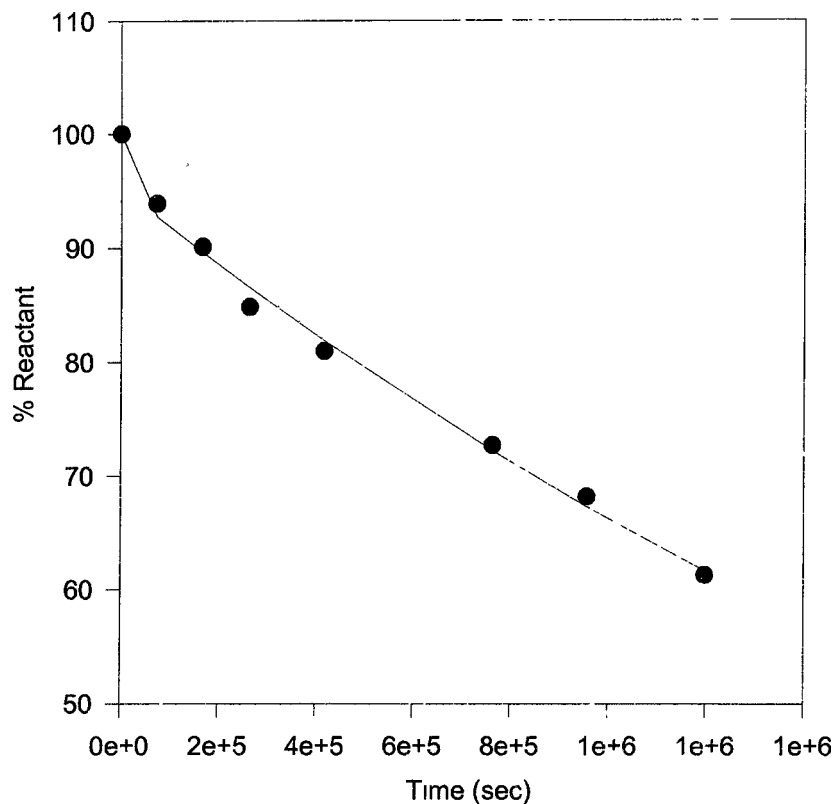
Graph 27. Exponential curve of the reaction as it goes to 100% completion. This reaction was run at 10mM with an excess of 5 equivalents of the $(CH_3)_3OBF_4$. The peaks at 7.1ppm and 6.97ppm were monitored for the data collection. Curve-fitting and rate determination was performed using SigmaPlot software.



Time (sec)	% Product			Plot Values
0	0	Amplitude	88 417	100.510
60	12.63	Rate Constant	2.759E-03	87.020
180	33.15		12.093	65.900
300	48.93		1.052E-11	50.734
420	62.57			39.842
540	68.14			32.020
660	71.1			26.403
780	78.68			22.370

Graph 28. Exponential curve of the reaction as it goes to 100% completion. This reaction was run at 10mM with an excess of 5 equivalents of the $(CH_3)_3OBF_4$. The peaks at 7.6ppm and 7.28ppm were monitored for the data collection. Curve-fitting and rate determination was performed using SigmaPlot software.

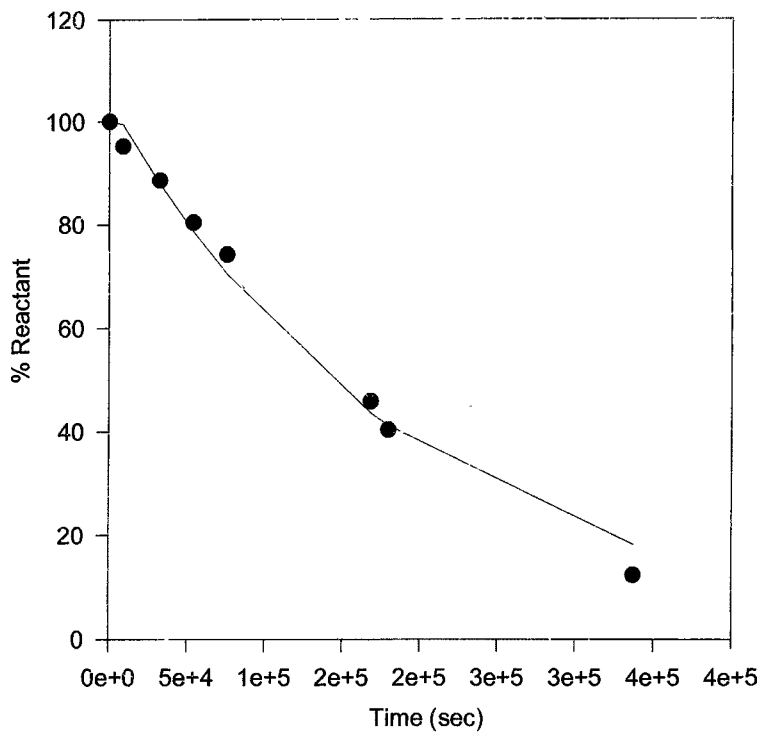
[(L4O)Zn(NAcSPh)] + MeI in CDCl₃



Time (sec)	% Product			Plot Values
0	0		4 747	100.000
73500	6.11		1 000E-03	92.744
166800	9.86	Amplitude:	95.253	89.654
264000	15.14	Rate Constant:	3.632E-07	86.544
417300	19.04			81.857
762900	27.33			72.201
956400	31.83			67.302
1198200	38.73			61.643

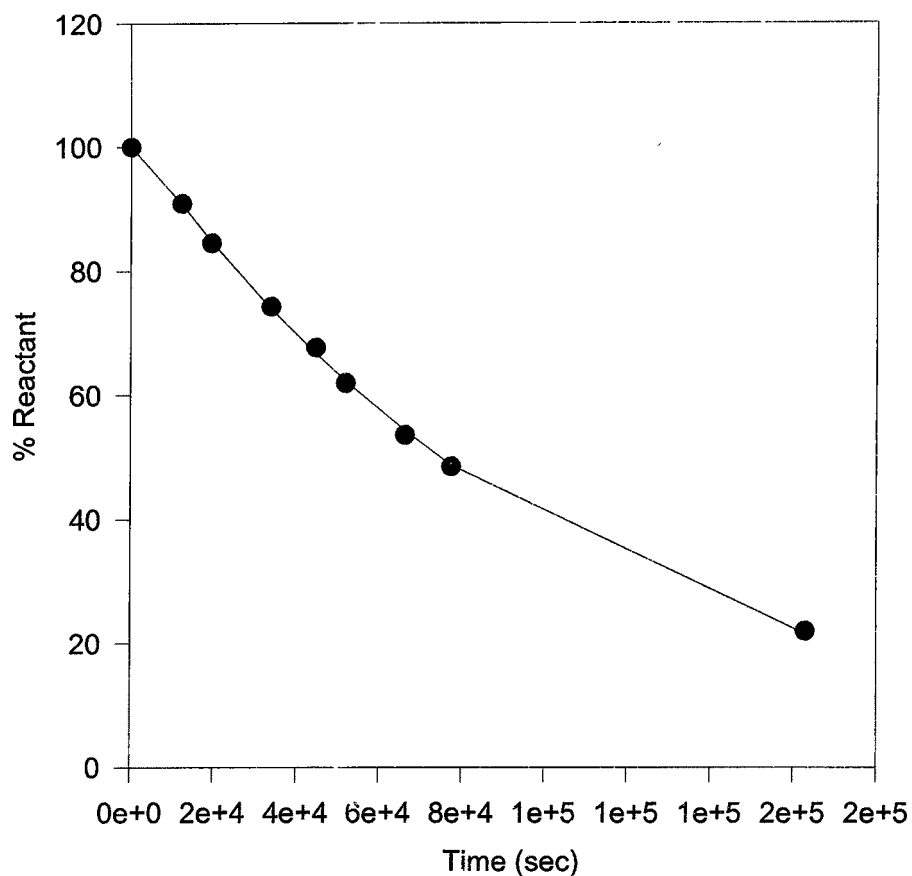
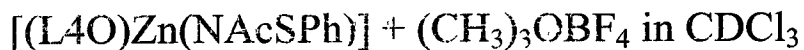
Graph 29. Exponential curve of the reaction as it goes to 100% completion. This reaction was run at 18mM with an excess of 10 equivalents of the MeI. The peaks at 1.43ppm and 1.28ppm were monitored for the data collection. Curve-fitting and rate determination was performed using SigmaPlot software.

[(L4O)Zn(NAcSPh)] + MeI in CD₃CN



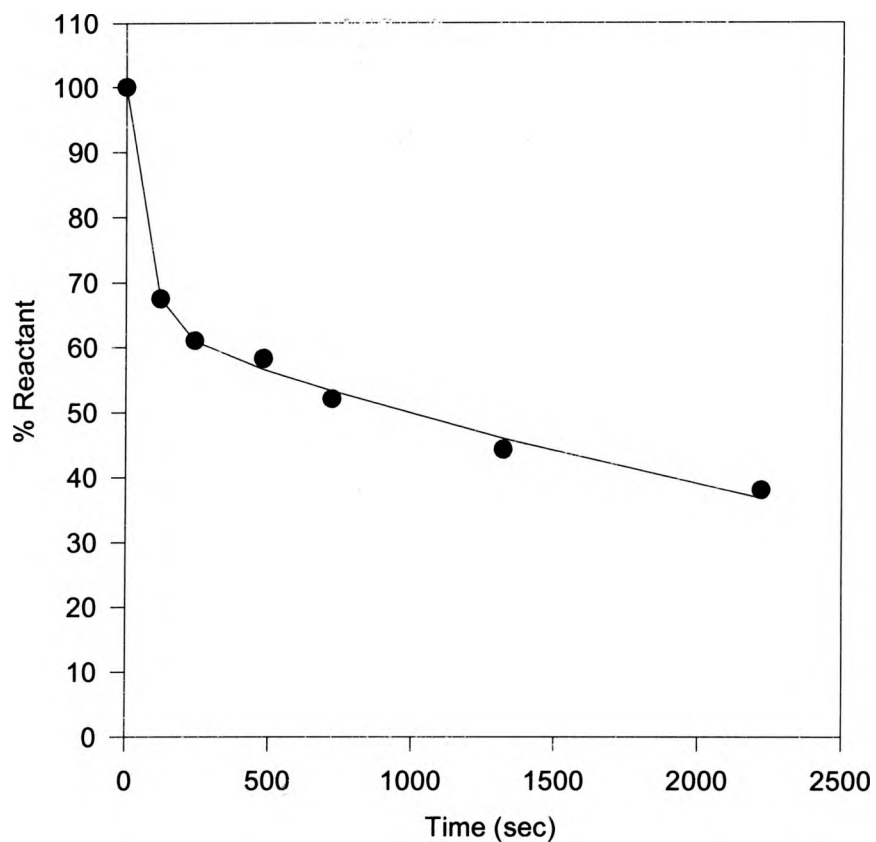
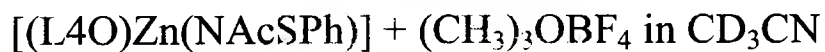
Time (sec)	% Product			Plot Values
0	0		-4.018	100.000
8700	4.73		5.190E-01	99.448
32400	11.38	Amplitude:	104.018	87.993
54000	19.58	Rate Constant:	5.164E-06	78.706
75600	25.78			70.399
168300	54.15			43.619
179700	59.68			41.125
337200	87.68			18.234

Graph 30. Exponential curve of the reaction as it goes to 100% completion. This reaction was run at 18mM with an excess of 10 equivalents of the MeI. The peaks at 1.4ppm and 1.35ppm were monitored for the data collection. Curve-fitting and rate determination was performed using SigmaPlot software.



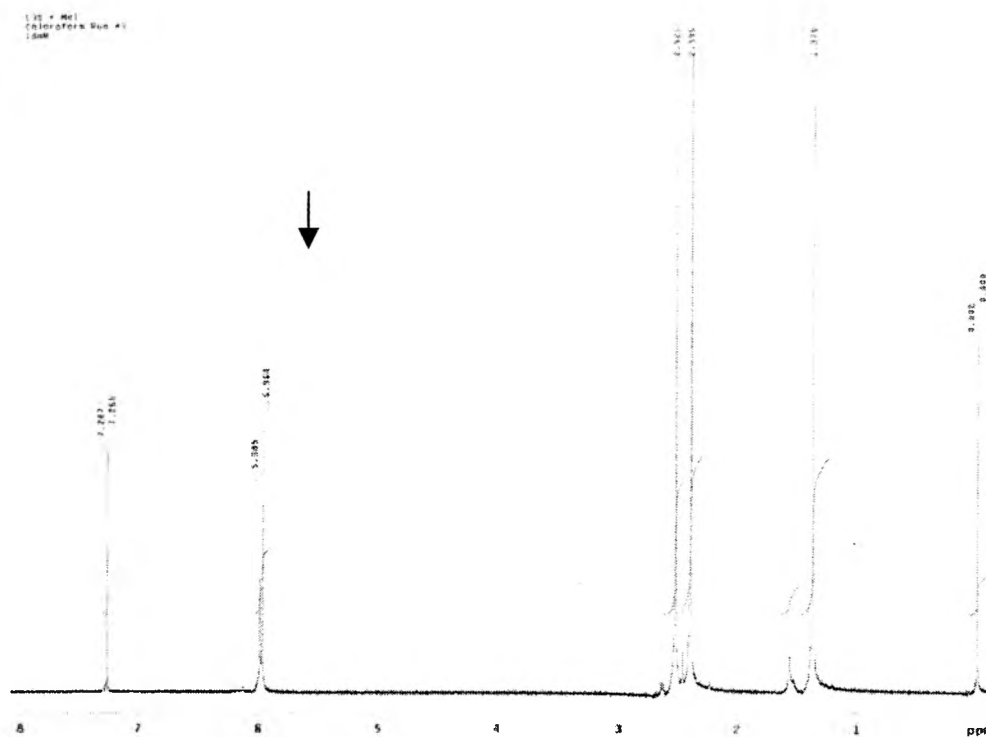
Time (sec)	% Product			Plot Values
0	0		-2.147	100.000
12300	9.13		1.080E+01	90.831
19500	15.51	Amplitude	102.147	84.799
33900	25.79	Rate Constant:	9.545E-06	73.908
44700	32.4			66.669
51900	38.11			62.241
66300	46.43			54.248
77400	51.45			48.794
162900	78.02			21.574

Graph 31. Exponential curve of the reaction as it goes to 100% completion. This reaction was run at 10mM with an excess of 5 equivalents of the $(CH_3)_3OBF_4$. The peaks at 8.06ppm and 6.86ppm were monitored for the data collection. Curve-fitting and rate determination was performed using SigmaPlot software.

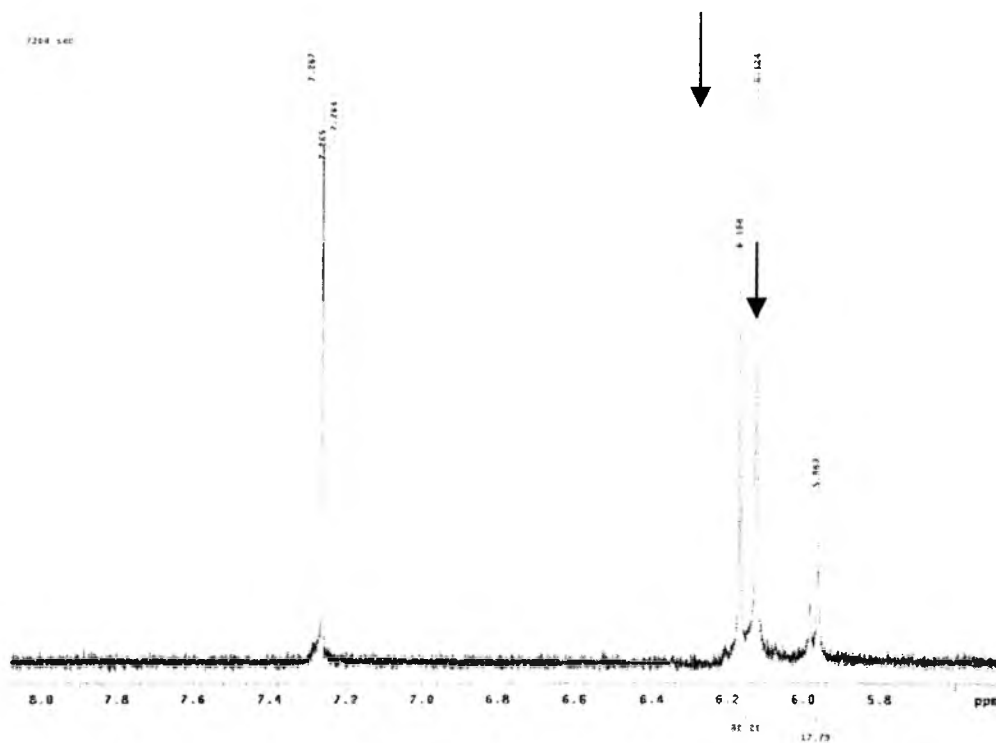


Time (sec)	% Product			Plot Values
0	0		36.259	99.995
120	32.46		1.539E-02	67.589
240	38.97	Amplitude:	63.737	60.957
480	41.72	Rate Constant:	2.480E-04	56.607
720	47.91			53.316
1320	55.74			45.945
2220	61.98			36.756

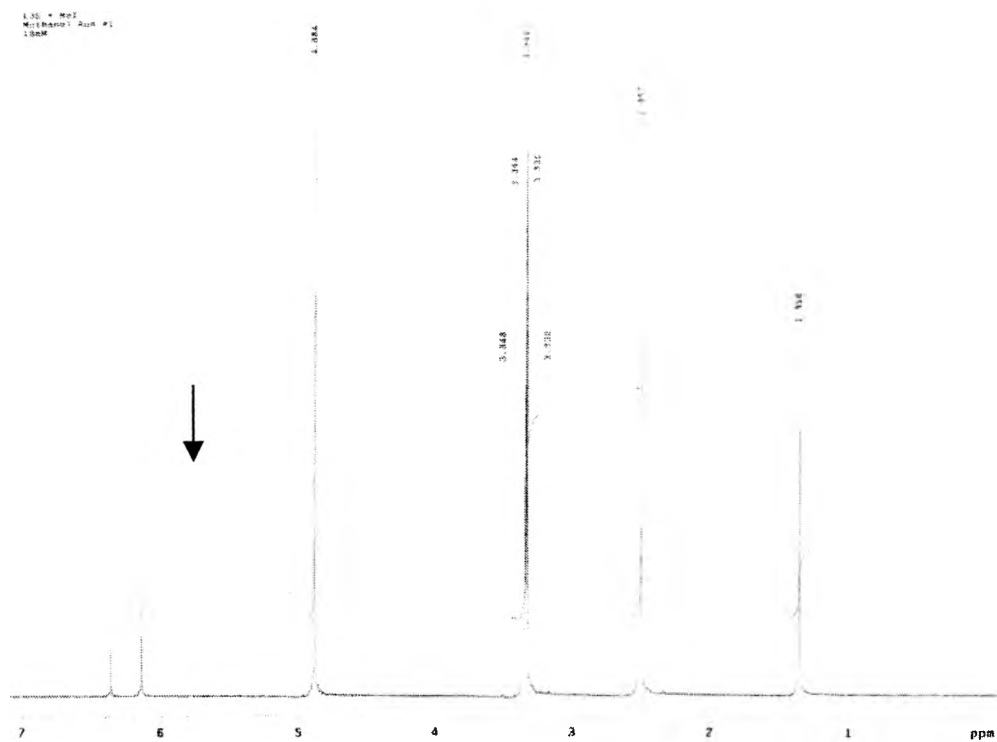
Graph 32. Exponential curve of the reaction as it goes to 100% completion. This reaction was run at 10mM with an excess of 5 equivalents of the $(CH_3)_3OBF_4$. The peaks at 7.23ppm and 8.60ppm were monitored for the data collection. Curve-fitting and rate determination was performed using SigmaPlot software.



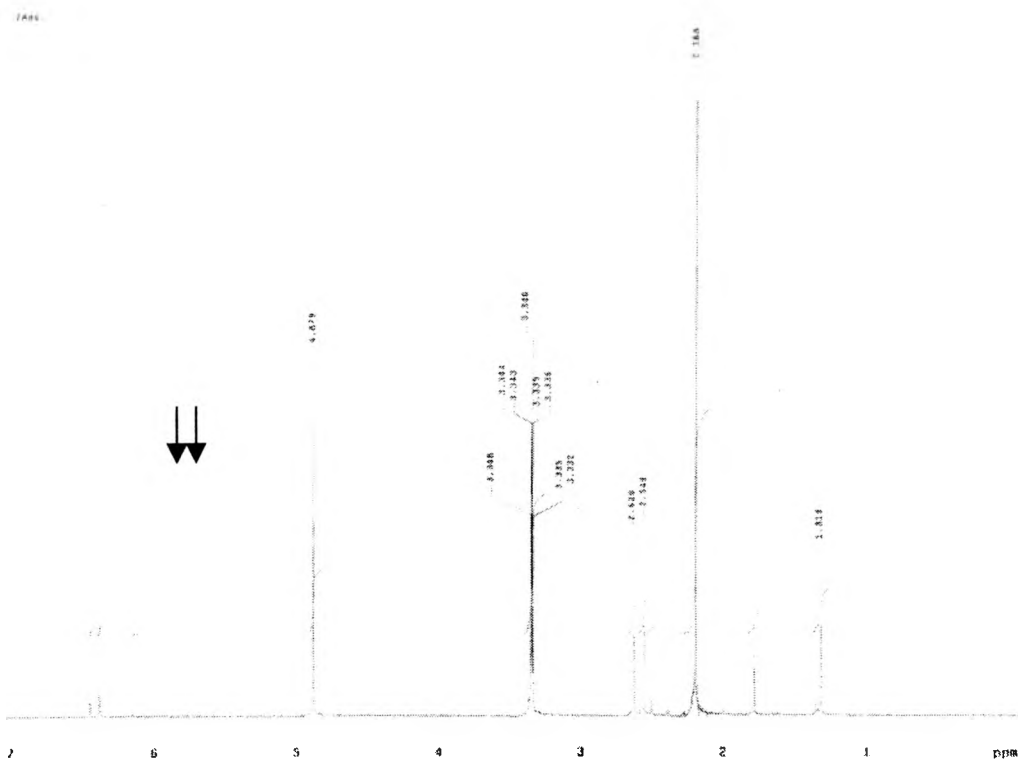
Spectra 1. [(L3S)ZnI] + MeI, chloroform, initial



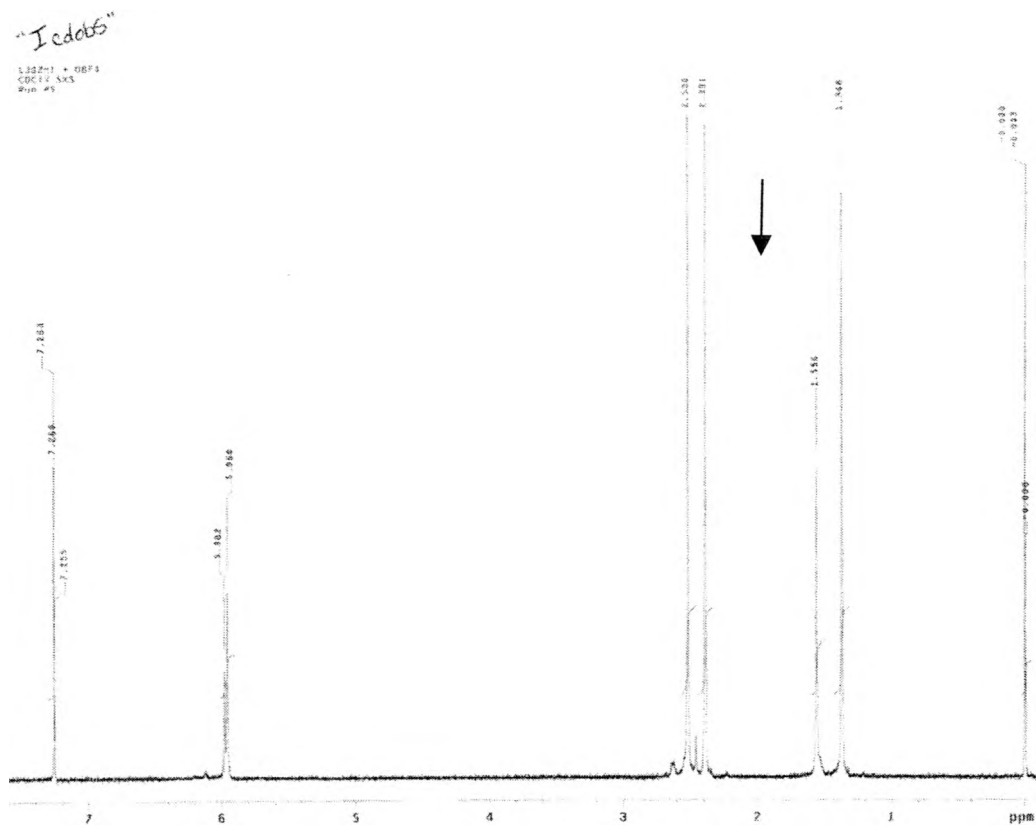
Spectra 2. [(L3S)ZnI] + MeI, chloroform, final



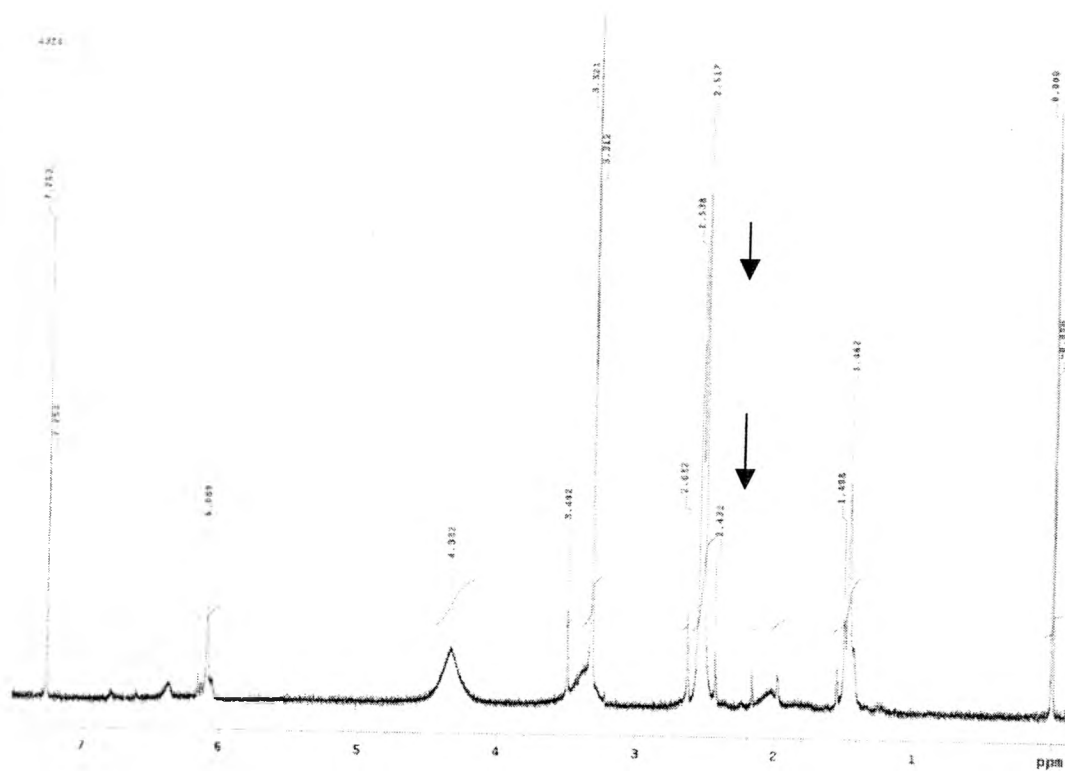
Spectra 5. [(L3S)ZnI] + MeI, methanol, initial



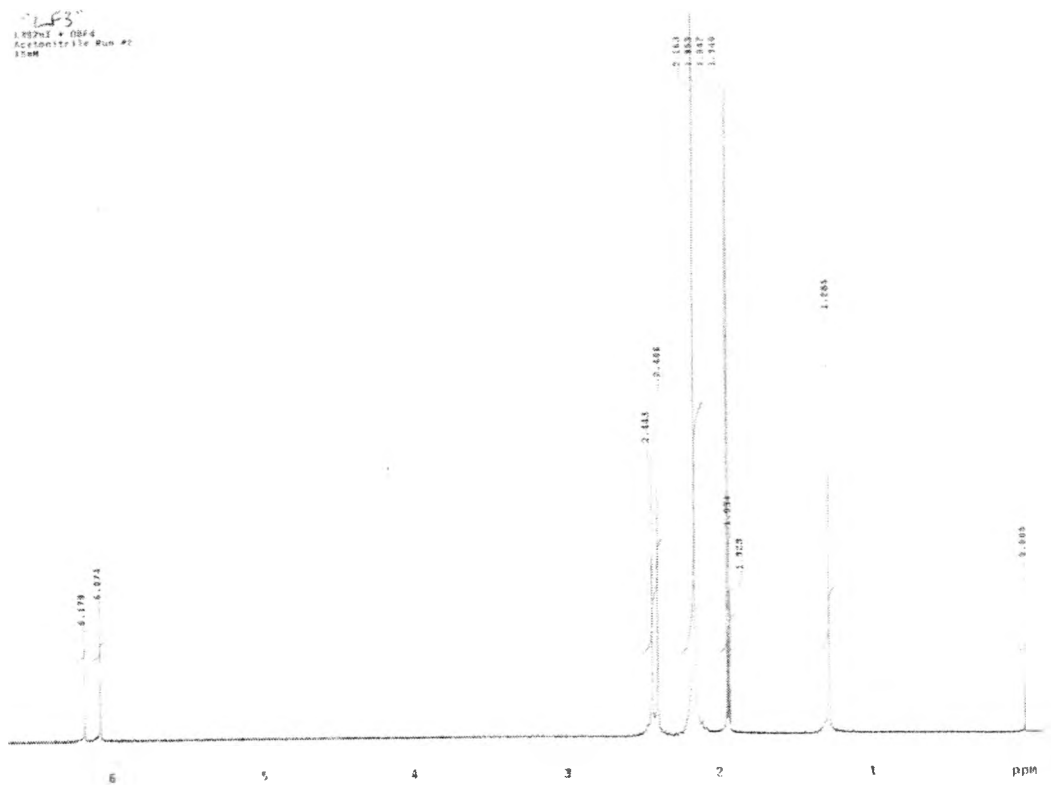
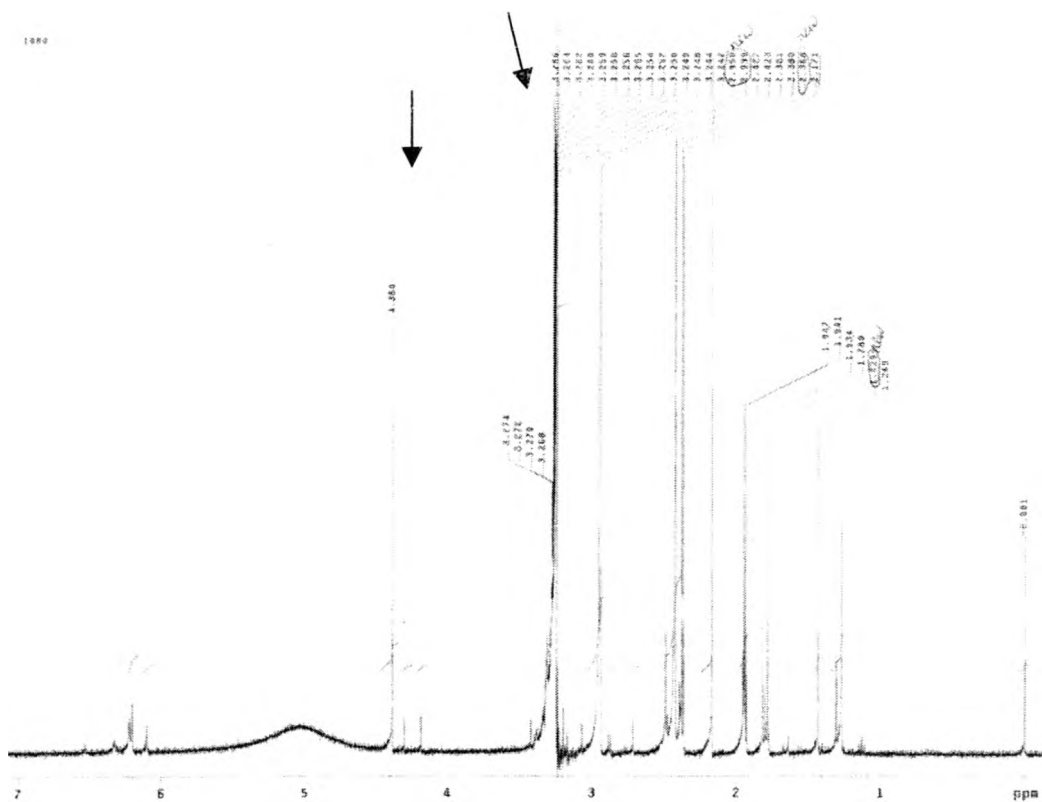
Spectra 6. [(L3S)ZnI] + MeI, methanol, final

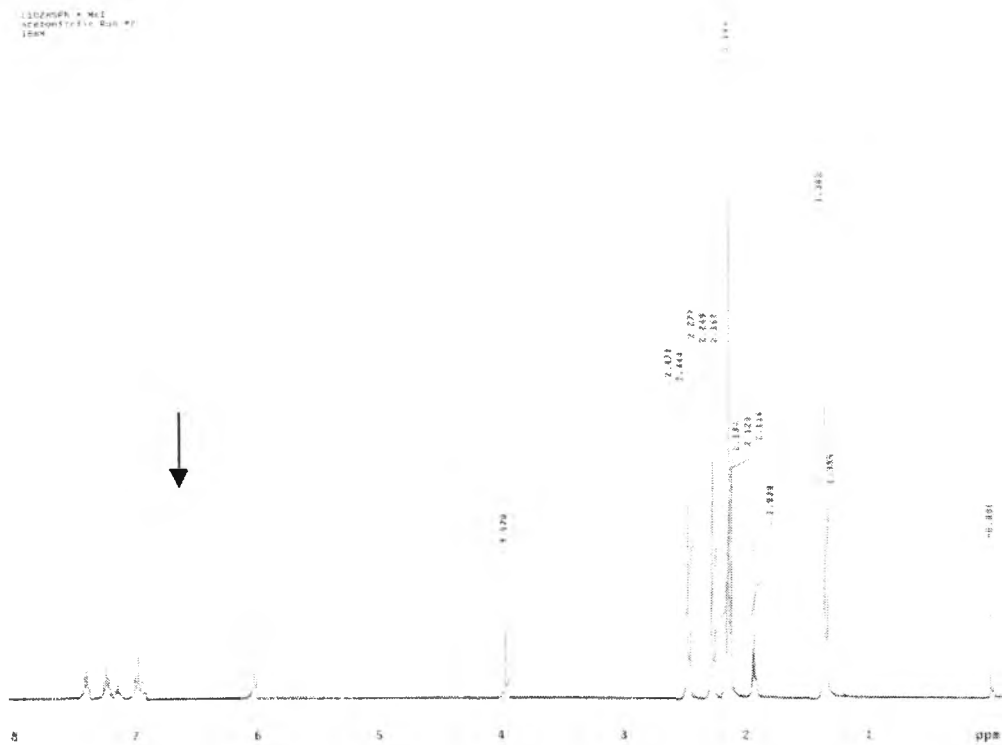


Spectra 7. [(L3S)ZnI] + (CH₃)₃OBF₄, chloroform, initial

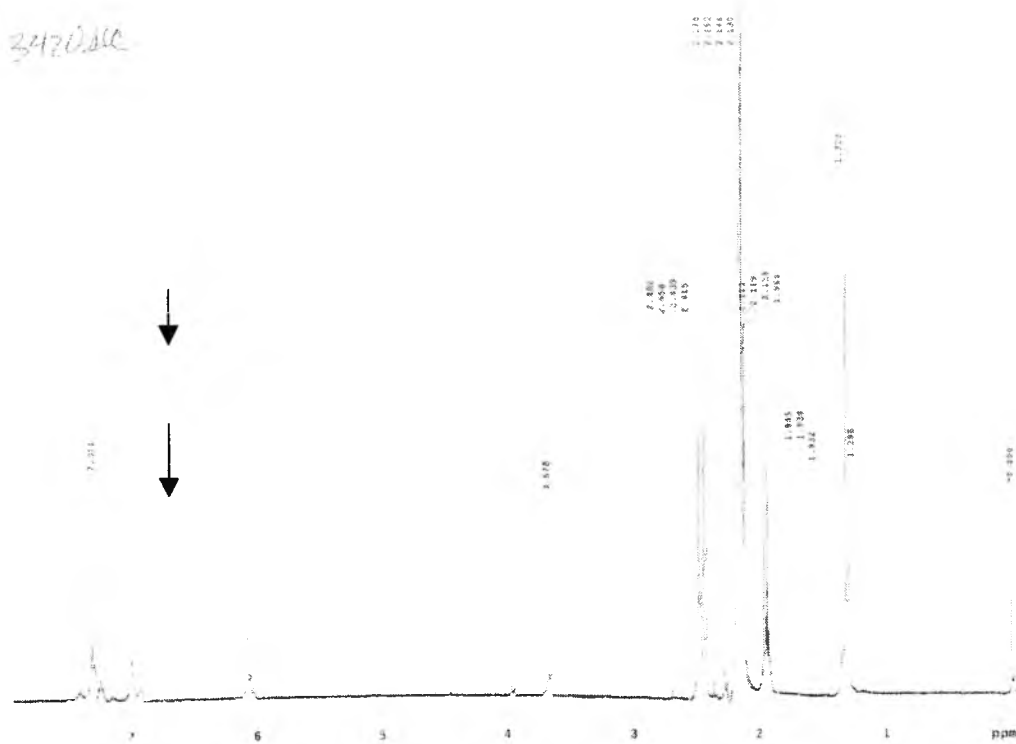


Spectra 8. [(L3S)ZnI] + (CH₃)₃OBF₄, chloroform, final

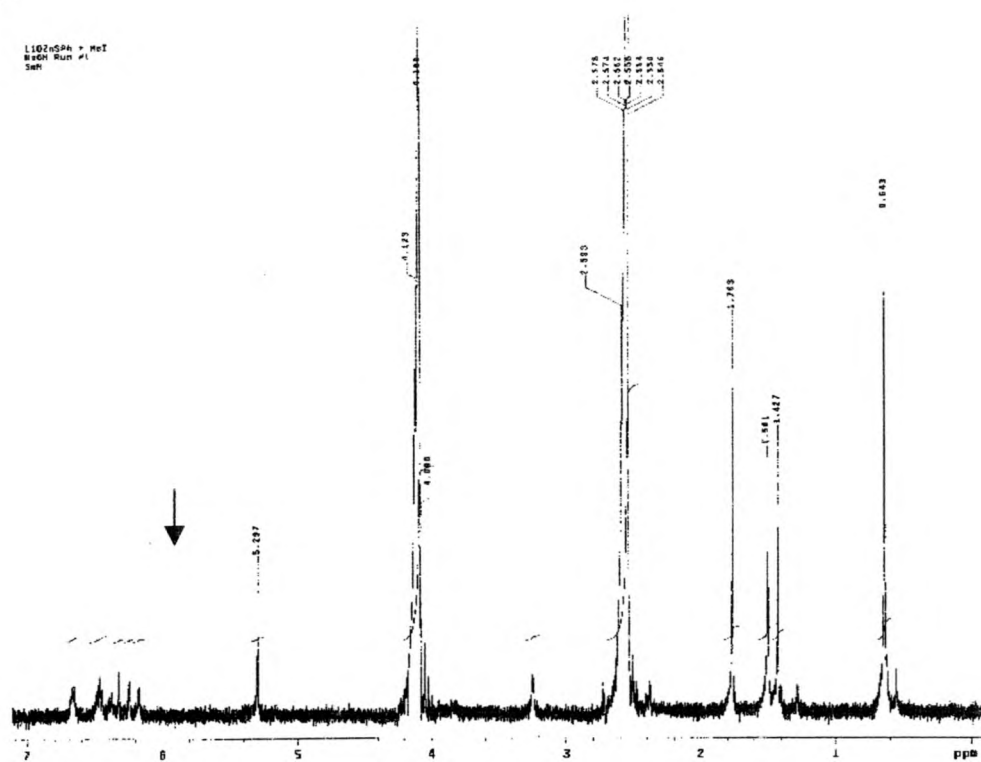
Spectra 9. [(L3S)ZnI] + (CH₃)₃OBF₄, acetonitrile, initialSpectra 10. [(L3S)ZnI] + (CH₃)₃OBF₄, acetonitrile, final



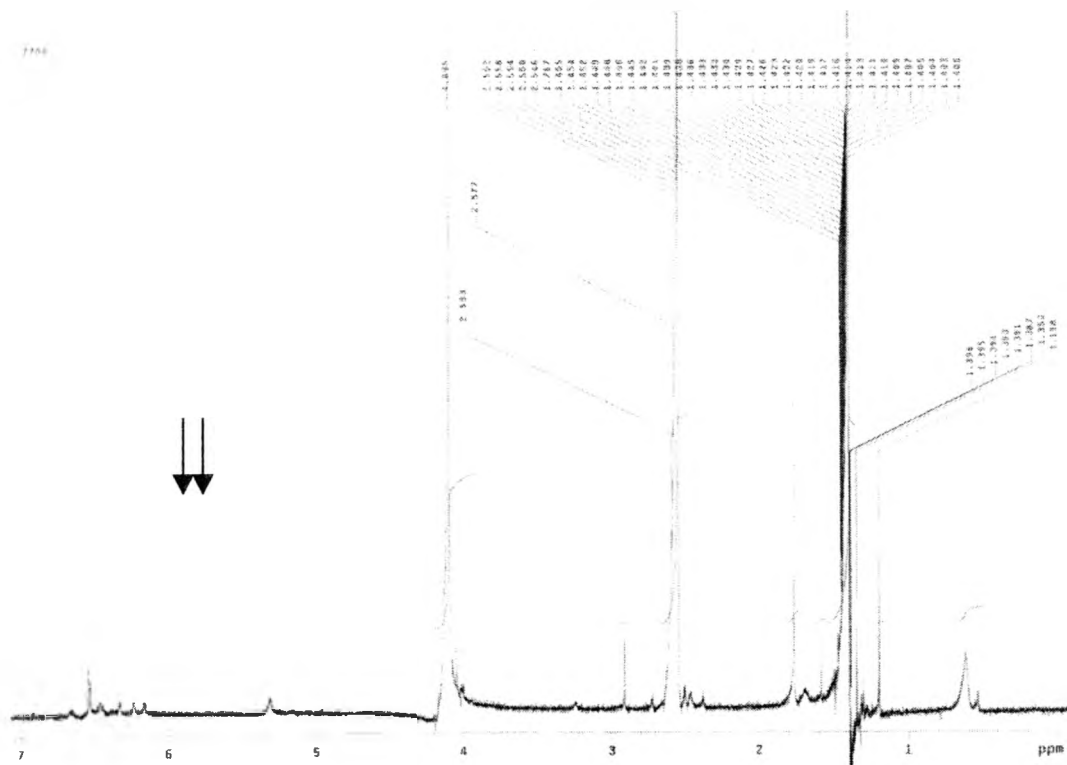
Spectra 15. $[(L1O)Zn(SPh)] + MeI$, acetonitrile, initial

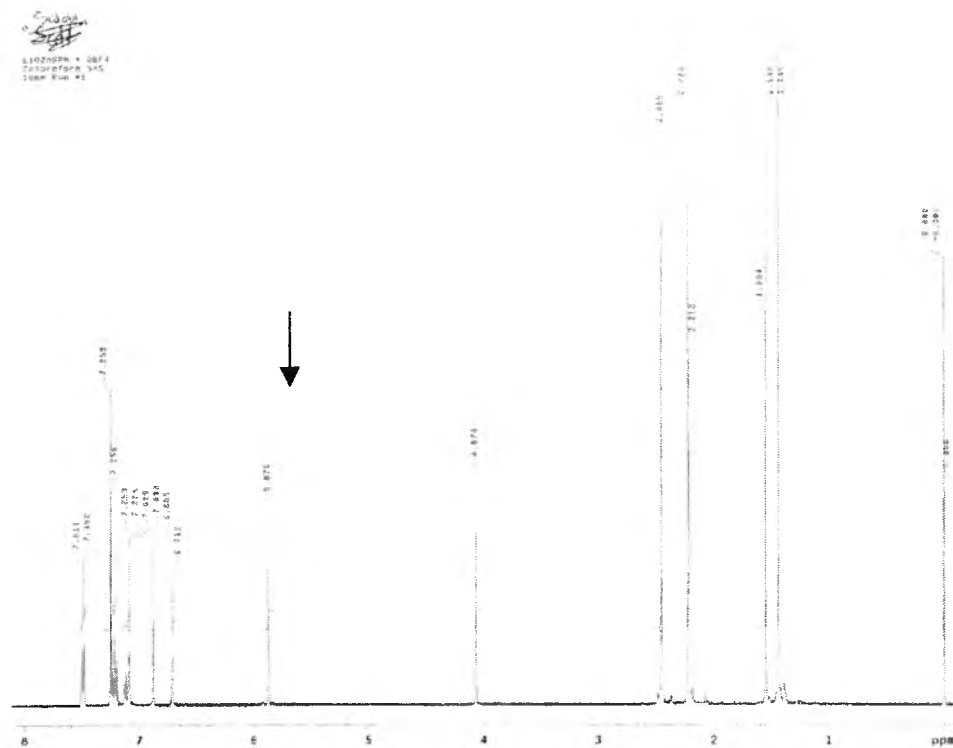


Spectra 16. $[(L1O)Zn(SPh)] + MeI$, acetonitrile, final

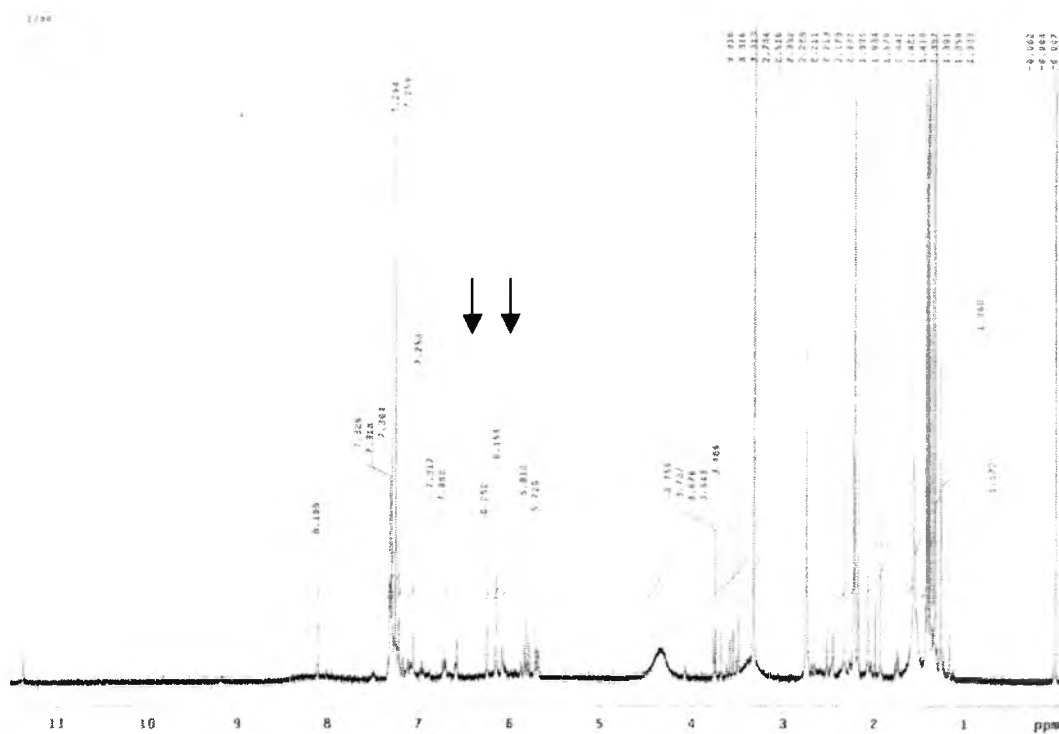


Spectra 17. [(L1O)Zn(NAcSPh)] + MeI, chloroform, initial

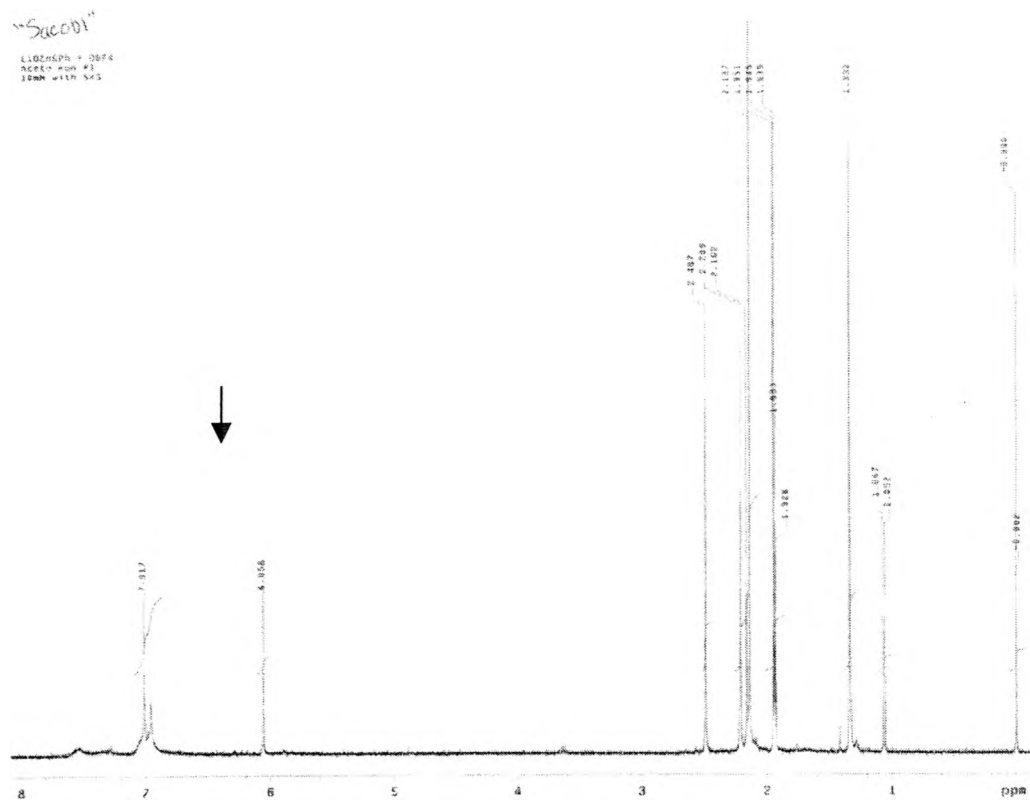




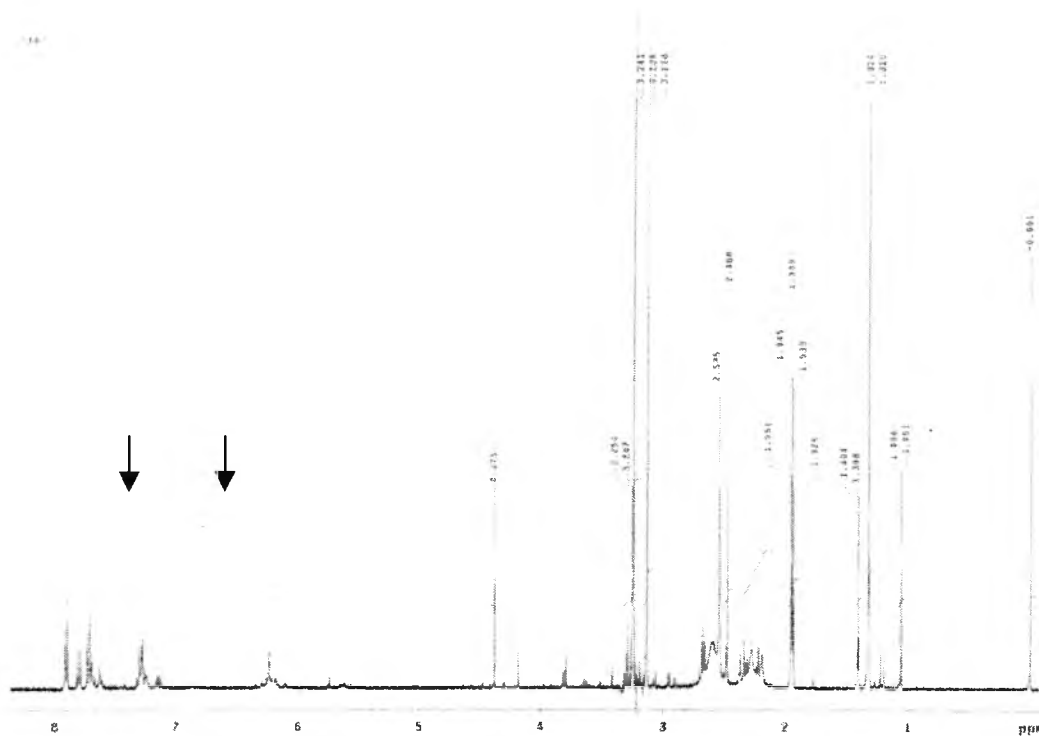
Spectra 19. [(L1O)Zn(SPh)] + (CH₃)₃OBF₄, chloroform, initial



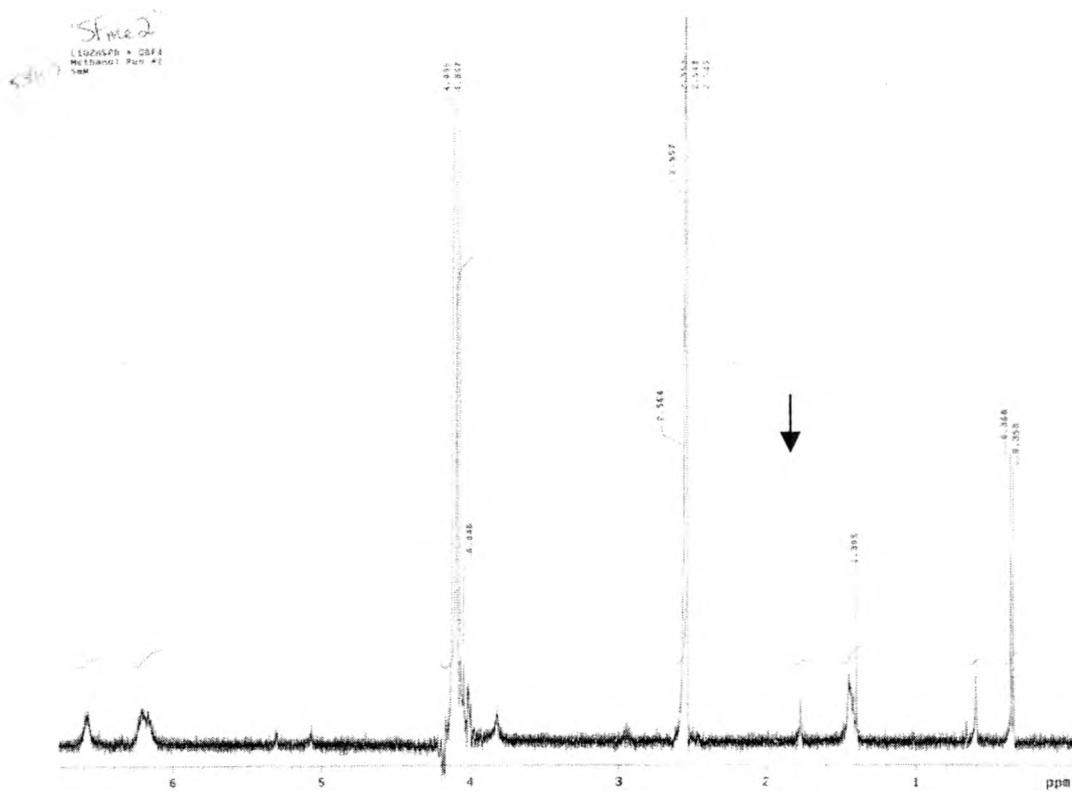
Spectra 20. [(L1O)Zn(SPh)] + (CH₃)₃OBF₄, chloroform, final



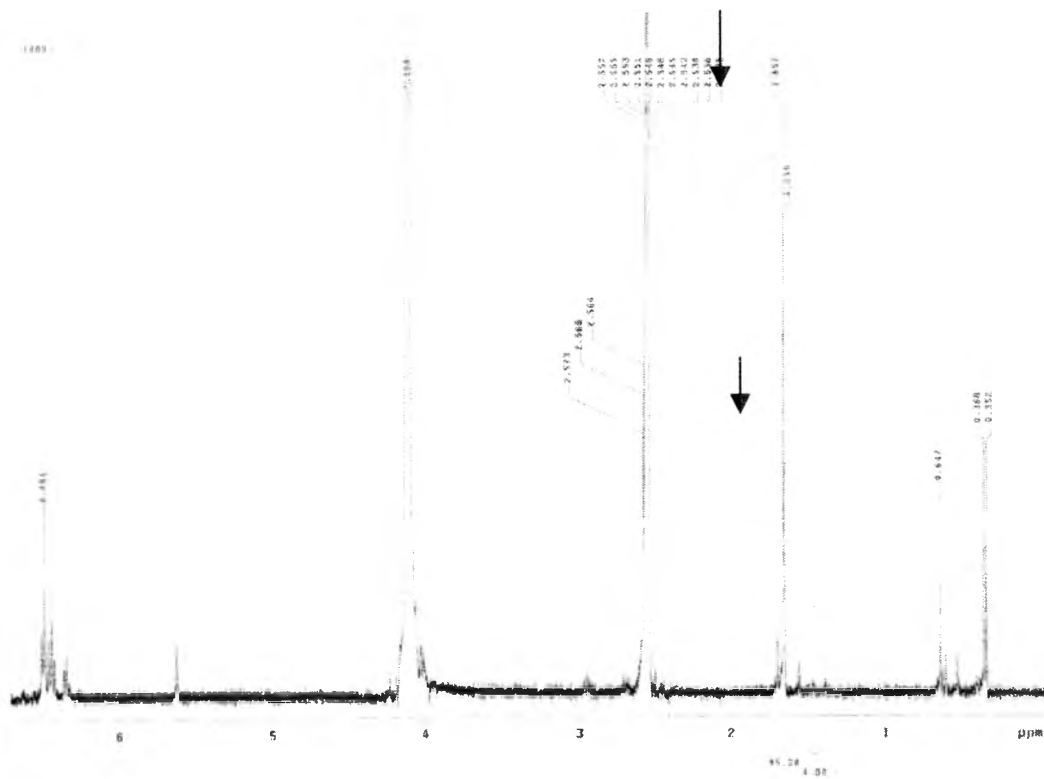
Spectra 21. $[(L1O)Zn(SPh)] + (CH_3)_3OBF_4$, acetonitrile, initial



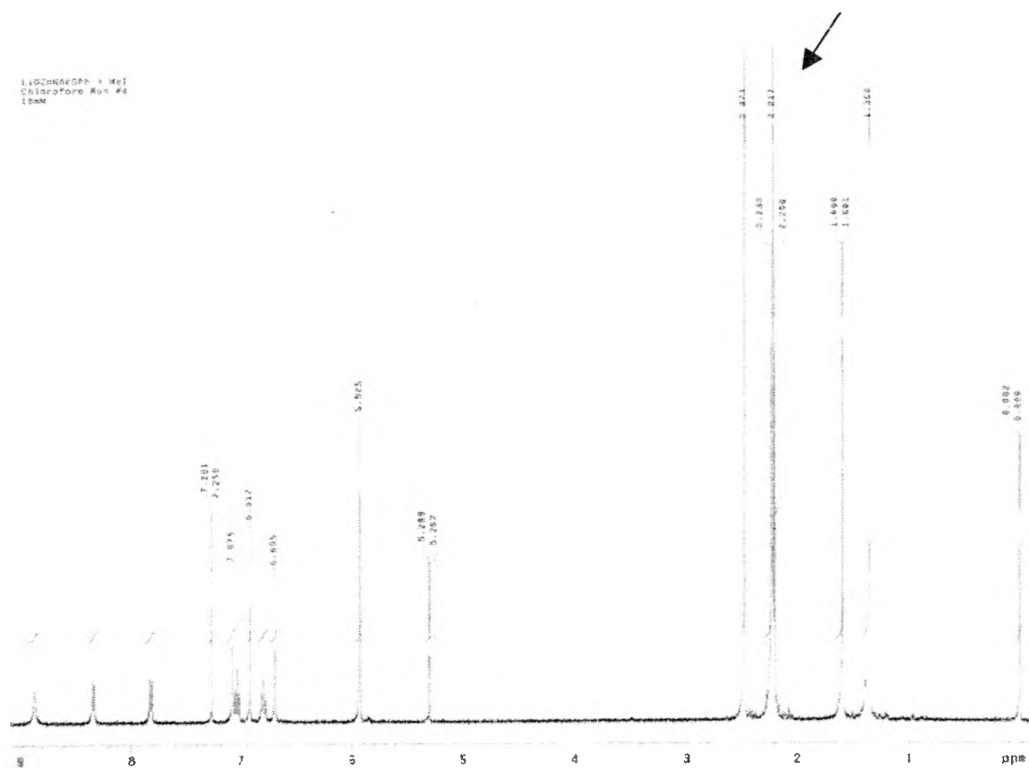
Spectra 22. $[(L1O)Zn(SPh)] + (CH_3)_3OBF_4$, acetonitrile, final



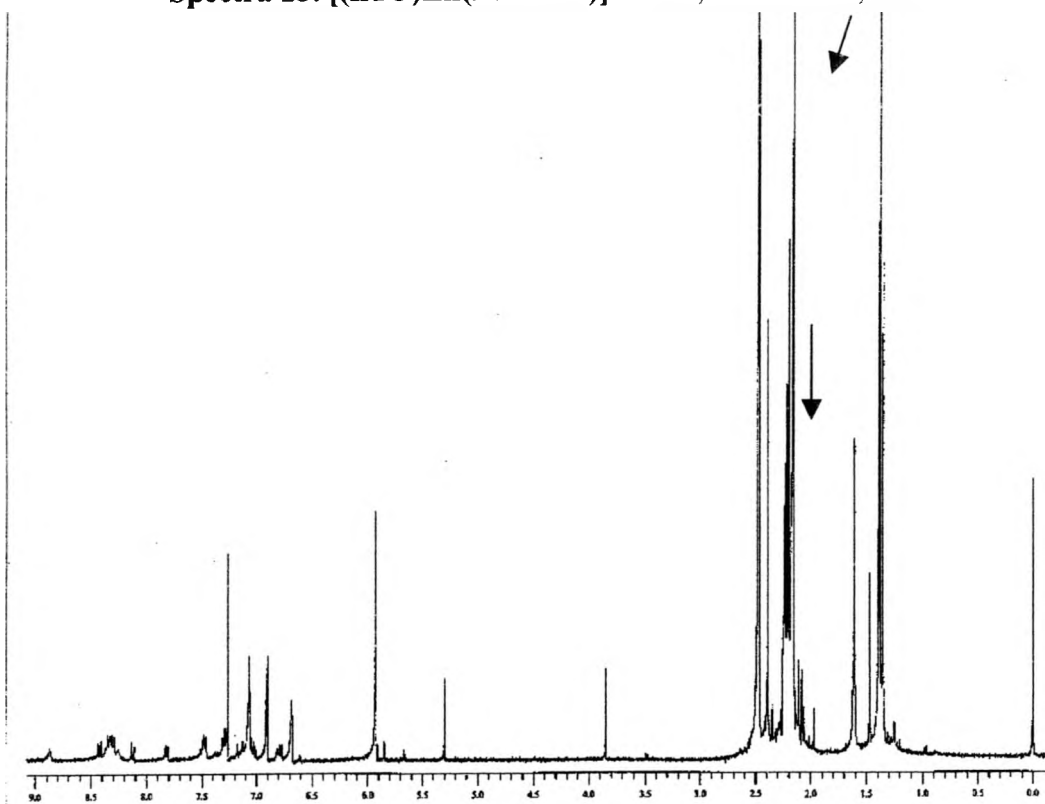
Spectra 23. [(L1O)Zn(SPh)] + (CH₃)₃OBF₄, methanol, initial



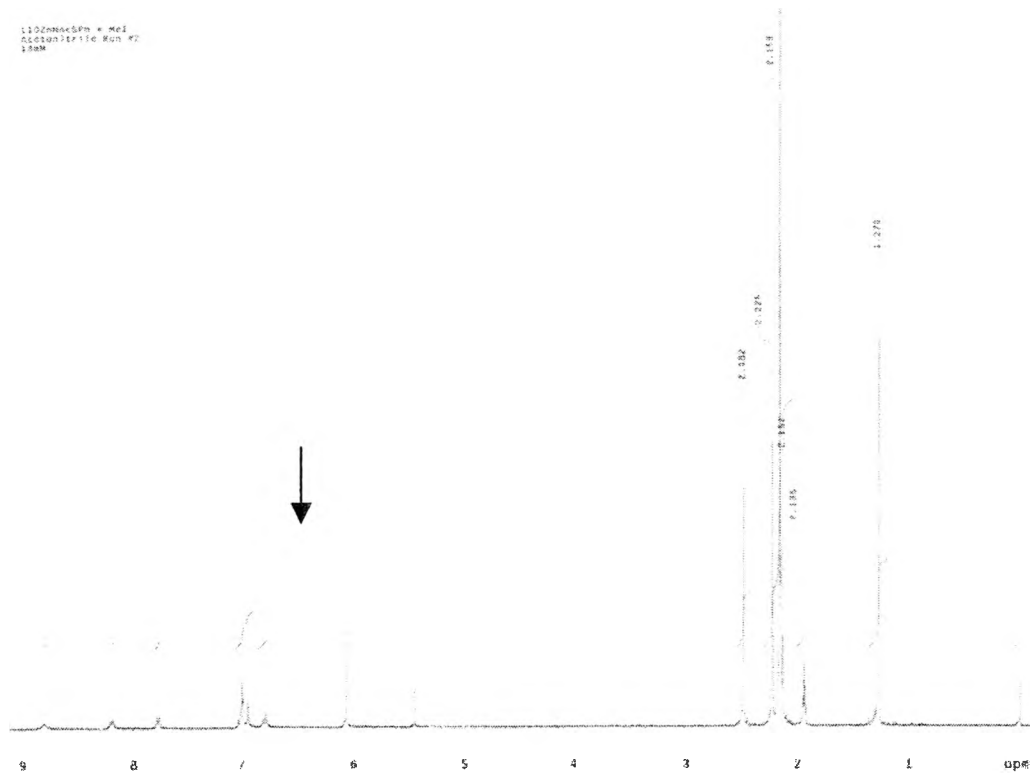
Spectra 24. [(L1O)Zn(SPh)] + (CH₃)₃OBF₄, methanol, final



Spectra 25. [(L1O)Zn(NAcSPH)] + MeI, chloroform, initial

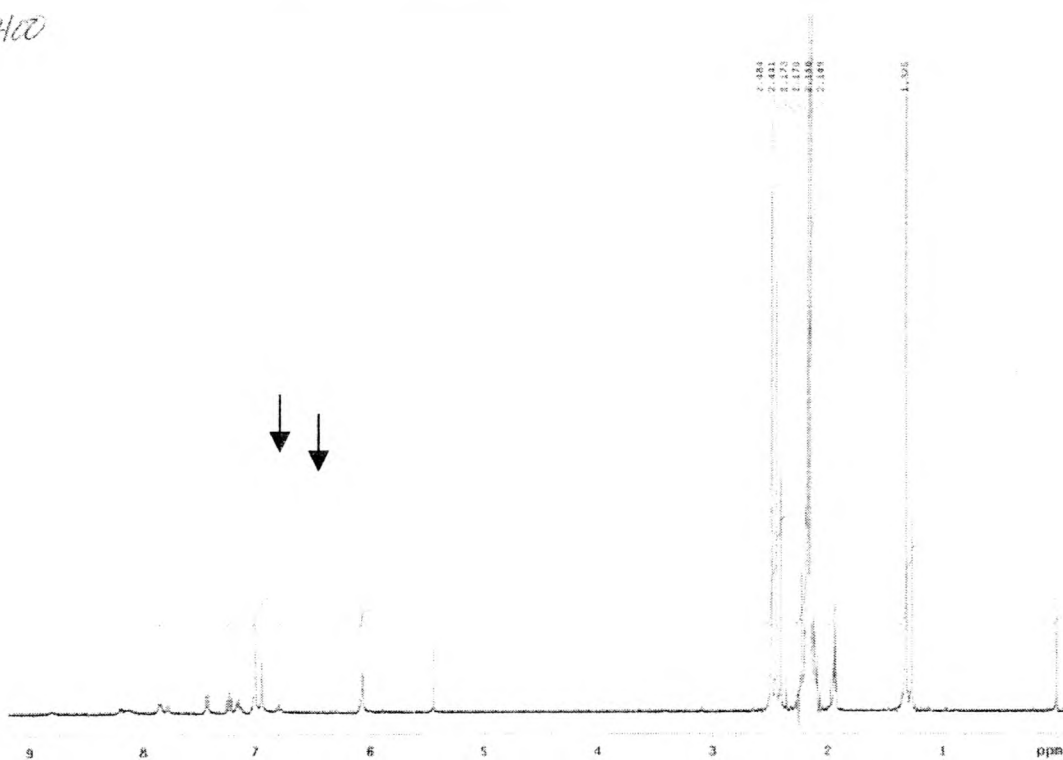


Spectra 26. [(L1O)Zn(NAcSPH)] + MeI, chloroform, final

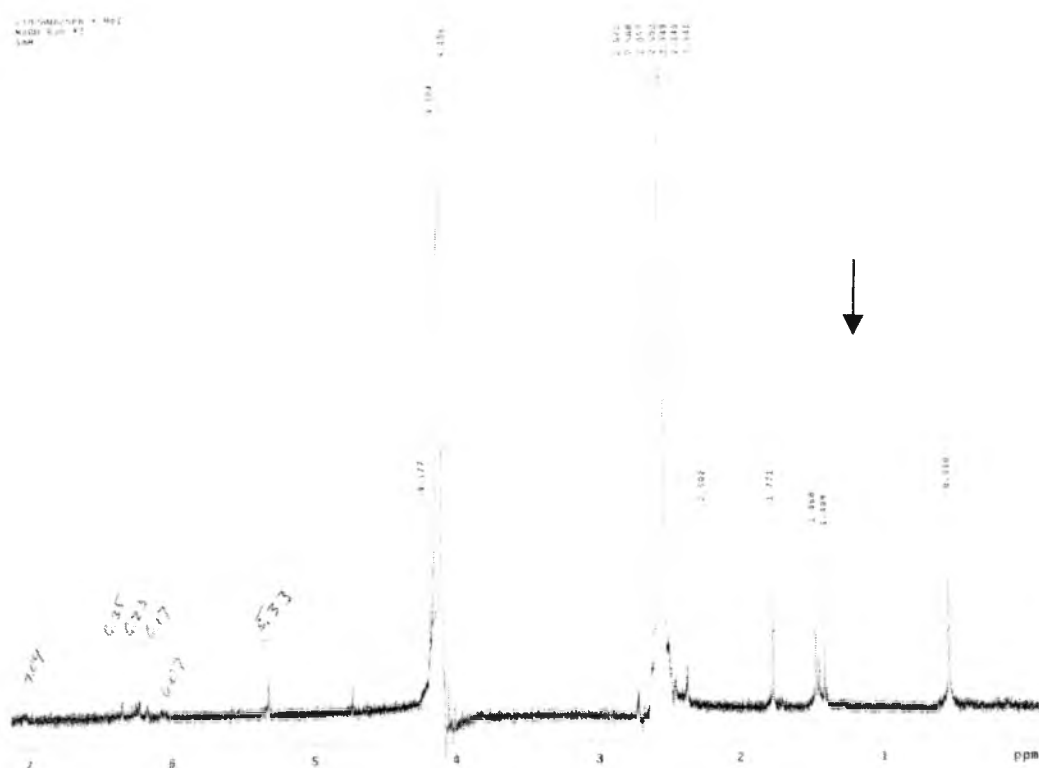


Spectra 27. [(L1O)Zn(NAcSPh)] + MeI, acetonitrile, initial

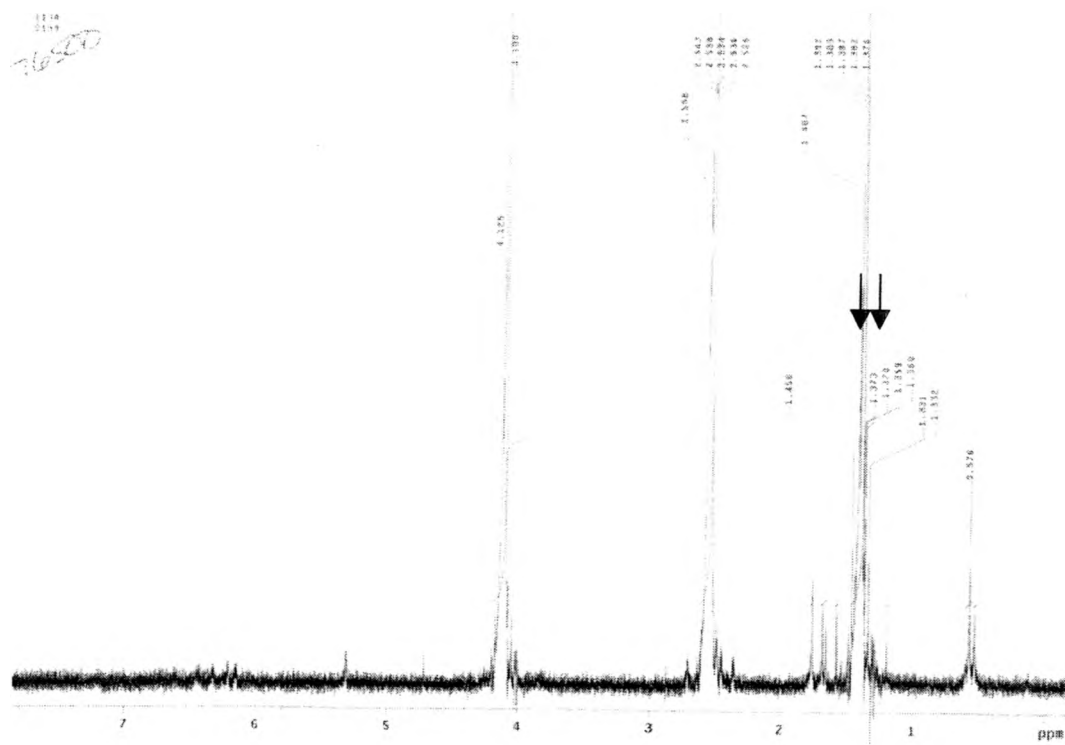
594100



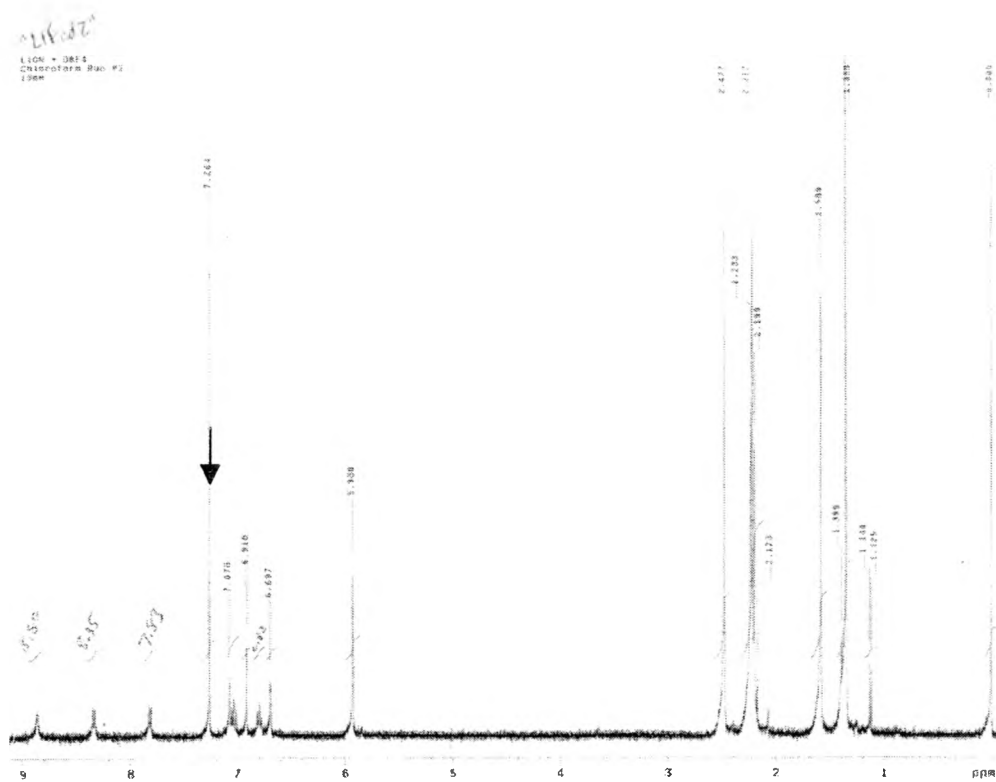
Spectra 28. [(L1O)Zn(NAcSPh)] + MeI, acetonitrile, final



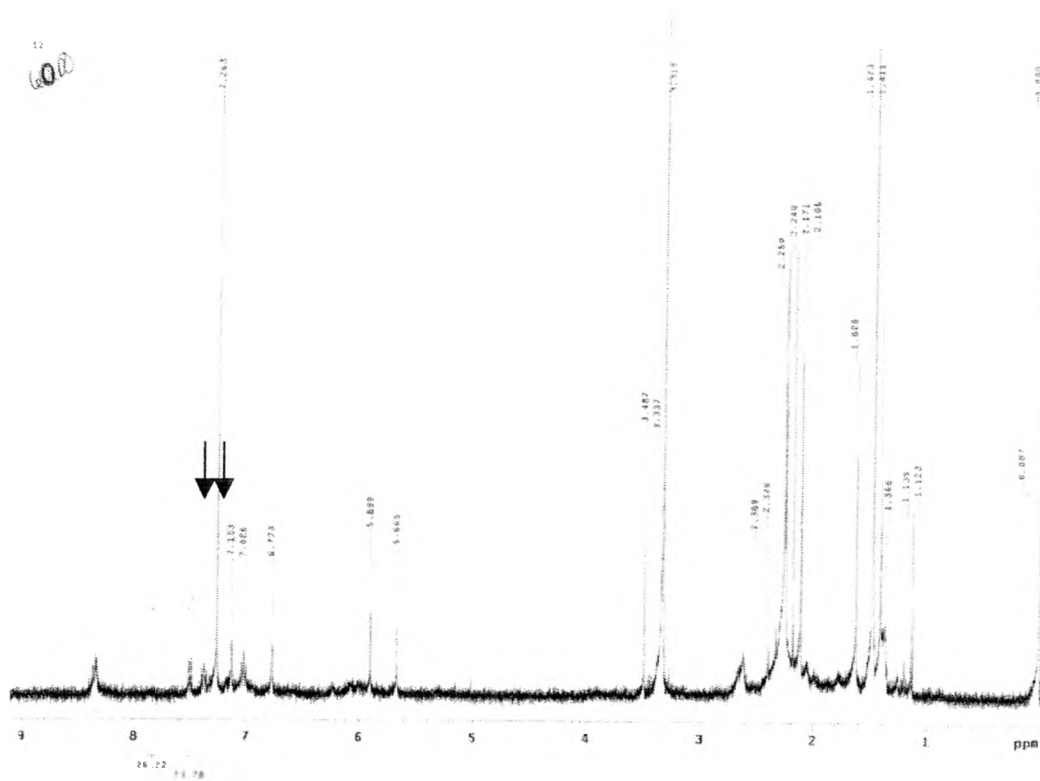
Spectra 29. $[(L1O)Zn(NAcSPh)] + MeI$, methanol, initial



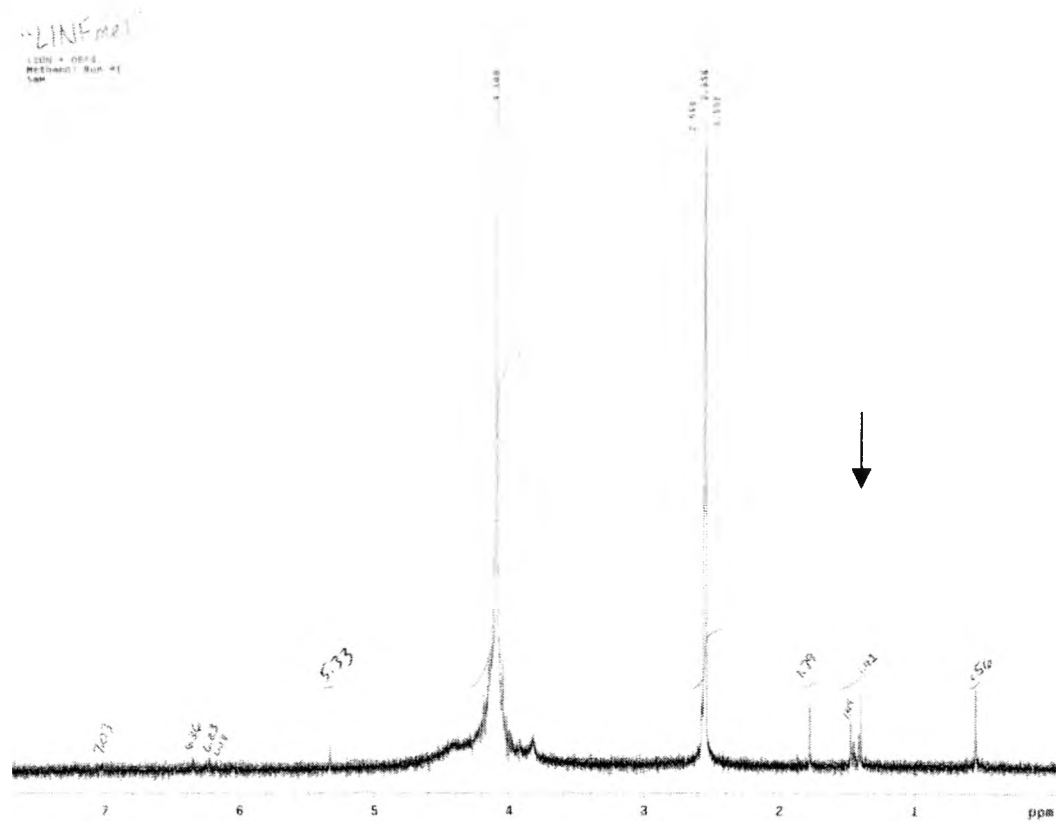
Spectra 30. $[(L1O)Zn(NAcSPh)] + MeI$, methanol, final



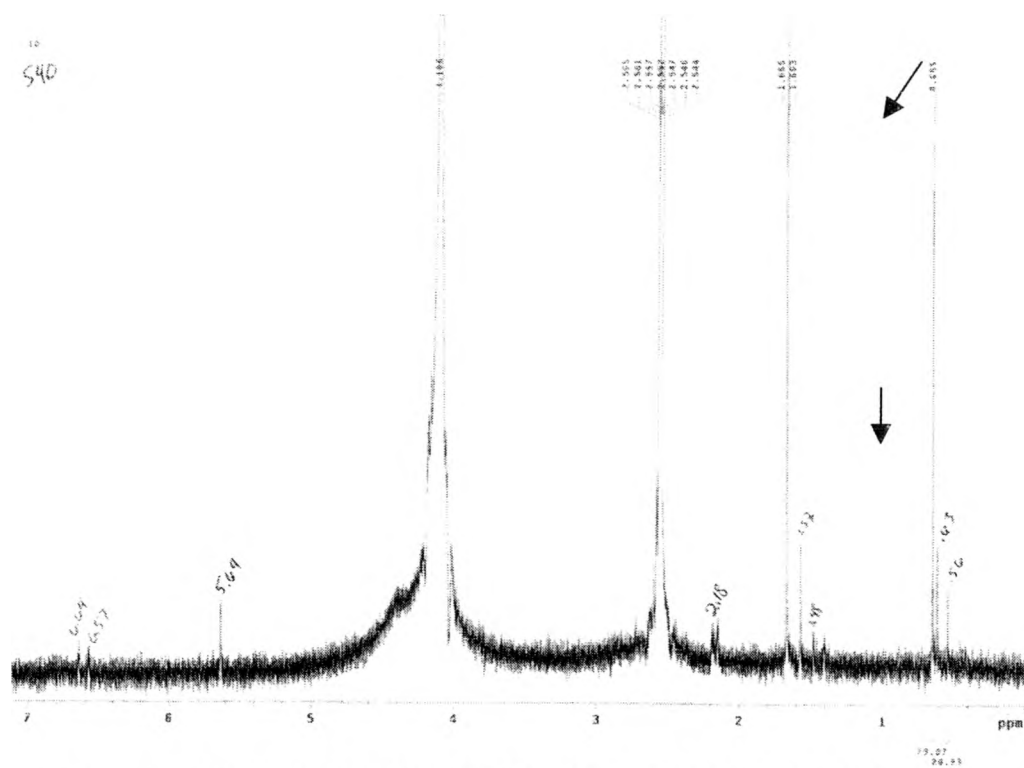
Spectra 31. [(L1O)Zn(NAcSPh)] + (CH₃)₃OBF₄, chloroform, initial



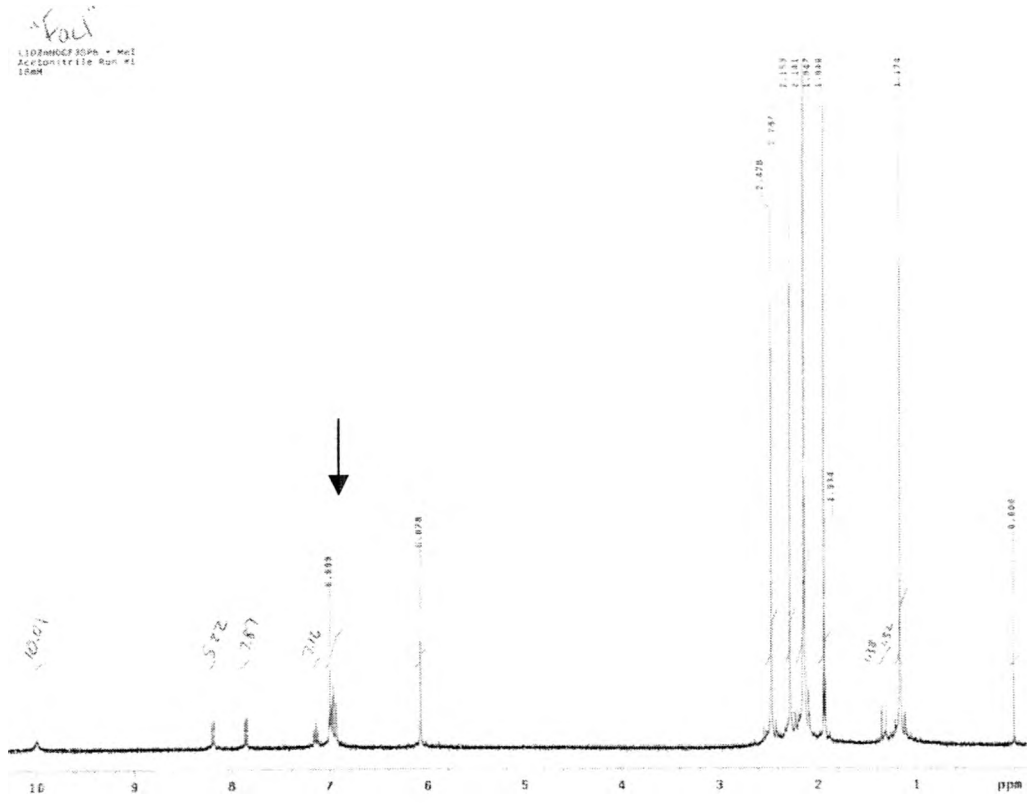
Spectra 32. [(L1O)Zn(NAcSPh)] + (CH₃)₃OBF₄, chloroform, final



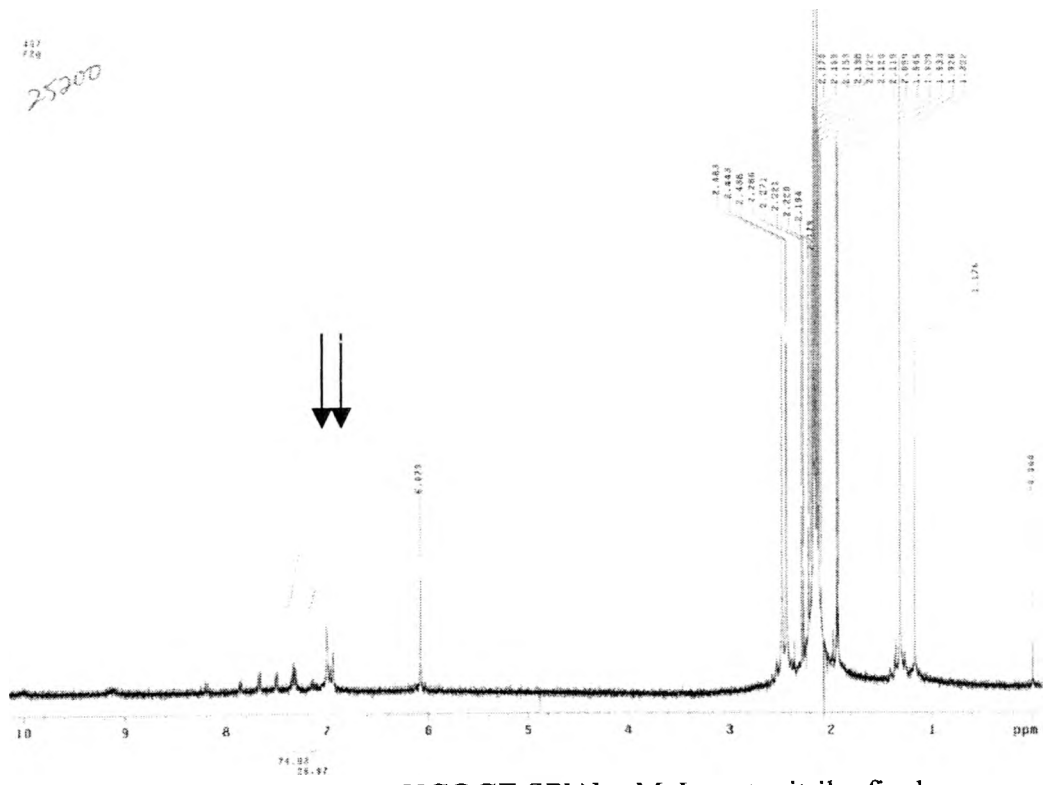
Spectra 35. $[(L1O)Zn(NAcSPh)] + (CH_3)_3OBF_4$, methanol, initial



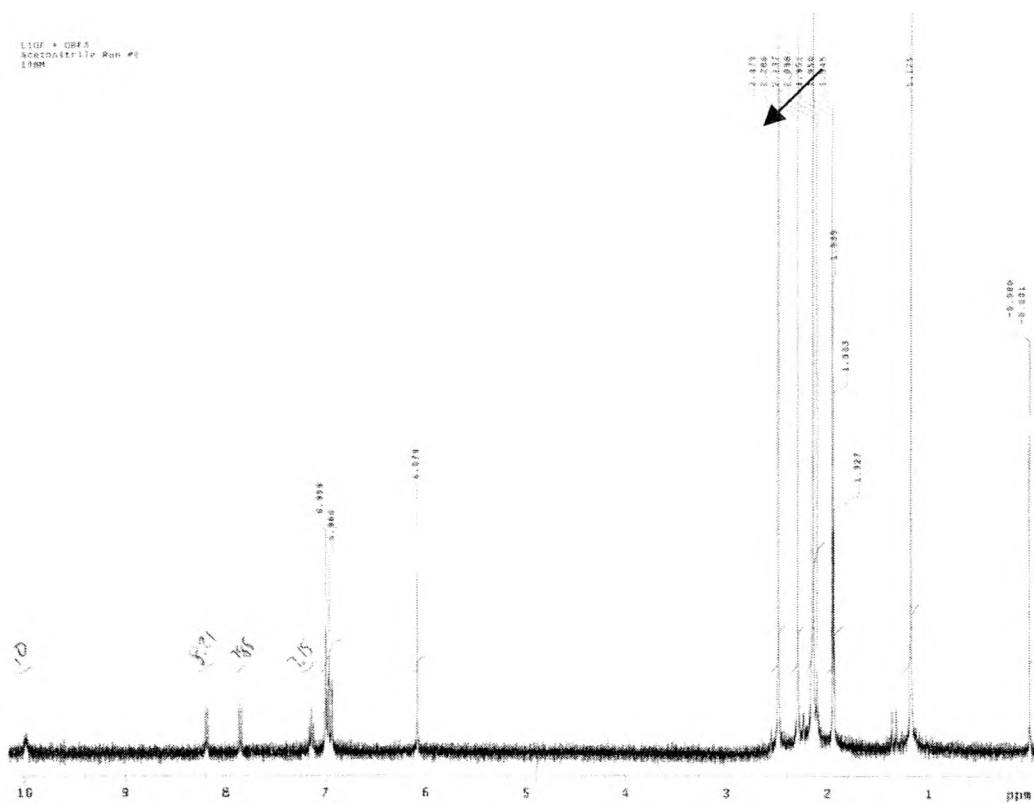
Spectra 36. $[(L1O)Zn(NAcSPh)] + (CH_3)_3OBF_4$, methanol, final



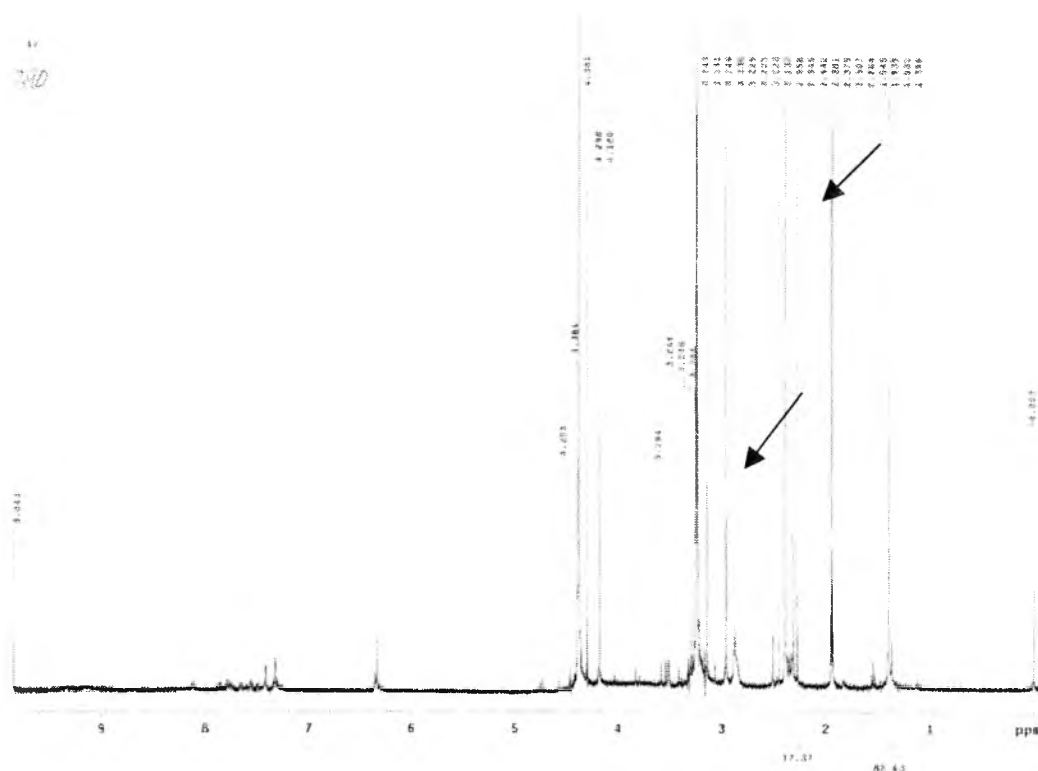
Spectra 39. [(L1O)Zn(NCOCF₃SPh)] + MeI, acetonitrile, initial



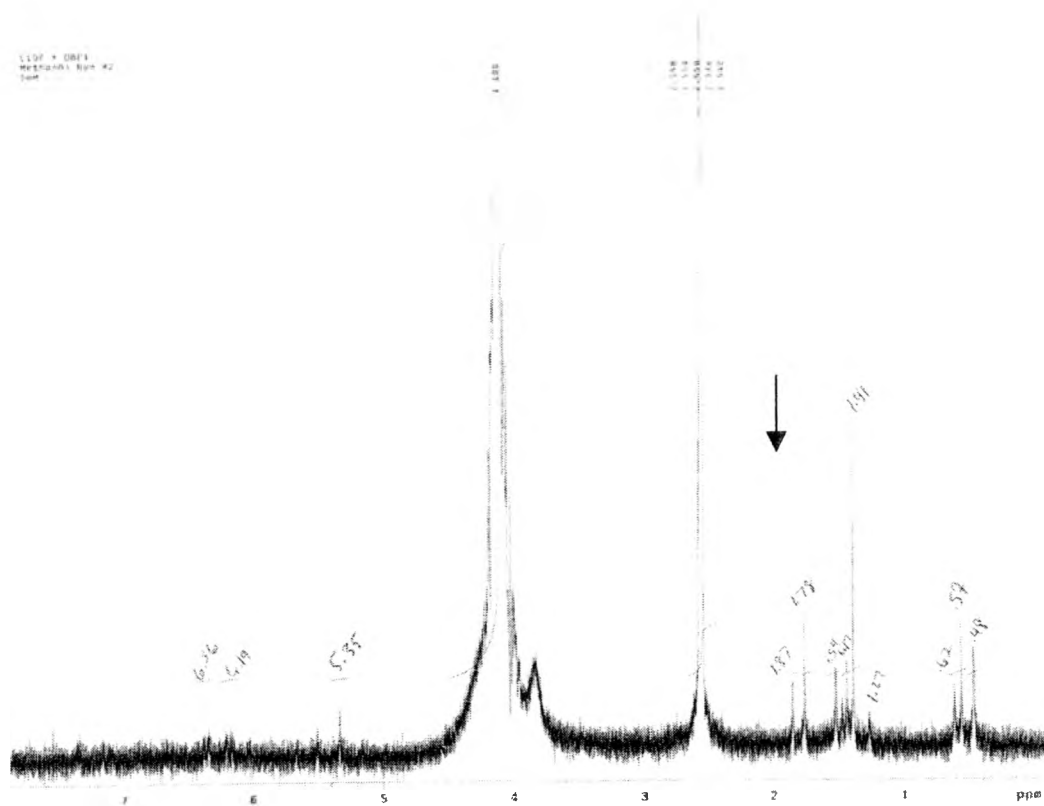
Spectra 40. [(L1O)Zn(NCOCF₃SPh)] + MeI, acetonitrile, final



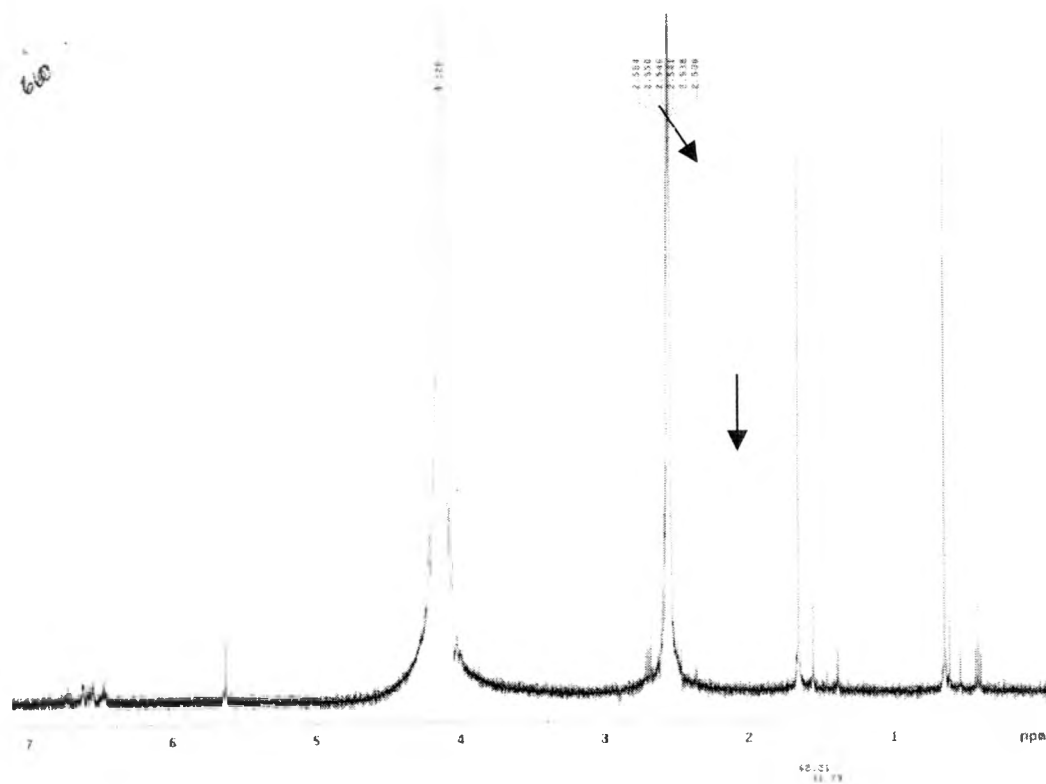
Spectra 45. [(L1O)Zn(NCOCF₃SPh)] + (CH₃)₃OBF₄, acetonitrile, initial



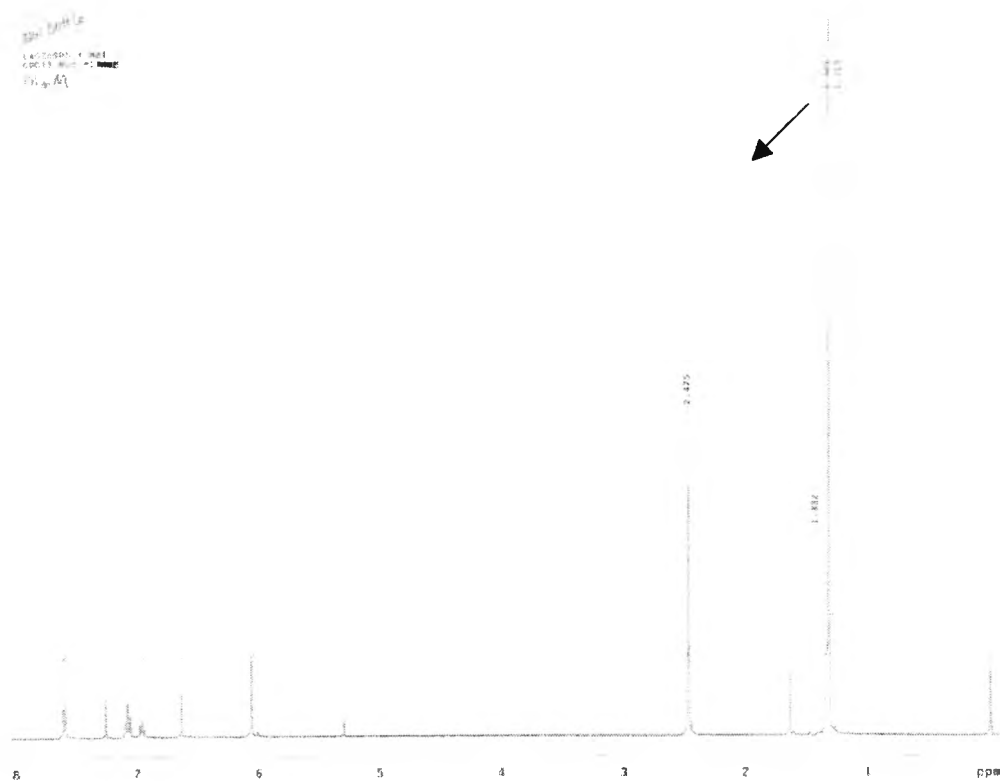
Spectra 46. [(L1O)Zn(NCOCF₃SPh)] + (CH₃)₃OBF₄, acetonitrile, final



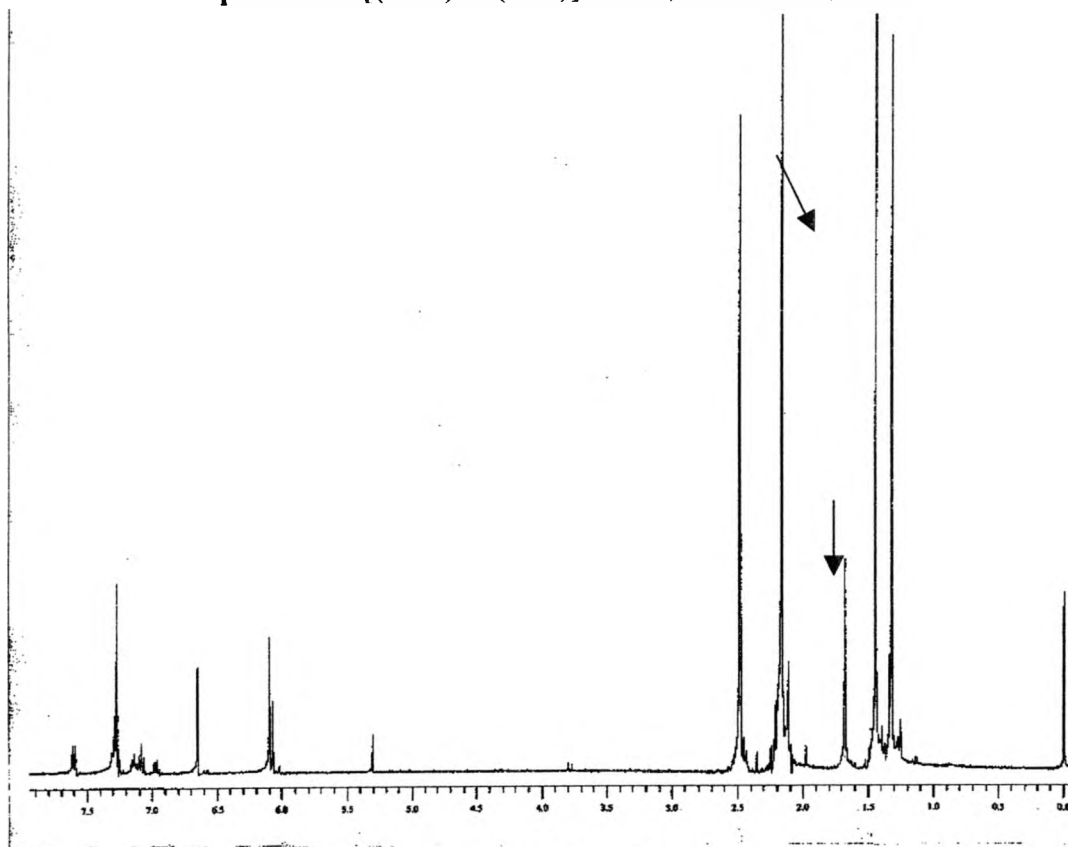
Spectra 47. [(L1O)Zn(NCOCF₃SPh)] + (CH₃)₃OBF₄, methanol, initial



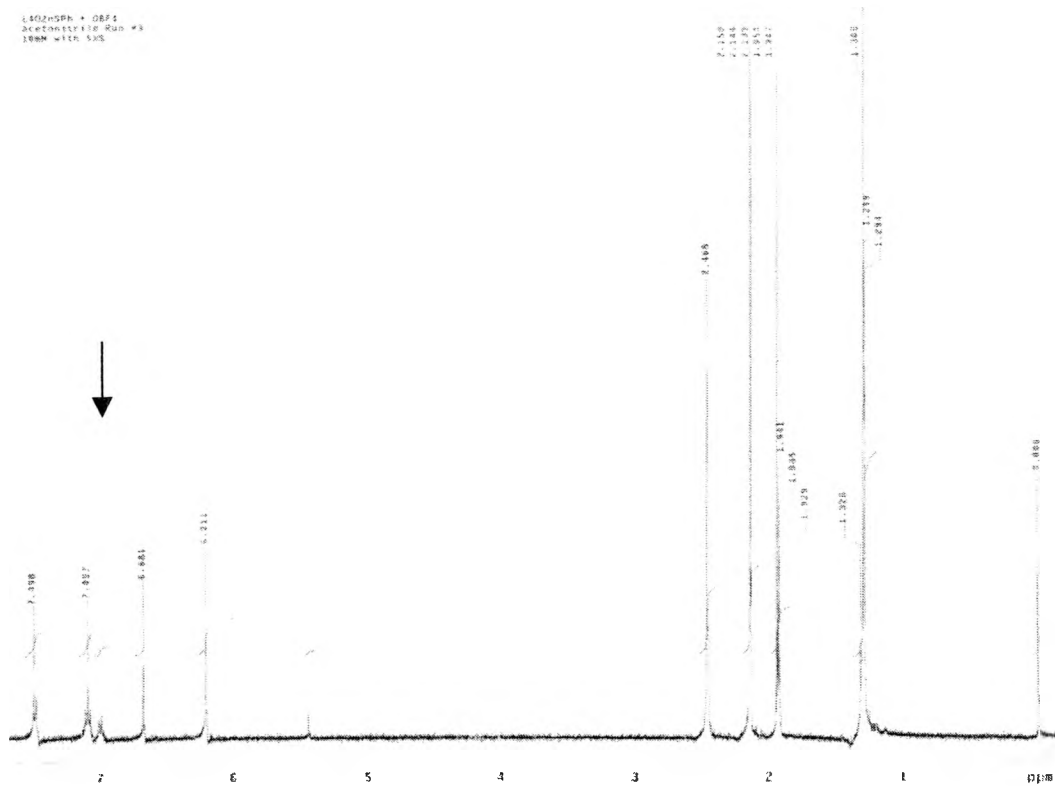
Spectra 48. [(L1O)Zn(NCOCF₃SPh)] + (CH₃)₃OBF₄, methanol, final



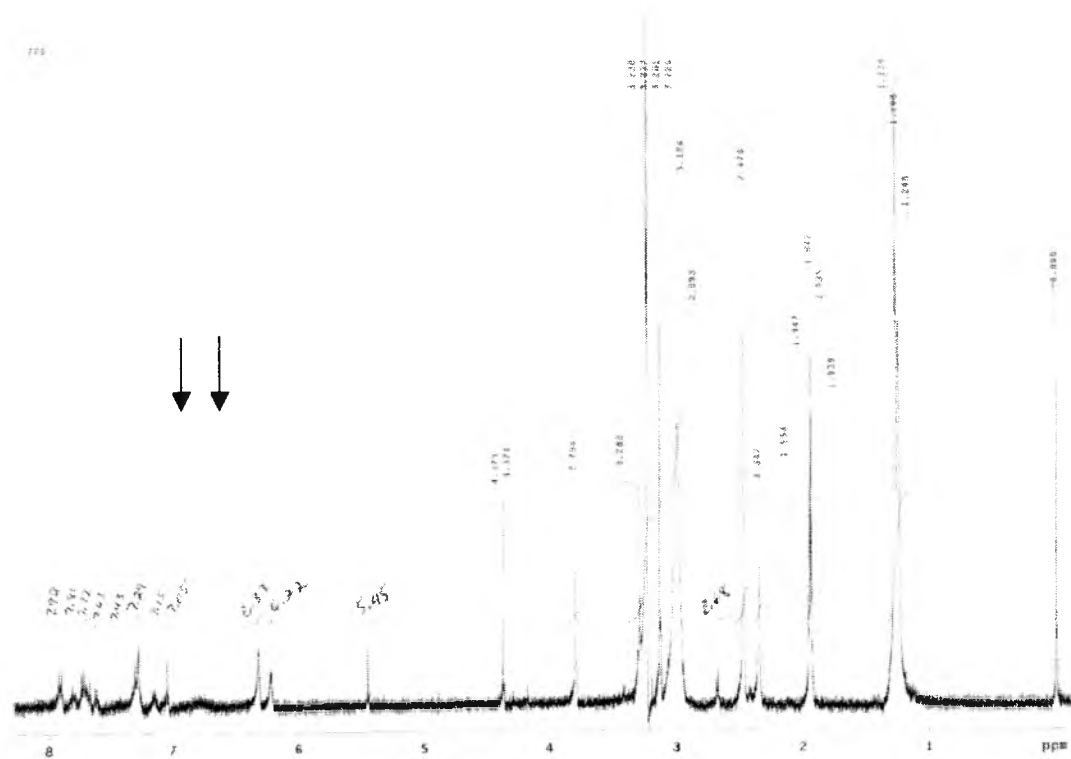
Spectra 49. [(L4O)Zn(SPh)] + MeI, chloroform, initial



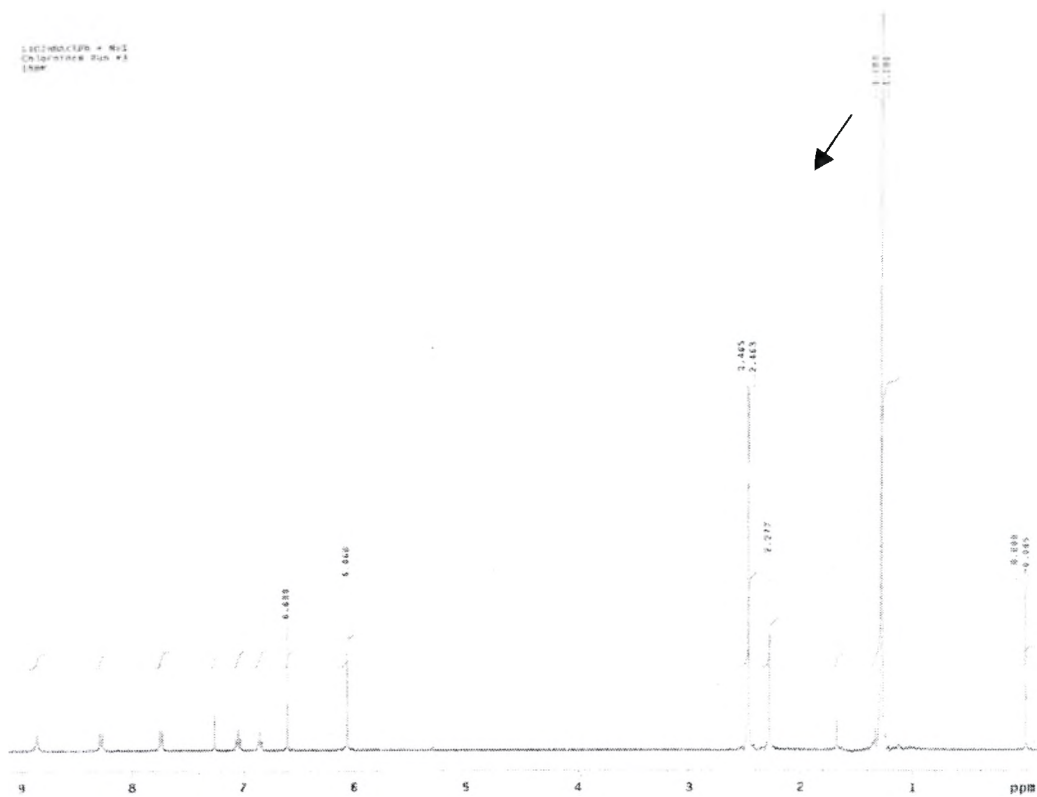
Spectra 50. [(L4O)Zn(SPh)] + MeI, chloroform, final



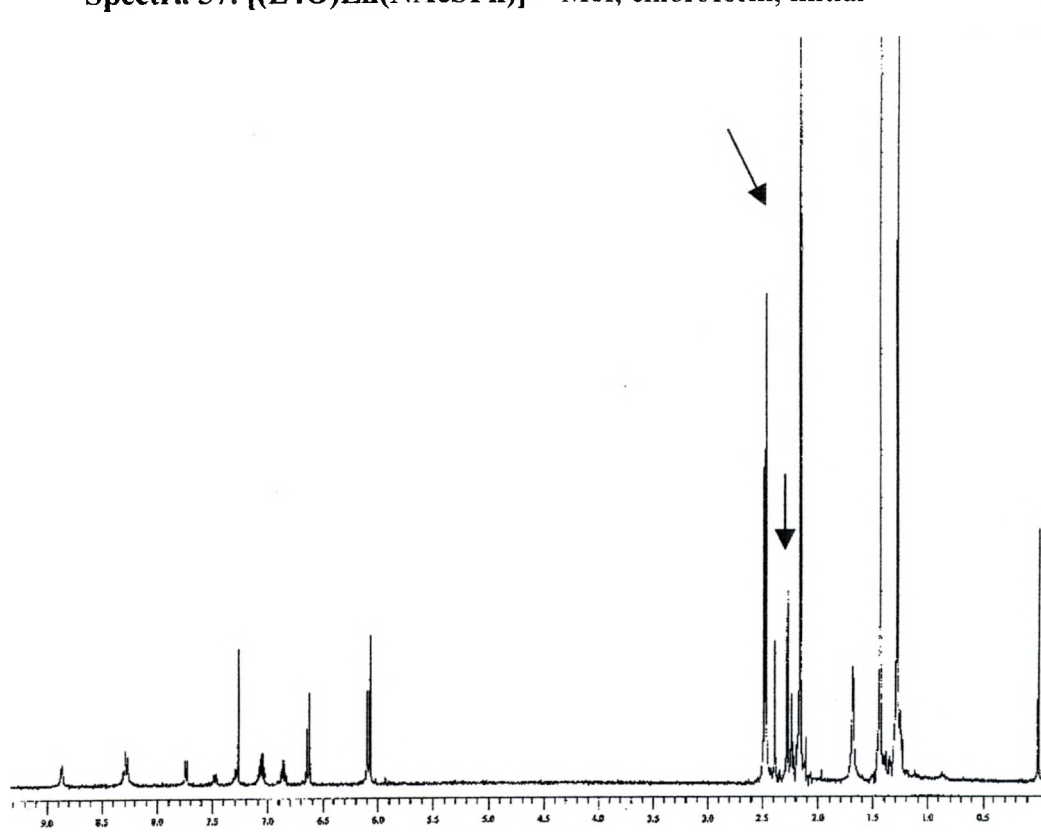
Spectra 55. [(L4O)Zn(SPh)] + (CH₃)₃OBF₄, acetonitrile, initial



Spectra 56. [(L4O)Zn(SPh)] + (CH₃)₃OBF₄, acetonitrile, final



Spectra 57. [(L4O)Zn(NAcSPh)] + MeI, chloroform, initial



Spectra 58. [(L4O)Zn(NAcSPh)] + MeI, chloroform, final

APPENDIX C: X-RAY CRYSTALLOGRAPHIC DATA

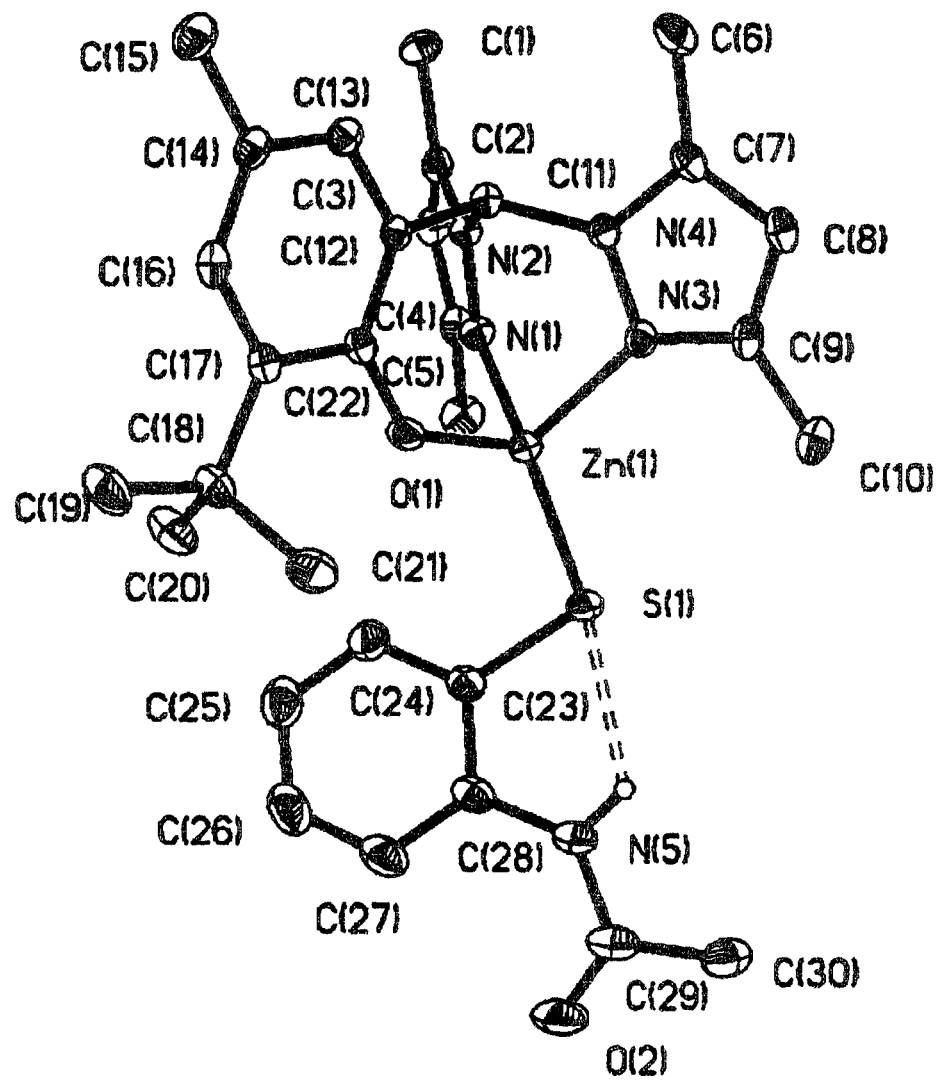


Table 2. Atomic coordinates [$\times 10^4$] and equivalent isotropic displacement parameters [$\text{\AA}^2 \times 10^3$] for 1. $U(\text{eq})$ is defined as one third of the trace of the orthogonalized U_{ij} tensor.

	x	y	z	$U(\text{eq})$
Zn(1)	3889(1)	7595(1)	1633(1)	38(1)
S(1)	5155(1)	7380(1)	1026(1)	58(1)
O(1)	2133(3)	7652(3)	1371(1)	52(1)
N(1)	4069(3)	8781(2)	2202(1)	40(1)
N(2)	3408(3)	8677(2)	2621(1)	34(1)
N(3)	4053(3)	6605(2)	2299(2)	40(1)
N(4)	3391(3)	6846(2)	2705(1)	37(1)
N(5)	5285(4)	6883(3)	-148(2)	57(1)
O(2)	5722(5)	6872(4)	-1026(2)	101(2)
C(1)	3035(5)	9587(4)	3488(2)	56(1)
C(2)	3612(4)	9485(3)	2982(2)	40(1)
C(3)	4424(4)	10115(3)	2786(2)	46(1)
C(4)	4690(4)	9659(3)	2310(2)	43(1)
C(5)	5543(5)	10015(4)	1934(2)	64(1)
C(6)	2960(5)	6182(4)	3628(2)	68(1)
C(7)	3569(4)	6132(3)	3129(2)	45(1)
C(8)	4369(4)	5424(3)	2981(2)	51(1)
C(9)	4659(4)	5743(3)	2476(2)	46(1)
C(10)	5506(5)	5276(4)	2137(2)	62(1)
C(11)	2627(3)	7781(3)	2663(2)	35(1)
C(12)	1382(4)	7729(3)	2242(2)	34(1)
C(13)	348(4)	7728(3)	2506(2)	39(1)
C(14)	-860(4)	7686(3)	2192(2)	43(1)
C(15)	-1952(4)	7662(4)	2483(2)	59(1)
C(16)	-1026(4)	7659(3)	1602(2)	45(1)
C(17)	-43(4)	7663(3)	1316(2)	40(1)
C(18)	-296(5)	7668(4)	660(2)	54(1)
C(19)	-1695(5)	7624(5)	396(2)	72(2)
C(20)	227(5)	8645(5)	451(2)	75(2)
C(21)	296(6)	6724(5)	437(2)	79(2)
C(22)	1207(4)	7683(3)	1644(2)	38(1)
C(23)	4464(4)	8111(4)	419(2)	51(1)
C(24)	3777(5)	8993(4)	451(3)	70(2)
C(25)	3299(6)	9554(5)	-27(3)	91(2)
C(26)	3501(7)	9263(6)	-549(3)	97(2)
C(27)	4164(6)	8400(5)	-598(2)	80(2)
C(28)	4649(4)	7807(4)	-120(2)	55(1)
C(29)	5754(5)	6459(5)	-573(2)	66(1)
C(30)	6344(6)	5443(5)	-431(3)	75(2)
Cl(2)	991(2)	7210(2)	-1338(1)	142(1)
Cl(3)	1824(10)	6270(11)	-878(4)	206(7)
Cl(1)	2425(3)	5327(3)	-1173(1)	175(1)

Table 3. Selected bond lengths [Å] and angles [°] for 1.

En(1)-O(1)	1.887(3)	Zn(1)-N(3)	2.023(3)
En(1)-N(1)	2.037(3)	Zn(1)-S(1)	2.2201(13)
O(1)-Zn(1)-N(3)	101.50(14)	O(1)-Zn(1)-N(1)	97.91(14)
N(3)-Zn(1)-N(1)	88.92(13)	O(1)-Zn(1)-S(1)	121.27(10)
N(3)-Zn(1)-S(1)	117.83(10)	N(1)-Zn(1)-S(1)	122.92(10)

Symmetry transformations used to generate equivalent atoms:

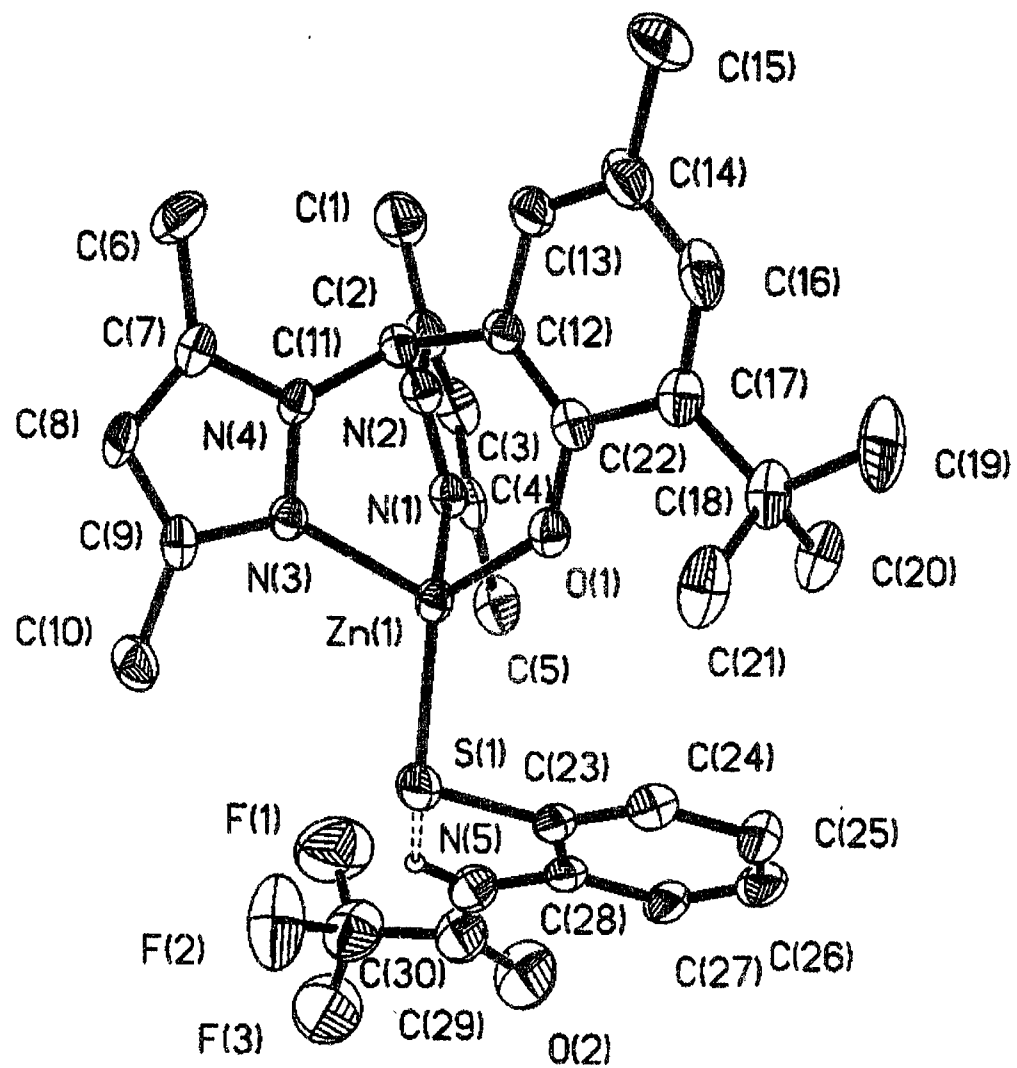


Table 2. Atomic coordinates [$\times 10^4$] and equivalent isotropic displacement parameters [$\text{\AA}^2 \times 10^3$] for 1. U(eq) is defined as one third of the trace of the orthogonalized U_{ij} tensor.

	x	y	z	U(eq)
Zn(1)	7022(1)	9262(1)	4008(1)	55(1)
S(1)	6451(2)	8556(2)	2829(2)	88(1)
N(1)	8543(5)	10184(5)	4346(4)	57(2)
N(2)	8671(5)	10765(5)	4975(5)	61(2)
N(3)	6522(5)	10287(5)	4293(4)	55(2)
N(4)	6908(5)	10743(5)	5000(4)	57(2)
N(5)	7934(8)	8498(7)	1716(6)	93(3)
O(1)	6739(5)	8501(4)	4909(4)	67(2)
O(2)	8982(9)	8245(8)	840(6)	163(4)
F(1)	9411(11)	10378(9)	957(7)	229(6)
F(2)	8629(11)	9556(8)	-27(6)	222(5)
F(3)	7812(10)	9845(8)	818(7)	207(5)
C(1)	10080(9)	12125(8)	5754(7)	108(4)
C(2)	9711(8)	11405(7)	5119(7)	77(3)
C(3)	10254(9)	11221(9)	4553(7)	92(4)
C(4)	9537(8)	10472(8)	4076(6)	74(3)
C(5)	9690(8)	10005(8)	3354(6)	94(4)
C(6)	6692(10)	11929(8)	5929(6)	104(4)
C(7)	6443(8)	11342(6)	5186(6)	66(3)
C(8)	5736(8)	11261(7)	4575(6)	75(3)
C(9)	5806(7)	10615(7)	4026(6)	65(3)
C(10)	5259(8)	10325(8)	3252(6)	88(3)
C(11)	7765(7)	10604(6)	5450(5)	60(2)
C(12)	7417(7)	9718(7)	5933(5)	58(2)
C(13)	7588(8)	9920(8)	6743(6)	79(3)
C(14)	7301(11)	9215(12)	7260(7)	105(4)
C(15)	7482(14)	9449(11)	8133(6)	171(7)
C(16)	6841(10)	8254(11)	6961(7)	101(4)
C(17)	6648(7)	7965(7)	6191(7)	70(3)
C(18)	6178(8)	6906(8)	5922(6)	80(3)
C(19)	5932(10)	6215(8)	6601(8)	138(6)
C(20)	6960(8)	6687(7)	5460(6)	93(4)
C(21)	5136(8)	6636(7)	5440(7)	109(4)
C(22)	6930(7)	8739(7)	5648(6)	61(2)
C(23)	7032(9)	7711(8)	2809(6)	77(3)
C(24)	6790(10)	6972(8)	3316(7)	95(4)
C(25)	7220(11)	6292(8)	3290(7)	100(4)
C(26)	7899(11)	6371(10)	2726(9)	110(5)
C(27)	8156(10)	7089(9)	2198(7)	97(4)
C(28)	7721(9)	7750(8)	2229(6)	80(3)
C(29)	8494(11)	8681(11)	1101(8)	111(4)
C(30)	8607(19)	9591(15)	700(11)	142(6)
Zn(2)	7102(1)	14250(1)	1272(1)	57(1)
S(2)	6612(2)	13637(2)	2431(2)	83(1)
O(3)	6982(5)	13438(4)	373(4)	68(2)
O(4)	8703(7)	13171(7)	4846(5)	124(3)
N(6)	7059(6)	15737(5)	247(4)	57(2)
N(7)	6561(5)	15208(5)	849(4)	55(2)
N(8)	8759(5)	15637(5)	401(4)	56(2)
N(9)	8640(5)	15170(5)	1073(4)	54(2)
N(10)	7990(7)	13603(6)	3790(6)	83(3)
F(4)	8955(8)	14825(7)	5552(5)	170(4)

F(5)	7395(7)	14314(7)	5237(6)	175(4)
F(6)	8459(10)	15295(6)	4560(5)	202(5)
C(31)	9818(8)	15079(8)	2160(6)	97(4)
C(32)	9624(8)	15440(7)	1406(5)	65(3)
C(33)	10357(7)	16073(7)	933(6)	73(3)
C(34)	9804(8)	16196(7)	306(5)	69(3)
C(35)	10183(9)	16796(10)	-384(6)	123(5)
C(36)	5156(7)	15145(8)	1686(6)	89(3)
C(37)	5839(7)	15550(7)	1037(6)	65(3)
C(38)	5868(9)	16252(8)	536(6)	78(3)
C(39)	6648(9)	16382(7)	40(6)	74(3)
C(40)	7040(10)	17064(8)	-595(6)	110(4)
C(41)	7839(7)	15511(6)	-146(5)	56(2)
C(42)	7379(6)	14591(6)	-639(5)	48(2)
C(43)	7412(7)	14729(7)	-1437(5)	58(2)
C(44)	6991(8)	13977(9)	-1974(6)	71(3)
C(45)	6988(10)	14154(9)	-2825(6)	111(4)
C(46)	6548(8)	13049(9)	-1700(7)	82(3)
C(47)	6505(7)	12838(7)	-922(6)	60(2)
C(48)	6024(8)	11780(7)	-680(6)	75(3)
C(49)	5599(10)	11045(7)	-1372(7)	116(5)
C(50)	5073(8)	11601(7)	-173(8)	114(4)
C(51)	6876(8)	11568(7)	-214(5)	81(3)
C(52)	6928(7)	13629(7)	-368(6)	59(2)
C(53)	7285(10)	12868(8)	2528(7)	88(3)
C(54)	7192(13)	12199(10)	1944(7)	131(5)
C(55)	7678(18)	11575(12)	2010(9)	186(9)
C(56)	8269(18)	11615(13)	2658(10)	199(10)
C(57)	8370(12)	12259(10)	3282(8)	134(6)
C(58)	7881(10)	12905(9)	3206(7)	91(4)
C(59)	8345(9)	13694(10)	4516(7)	86(3)
C(60)	8331(12)	14577(12)	4946(8)	102(4)

Table 3. Selected bond lengths [Å] and angles [°] for 1.

Zn(1)-O(1)	1.913(6)	Zn(1)-N(3)	2.011(6)
Zn(1)-N(1)	2.017(7)	Zn(1)-S(1)	2.235(3)
Zn(2)-O(3)	1.903(6)	Zn(2)-N(7)	2.018(6)
Zn(2)-N(9)	2.044(7)	Zn(2)-S(2)	2.246(3)
O(1)-Zn(1)-N(3)	101.5(3)	O(1)-Zn(1)-N(1)	96.9(3)
N(3)-Zn(1)-N(1)	90.2(3)	O(1)-Zn(1)-S(1)	121.0(2)
N(3)-Zn(1)-S(1)	115.5(2)	N(1)-Zn(1)-S(1)	125.5(2)
O(3)-Zn(2)-N(7)	100.1(3)	O(3)-Zn(2)-N(9)	94.9(3)
N(7)-Zn(2)-N(9)	91.0(3)	O(3)-Zn(2)-S(2)	122.2(2)
N(7)-Zn(2)-S(2)	118.7(2)	N(9)-Zn(2)-S(2)	123.1(2)

Symmetry transformations used to generate equivalent atoms:

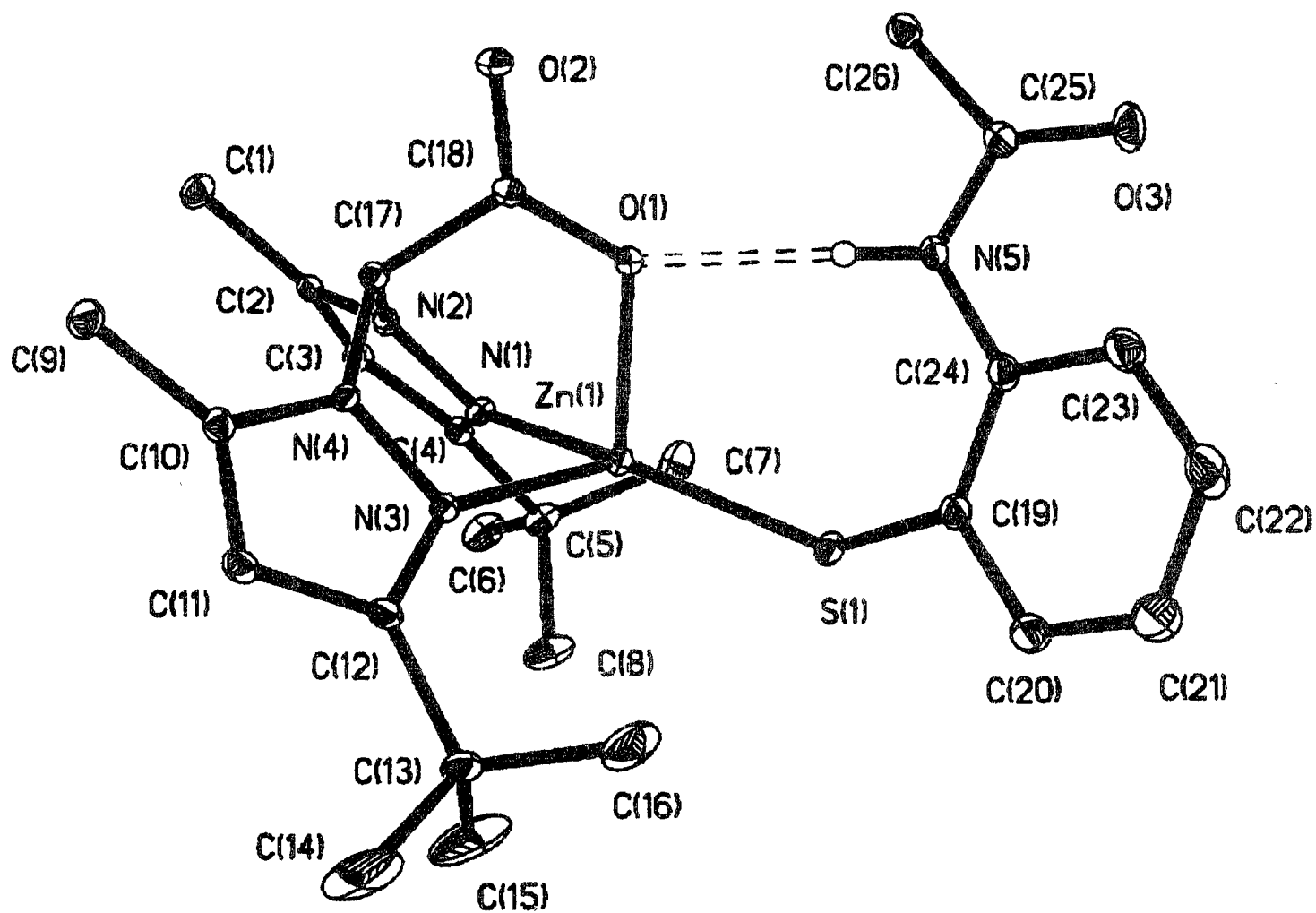


Table 2. Atomic coordinates [$\times 10^4$] and equivalent isotropic displacement parameters [$\text{\AA}^2 \times 10^3$] for 1. $U(\text{eq})$ is defined as one third of the trace of the orthogonalized U_{ij} tensor.

	x	y	z	U(eq)
Zn(1)	2565(1)	1922(1)	3763(1)	17(1)
S(1)	1932(1)	-11(1)	3787(1)	23(1)
O(1)	3578(1)	2140(2)	4774(1)	21(1)
O(2)	4651(1)	3458(2)	5386(1)	27(1)
O(3)	3907(2)	-2156(3)	6325(2)	48(1)
N(1)	3156(1)	2315(3)	2965(1)	19(1)
N(2)	3707(1)	3340(2)	3260(1)	17(1)
N(3)	2311(1)	3963(2)	3757(2)	19(1)
N(4)	2991(1)	4730(2)	3896(2)	17(1)
N(5)	3343(1)	-282(3)	5565(2)	24(1)
C(1)	4770(2)	4577(3)	2926(2)	28(1)
C(2)	4129(2)	3537(3)	2749(2)	19(1)
C(3)	3837(2)	2607(3)	2107(2)	21(1)
C(4)	3231(2)	1868(3)	2253(2)	20(1)
C(5)	2710(2)	731(3)	1741(2)	26(1)
C(6)	2839(2)	580(4)	912(2)	37(1)
C(7)	2943(2)	-608(4)	2237(2)	38(1)
C(8)	1823(2)	1058(5)	1557(2)	41(1)
C(9)	3463(2)	7123(3)	4045(2)	33(1)
C(10)	2833(2)	6077(3)	3891(2)	21(1)
C(11)	2024(2)	6184(3)	3748(2)	25(1)
C(12)	1721(2)	4857(3)	3660(2)	23(1)
C(13)	852(2)	4422(4)	3462(2)	36(1)
C(14)	345(4)	5661(8)	3394(10)	156(6)
C(15)	562(4)	3700(11)	2551(4)	92(3)
C(16)	795(4)	3366(9)	4081(4)	62(2)
C(17)	3759(2)	4087(3)	4014(2)	18(1)
C(18)	4036(2)	3160(3)	4804(2)	18(1)
C(19)	1883(2)	-248(3)	4804(2)	26(1)
C(20)	1120(2)	-424(4)	4831(2)	42(1)
C(21)	1020(2)	-767(5)	5570(3)	57(1)
C(22)	1681(2)	-920(5)	6310(3)	52(1)
C(23)	2441(2)	-747(4)	6297(2)	37(1)
C(24)	2549(2)	-434(3)	5552(2)	26(1)
C(25)	3966(2)	-1125(3)	5956(2)	27(1)
C(26)	4754(2)	-709(3)	5881(2)	28(1)
C(16A)	781(14)	3059(22)	3820(13)	19(5)
C(15A)	380(8)	4559(14)	2618(9)	9(3)
C(14A)	533(9)	5507(16)	4026(8)	13(3)

Table 3. Selected bond lengths [Å] and angles [°] for 1.

Zn(1)-O(1)	2.002(2)	Zn(1)-N(1)	2.050(2)
Zn(1)-N(3)	2.058(2)	Zn(1)-S(1)	2.2219(8)
O(1)-Zn(1)-N(1)	91.52(9)	O(1)-Zn(1)-N(3)	91.63(9)
N(1)-Zn(1)-N(3)	88.80(10)	O(1)-Zn(1)-S(1)	112.50(6)
N(1)-Zn(1)-S(1)	124.48(7)	N(3)-Zn(1)-S(1)	136.25(7)

Symmetry transformations used to generate equivalent atoms:

Table 2. Atomic coordinates [$\times 10^4$] and equivalent isotropic displacement parameters [$\text{\AA}^2 \times 10^3$] for 1. $U(\text{eq})$ is defined as one third of the trace of the orthogonalized U_{ij} tensor.

	x	y	z	U(eq)
Zn(1)	2416(1)	2118(1)	380(1)	24(1)
S(1)	3260(1)	3595(1)	211(1)	28(1)
S(2)	705(1)	1618(1)	1056(1)	33(1)
N(1)	4101(2)	1362(2)	576(1)	22(1)
N(2)	5023(2)	1515(2)	26(1)	21(1)
N(3)	2506(2)	1670(2)	-804(1)	23(1)
N(4)	3666(2)	1855(2)	-1140(1)	20(1)
N(5)	-1005(2)	1946(2)	2383(2)	33(1)
C(1)	7367(3)	1129(2)	-191(2)	33(1)
C(2)	6156(3)	1073(2)	256(2)	25(1)
C(3)	5933(3)	612(2)	966(2)	29(1)
C(4)	4653(3)	805(2)	1145(2)	26(1)
C(5)	3896(3)	475(2)	1840(2)	37(1)
C(6)	4651(3)	1899(2)	-2501(2)	30(1)
C(7)	3565(3)	1743(2)	-1955(2)	24(1)
C(8)	2308(3)	1475(2)	-2135(2)	29(1)
C(9)	1685(3)	1430(2)	-1406(2)	27(1)
C(10)	327(3)	1150(2)	-1240(2)	38(1)
C(11)	4768(2)	2186(2)	-636(2)	20(1)
C(12)	4682(3)	3258(2)	-369(2)	22(1)
C(13)	5918(3)	3476(2)	131(2)	31(1)
C(14)	4645(3)	3862(2)	-1137(2)	30(1)
C(15)	-220(3)	2677(2)	1187(2)	25(1)
C(16)	-222(3)	3447(2)	654(2)	31(1)
C(17)	-969(3)	4257(2)	770(2)	32(1)
C(18)	-1722(3)	4315(2)	1431(2)	32(1)
C(19)	-1752(3)	3563(2)	1969(2)	31(1)
O(1)	-2574(2)	2320(2)	3246(1)	40(1)
C(20)	-1015(3)	2741(2)	1852(2)	26(1)
C(21)	-1763(3)	1766(2)	3014(2)	33(1)
C(22)	-1506(4)	813(3)	3417(2)	51(1)

Table 3. Selected bond lengths [Å] and angles [°] for 1.

Zn(1)-N(1)	2.054(2)	Zn(1)-N(3)	2.077(2)
Zn(1)-S(2)	2.2482(9)	Zn(1)-S(1)	2.2573(9)
N(1)-Zn(1)-N(3)	85.81(9)	N(1)-Zn(1)-S(2)	116.31(7)
N(3)-Zn(1)-S(2)	116.73(7)	N(1)-Zn(1)-S(1)	99.00(7)
N(3)-Zn(1)-S(1)	97.04(7)	S(2)-Zn(1)-S(1)	131.45(3)

Symmetry transformations used to generate equivalent atoms:

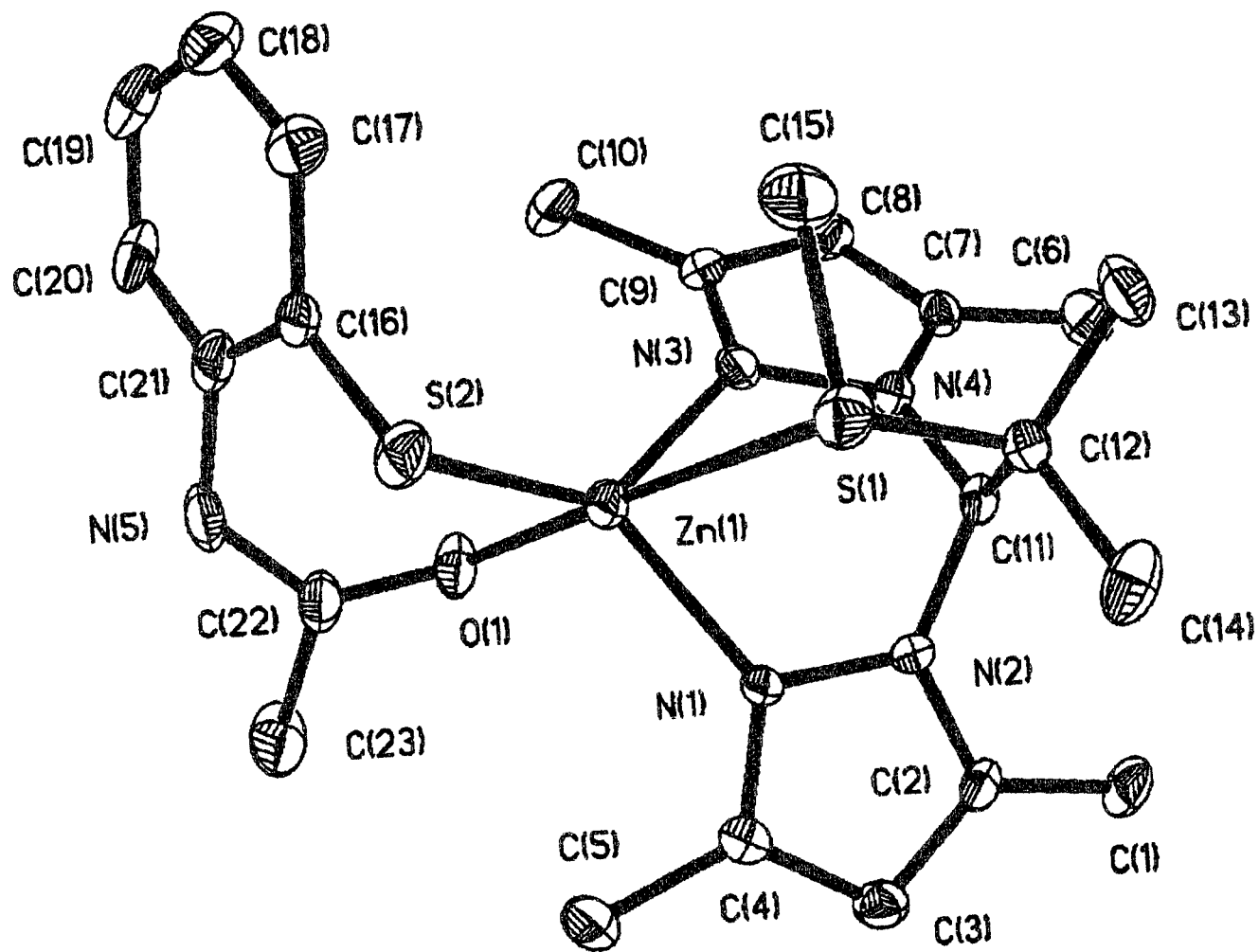


Table 2. Atomic coordinates [$\times 10^4$] and equivalent isotropic displacement parameters [$\text{\AA}^2 \times 10^3$] for 1. $U(\text{eq})$ is defined as one third of the trace of the orthogonalized U_{ij} tensor.

	x	y	z	U(eq)
Zn(1)	2662(1)	1290(1)	1511(1)	45(1)
N(1)	3850(4)	1595(5)	768(4)	42(2)
N(2)	3881(4)	1280(5)	-97(4)	40(2)
N(3)	2209(4)	195(5)	659(4)	40(2)
N(4)	2502(4)	192(5)	-206(4)	38(2)
N(5)	2743(6)	526(7)	3814(5)	78(3)
O(1)	3330(4)	329(5)	2433(4)	61(2)
S(1)	1827(2)	2528(2)	246(2)	59(1)
S(2)	1892(2)	2194(2)	2536(2)	62(1)
C(1)	5058(6)	1080(7)	-1330(5)	61(3)
C(2)	4784(6)	1393(7)	-422(5)	44(2)
C(3)	5348(6)	1771(6)	244(5)	51(2)
C(4)	4746(6)	1883(7)	965(5)	47(2)
C(5)	5015(6)	2244(8)	1877(5)	70(3)
C(6)	2473(7)	-898(7)	-1545(6)	71(3)
C(7)	2259(6)	-684(7)	-605(5)	43(2)
C(8)	1810(6)	-1252(7)	-2(5)	54(2)
C(9)	1784(5)	-690(7)	771(5)	40(2)
C(10)	1332(6)	-961(6)	1631(5)	58(3)
C(11)	2980(6)	1049(6)	-578(5)	43(2)
C(12)	2328(6)	1970(7)	-763(5)	49(2)
C(13)	1516(6)	1647(8)	-1402(5)	77(4)
C(14)	2938(7)	2780(7)	-1167(6)	73(3)
C(15)	631(6)	2062(9)	346(6)	92(4)
C(16)	1285(6)	1216(7)	3059(5)	50(2)
C(17)	257(7)	1107(8)	2931(6)	61(3)
C(18)	-267(8)	404(9)	3367(7)	75(3)
C(19)	182(9)	-253(9)	3916(7)	83(4)
C(20)	1168(8)	-200(8)	4046(6)	72(3)
C(21)	1705(7)	512(8)	3621(6)	64(3)
C(22)	3458(7)	377(8)	3257(6)	65(3)
C(23)	4445(6)	256(10)	3642(6)	106(5)
B(1)	3068(9)	1056(14)	6296(11)	71(4)
F(3)	3533(17)	967(37)	5575(9)	113(14)
F(1)	3055(30)	242(35)	6716(43)	237(29)
F(2)	2202(5)	1512(6)	6214(6)	150(3)
F(4)	3607(25)	1690(30)	6779(29)	158(17)
F(3')	2989(37)	261(25)	5744(22)	159(15)
F(4')	3741(17)	1672(27)	6043(46)	165(24)
F(1')	3266(23)	697(41)	7081(14)	124(18)

Table 3. Selected bond lengths [Å] and angles [°] for 1.

Zn(1)-N(3)	2.045(7)	Zn(1)-N(1)	2.047(6)
Zn(1)-O(1)	2.102(6)	Zn(1)-S(2)	2.254(2)
Zn(1)-S(1)	2.773(3)		
<hr/>			
N(3)-Zn(1)-N(1)	91.8(3)	N(3)-Zn(1)-O(1)	96.2(2)
N(1)-Zn(1)-O(1)	98.3(2)	N(3)-Zn(1)-S(2)	132.9(2)
N(1)-Zn(1)-S(2)	131.7(2)	O(1)-Zn(1)-S(2)	94.2(2)
N(3)-Zn(1)-S(1)	82.6(2)	N(1)-Zn(1)-S(1)	79.9(2)
O(1)-Zn(1)-S(1)	177.8(2)	S(2)-Zn(1)-S(1)	87.91(9)

Symmetry transformations used to generate equivalent atoms:

VITA

Jennifer Nicole Smith was born in Louisville, Kentucky, on January 13, 1980, the daughter of Karlene Ann Smith and Dr. Thomas Michael Smith. In 1983, she and her family moved to Austin, Texas. After completing her work at Westlake High School, Austin, Texas, in 1998, she entered the University of Texas at Austin. She received the degree of Bachelor of Science in Biochemistry from the University of Texas at Austin, in December, 2001. The following January, she entered the Graduate School of Southwest Texas State University, San Marcos, Texas. Jennifer co-authored a research publication entitled "Control of Thiolate Nucleophilicity and Specificity in Zinc Metalloproteins by Hydrogen Bonding: Lessons from Model Compound Studies," which is published in the *Journal of the American Chemical Society*, **2003**, *125(4)* 868-869. In November, 2002, she attended the Southwest Regional Meeting of the American Chemical Society, Austin, Texas, to present a seminar entitled "Alkylation of Zinc Thiolate Proteins: Controlling Reactivity in Model Compounds." She currently resides in Austin, Texas.

Permanent Address: 1625 Churchwood Cove
 Austin, Texas 78746

This thesis was typed by Jennifer Nicole Smith.

